Quantum Fluctuations and Criticality of Interacting Dirac Fermions

Elliot Christou

A dissertation submitted in partial fulfillment

of the requirements for the degree of

Doctor of Philosophy

of

University College London.

Department of Physics

University College London

October 10, 2019

I, Elliot Christou, confirm that the work presented in this Thesis is my own. Where information has been derived from other sources, I confirm that this has been indicated in the work.

Abstract

This Thesis explores the formation of novel phases in Dirac systems that are driven by strong many-body interactions and collective quantum fluctuations. The central focus is the half-filled honeycomb lattice, which is the prototypical Dirac semimetal with low-energy excitations described by Dirac fermions.

Of particular interest are exotic phases of matter that are not favoured at mean-field but are stabilised by fluctuations. Self-consistent path integral techniques are used to demonstrate that extended repulsive interactions favour charge order that breaks translational and other lattice symmetries. This charge order outcompetes interaction induced topological insulating phases, which are dominant at the mean-field level. The interacting quantum critical point was found to be near the critical point of a topological Lifshitz transition.

Interacting Dirac fermions exhibit perhaps the simplest example of fermionic quantum criticality. Gross-Neveu-Yukawa field theories describe the universality class of semimetal-insulator transitions, which are driven by on-site and nearest neighbour repulsive interactions on the honeycomb lattice. The Dirac fermions couple to the dynamical order parameter fields and play a crucial role in determining the universal behaviour. Naturally, this variety of criticality is outside of the Ginzburg-Landau-Wilson paradigm. This idea is extended to include the translational symmetry breaking charge order. Here it is found that the breaking of crystal symmetries corresponds to Lorentz violating effective field theories. The criticality is analysed with the renormalisation group.

The low energy excitations at the topological transition are gapless semi-Dirac fermionic quasiparticles that disperse linearly in one direction and quadratically in

the other. The instabilities induced by generic short-range repulsions are investigated. The criticality of this anisotropic system is analysed with the renormalisation group in two spatial dimensions, and it is found to exhibit anisotropic order parameter correlations.

Impact Statement

This Thesis comprises fundamental research into strongly interacting and correlated quantum electron systems. The immediate benefit of this research will be to researchers working on novel electronic phases, quantum criticality, quantum materials, and solid-state physics. Harnessing the new phenomena of correlated topological quantum materials, and controlling their quantum states, is paramount to delivering quantum technologies.

Acknowledgements

First of all, I would like to thank my supervisor Frank Krüger for his guidance, patience and support, both in and outside of physics, and who has always been generous with his time. I am thankful to Andrew Green for his useful advice throughout. I am grateful to Andrew James for the numerous constructive discussions over coffee and lunch. Further, I would like to thank my collaborators and colleagues for their many useful comments and discussions. In particular, Fernando de Juan for sharing his symmetry wizardry, and Bruno Uchoa for sharing his knowledge of Dirac fermions. Also, those at UCL who regularly provided insight and understanding: Philip Crowley, Luke Davis, Andrew Hallam, Tom Kirk, Alex Sato, Miki Uryszek and Adam Walker. I am grateful to all the support staff and others that have helped along the way. Special thanks goes to Felix Flicker for continuously providing advice that started in my first year at Bristol. Additional thanks go to Jasper van Wezel and Martin Gradhand for answering my numerous questions and guiding me during my undergraduate research, as well as to Jasper for inviting me to Amsterdam. Thanks to my parents Michael and Tracy and my brothers Alex, Max and Miles for everything they have done for me. Thanks to my Bristol and London friends for all the good times and support. Finally, I owe an enormous amount to Danielle for her unwavering love, care, belief and much, much more. Cheers!

Contents

List of Figures

List of Tables

Chapter 1

Introduction

Emergence and universality are two ideas at the heart of modern physics, and in particular the study of *quantum matter*. This is a topic that concerns both the electrons in the most unexceptional of metals, as well as the interiors of neutron stars [1]. At the heart of the principle of emergence is that "the whole is greater than the sum of its parts" [2]. This correctly identifies that a macroscopic number of interacting particles, acting as a collective, can exhibit phenomena that are profoundly different to the properties of the non-interacting constituents. In doing so, emergent phases of matter are formed. This is particularly true for quantum matter in which Heisenberg's uncertainty principle inhibits the distinction of the individual particles. Such ideas are profoundly important when dealing with the seemingly unsurmountable task of 10^{26} electrons, that are all interacting in accordance with the laws of electromagnetism.

There are many strongly correlated systems that remain enigmatic. These include the high-temperature superconductors [3] that also exhibit the mysterious bad metal and pseudogap phases, as well as the quark-gluon plasma that is thought to have formed within fractions of a second of the Big Bang. There are however multiple examples of quantum matter that are well understood, such as the transport of electricity in everyday metals, and the superfluid phase of low temperature helium. To a large extent, these phenomena were explained by the two deep insights provided by Landau: the Fermi liquid and the order parameter [4]. The Fermi liquid theory posits that interacting fermions, typically in metals, can be described by emergent

non-interacting fermionic quasiparticles with renormalised properties, such as the increase of their mass. The concept of the order parameter ϕ measures long-range correlations of collective fermionic ψ degrees of freedom $\phi \sim \langle \psi^\dagger \psi \rangle$, and characterises the transformation of matter at a phase transition between a disordered, high symmetry phase ($\phi = 0$) and an ordered, broken symmetry phase ($\phi \neq 0$).

Another principle of fundamental importance is that of universality, which dictates that microscopically distinct physical systems can display identical long-distance, low-energy properties. Universal features are often observed when the emergent characteristic length scale, the correlation length ξ, is considerably larger than all microscopic scales of the system. The prototypical example of universality is a system in the vicinity of a classical finite temperature continuous phase transition. The system transitions from disordered to ordered as the temperature is lowered past the critical temperature T_c.

At the critical point, the correlation length diverges as a power law $\xi \sim (T - T_c)^{-\nu}$, indicating the system becomes scale invariant, or self-similar, with no well defined length scale. This universal power law scaling behaviour is also observed in the growth of the order parameter below T_c, $\phi \sim (T_c - T)^{\beta}$, as well as in various thermodynamic quantities such as the specific heat. Remarkably, it is only the symmetry of the order parameter and the dimensionality of the system that govern the universality class of a classical continuous phase transition. Hence, in physically distinct transitions it is possible to observe the same set of critical exponents, which include ν and β. A well known example is that the uniaxial ferromagnetic and liquid-gas transitions both belong to the Z_2 Ising universality class.

The culmination of these ideas was the Ginzburg-Landau-Wilson fluctuating order parameter theory of continuous phase transitions [5] described by the action

$$S_{\mathrm{GLW}} = \int \phi^\dagger(-\partial^2 + m^2)\phi + \lambda\phi^4. \tag{1.1}$$

The critical properties can be studied systematically within the framework of the renormalisation group [6–9]. Through this it is understood that dimensionality plays an important role. In fact, for a given theory there is a critical dimension, above

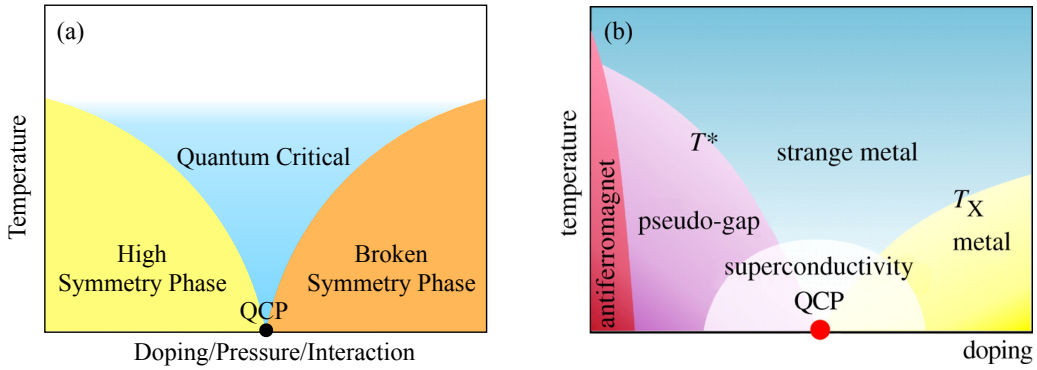

Figure 1.1: (a) Generic phase diagram of a continuous quantum phase transition tuned by a non-thermal parameter such as chemical doping, pressure or interactions between particles. Above the quantum critical point (QCP) (black dot) is the quantum critical fan, which persists to high temperatures determined by microscopic properties of the system. (b) Generic schematic phase diagram of the cuprate superconductors as a function of temperature and hole doping. A superconducting dome forms in the vicinity of the quantum critical point separating the antiferromagnetic insulator at low doping and the metal (Fermi-liquid) at high doping. The two mysterious non-Fermi liquid phases are the pseudogap, and strange metal that occupies a wide region reminiscent of the quantum critical fan. Some phases, such as the charge order, have been omitted for simplicity. Figure (b) is from Ref. [3].

which Landau's mean-field theory exactly describes the criticality. However, below this critical dimension interactions λ and order parameter fluctuations are no longer negligible, and become more potent as the dimensionality is lowered.

In recent years, the focus has shifted to phase transitions at the absolute zero of temperature, where the physics is inherently quantum mechanical [1, 10, 11]. These quantum phase transitions describe the distinct change in the properties of matter due to a small variation in a non-thermal parameter, such as pressure or chemical doping, which ultimately change the relative strength of interactions V between the constituent (quasi-)particles, see Fig. 1.1(a). In the region of the quantum critical point V_c there is a vanishing characteristic energy scale $\Delta \sim \xi^{-z} \sim |V - V_c|^{\nu z}$ associated with the diverging correlation length $\xi \sim |V - V_c|^{-\nu}$. Here z is the dynamical exponent associated with the relative scaling of space and time, and governs the ensuing gapless excitations $\omega \sim k^z$.

Surprisingly, the quantum critical region extends to finite temperatures where the system is ignorant of the finite energy gap $k_B T \ll \Delta$, and is roughly bounded

by $k_B T \sim \Delta$. Therefore quantum critical fluctuations can persist and dominate the phase diagram to amazingly high temperatures. Such fluctuations can induce new types of order, with the prototypical example being the cuprate high temperature superconductor phase diagram between metallic Fermi liquid and antiferromagnetic insulator states [3], see Fig. 1.1b. In the vicinity of the antiferromagnetic quantum critical point, quantum critical fluctuations stabilise the superconducting phase to remarkably high temperatures. Fathoming the underlying universal mechanisms that may lead to room temperature superconductivity is an ongoing research area. Finally, it is worth noting that non-universal physics will set in at energy scales determined by microscopic properties of the system [12].

There are a growing number of instances where quantum criticality goes beyond the Ginzburg-Landau-Wilson paradigm, that has had so much success in the classical case. A prevalent example, and a central focus of this Thesis, is the impact of gapless fermionic excitations, such as in a metal or semimetal, that couple to the dynamical order parameter field. In short, if the fermionic spectrum $\hat{\varepsilon}$ is gapless, then there is no energy scale on which the fermions can be successfully integrated out in a controlled manner, without also integrating out all order parameter modes. Without being overly formal, this can be sketched out with the fermion-order parameter (Hubbard-Stratonovich) action

$$S = \int \psi^\dagger (\hat{G}^{-1} + \hat{\phi})\psi + \frac{1}{V}\hat{\phi}^\dagger \hat{\phi}, \tag{1.2}$$

where $\hat{G}^{-1} = \hat{\partial}_\tau + \hat{\varepsilon}$ is the fermionic propagator in imaginary time $\tau \in [0, \hbar/k_B T]$. Here it is to be understood that in the broken symmetry state $\langle\hat{\phi}\rangle \neq 0$ the previously gapless fermionic spectrum is now massive $\hat{\varepsilon}' \sim \hat{\varepsilon} + \langle\hat{\phi}\rangle$. Although the fermions can be formally integrated out at criticality, it is highly questionable [13] whether $\mathrm{tr}\ln(\hat{G}^{-1} + \hat{\phi})$ may be expanded (when $\langle\hat{\phi}\rangle = 0$) to obtain anything even remotely resembling the Ginzburg-Landau-Wilson action Eq. (1.1)

$$S \to \int \mathrm{tr}\ln(\hat{G}^{-1} + \hat{\phi}) + \frac{1}{V}\hat{\phi}^\dagger\hat{\phi} \stackrel{?}{=} \int \hat{\phi}\left(\frac{1}{V} + \mathrm{tr}\,\hat{G}\hat{G}\right)\hat{\phi} + \mathrm{tr}\,(\hat{G}\hat{\phi})^4 + \cdots . \tag{1.3}$$

Another way of thinking about this issue of fermionic quantum criticality, is that the expansion would assume that there are well defined fermionic quasiparticles, which is in contradiction to the fact that there are no sharp quasiparticle excitations in the vicinity of a quantum critical point [1]. The resolution is to treat fermionic and order parameter fields in Eq. (1.2) on equal footing. Another notable example of quantum criticality beyond the conventional paradigm is the Landau-forbidden continuous transition between ordered insulating states with fractionalised critical excitations, which is known as deconfined quantum criticality [14].

Outline of Thesis

This Thesis explores the formation of novel phases in two-dimensional Dirac systems that are driven by strong many-body interactions and collective quantum fluctuations. The central focus is the half-filled (graphene) honeycomb lattice in two spatial dimensions, which is the prototypical Dirac semimetal [15]. Remarkably, the low-energy excitations are well described by linearly dispersing Dirac fermions [16, 17], which couple to the order-parameter fields and play a crucial role in determining the universal behaviour [1, 9, 18]. The symmetry breaking leads to the opening of a gap in the fermionic spectrum and therefore goes hand-in-hand with a semimetal-to-insulator transition [19, 20]. These nodal semimetals with point-like Fermi surfaces represent perhaps the simplest example of fermionic quantum criticality. In high energy physics this has been known for some time, and goes under the guise of spontaneous fermion mass generation and chiral symmetry breaking in the Gross-Neveu-Yukawa model [21, 22]. In recent years Gross-Neveu-Yukawa models and sign-free lattice Quantum Monte Carlo simulations have helped to push the understanding of fermionic criticality beyond the Ginzburg-Landau-Wilson paradigm [23–32]. Ultimately, the study of quantum phase transitions in nodal semi-metals might serve as a stepping stone towards an understanding of quantum criticality in metals with extended Fermi surfaces [33].

An additional motivation to study Dirac systems is their susceptibility towards topologically non-trivial phases of matter. An example are the quantum Hall insulat-

ing states that exhibit quantised Hall conductance due to their topologically protected metallic edge states [34–36]. Indeed, it was on the honeycomb lattice that Haldane first proposed that there could be quantum Hall states in the absence of Landau level quantisation, so long as there was a mechanism that induced complex chiral hopping, or equivalently broken time reversal symmetry [37]. This idea was later generalised to topological insulators that display a quantum spin Hall effect [38–40], which was brought to experimental fruition in semiconducting heterostructures [36, 41]. Here the key feature was spin-orbit coupling that induced helical chiral hopping. Even the semimetallic state has a topological interpretation in which the Dirac points are vortex-antivortex pairs with opposite chirality [42, 43]. These topological classifications are also beyond the Ginzburg-Landau-Wilson paradigm, as it is not possible to construct a local order parameter that distinguishes a non-trivial quantum Hall state from a topologically trivial band insulator [44]. What's more, phase transitions between topologically distinct phases result in critical phases with exotic gapless excitations [45–48], which imply novel quantum critical properties [42, 49–56].

Chapter 2 presents an introduction to the physics of fermions on the half-filled two dimensional honeycomb lattice. The remarkable fact that the low-energy physics is well described by Dirac fermions is demonstrated. The semimetal-sublattice charge density wave insulator transition driven by strong nearest neighbour repulsion is discussed. The Landau free energy is obtained using standard mean-field theory. An equivalent formulation using the path integral saddle point expansion is presented. It is demonstrated that even at the mean-field level, the gapless Dirac fermions play a crucial role, and the universality is not of the standard Ginzburg-Landau-Wilson mean-field variety.

Chapter 3 concerns the broken symmetry state induced by strong next-nearest neighbour repulsion on the honeycomb lattice. This work was motivated by the proposal of Raghu *et al.* [57] that these interactions could dynamically generate the complex chiral hopping of the Haldane model. Therefore, the interactions could spontaneously break the symmetry into non-trivial topological states, referred to as topological Mott insulating states. This was the first example unifying ideas of

strongly correlated physics and topological band theory. Further examples on this theme can be found in recent review articles [44, 58]. The topological Mott insulating states turn out to compete with charge ordering that breaks the lattice translational symmetry at the mean-field level. This competition implies that beyond mean-field quantum fluctuations are pivotal to determining the phase diagram.

After first introducing Haldane's model, the fate of the topological Mott insulating states is analysed using a self-consistent path integral method to quadratic order in the collective quantum fluctuations. An analytical treatment is achieved by deriving the low-energy theory of the ordering. Although the topological phases are stable at mean-field, it is concluded that fluctuations induce charge ordering. Surprisingly, the low-energy excitations of the charge ordered broken symmetry state are found to be of the gapless semi-Dirac form, with linear and quadratic dispersions along perpendicular axes.

Chapter 4 presents a systematic study of the quantum criticality associated with the lattice symmetry breaking charge order. This is motivated by the unconventional low-energy excitations predicted in the fluctuation induced broken symmetry state. It is first demonstrated that the translational and rotational symmetry breaking charge order parameters on the lattice, couple to the Dirac fermions in the low-energy effective field theory as a combination of mass- and emergent non-Abelian gauge fields. Following this, the Wilsonian renormalisation group and scaling analysis framework to analyse universal properties is introduced. The one-loop renormalisation group analysis of the Gross-Neveu-Yukawa field theory, relevant to the sublattice charge density wave, is presented in detail. The coupling to the Dirac fermions plays a crucial role in determining the quantum critical fixed point, which is endowed with emergent Lorentz invariance: $z = 1$ and a single terminal velocity. In addition, the quasiparticle residue vanishes as a power law indicating the breakdown of well defined fermionic quasiparticles.

The study of the lattice symmetry breaking field theory then builds upon the analysis of the Gross-Neveu-Yukawa theory. The former critical fixed point is unstable, and the system flows to a new fixed point that breaks the emergent Lorentz

invariance, indicating new universal behaviour. In addition, lattice symmetry allowed cubic terms in the Landau theory are found to vanish at the critical point. These terms would otherwise indicate a first-order transition, but are suppressed by the gapless fermionic excitations, making this an example of fermion-induced quantum criticality. Finally, perturbing into the broken symmetry state reveals the system is in the vicinity of a topological critical point hosting semi-Dirac excitations, consistent with the path integral approach.

Chapter 5 studies the instabilities of a topologically critical system, hosting semi-Dirac fermions, to strong generic short-range interactions. The ensuing criticality is found to be distinct from that of conventional Dirac fermions, owing in part to the enhanced density of states. What's more, the anisotropy in the fermionic sector induces anisotropy in the order parameter correlations.

Chapter 6 concludes the Thesis and suggests possibilities for further work.

Chapter 2

The Honeycomb Lattice and the Semimetal-Insulator Transition

In the absence of interactions the two dimensional honeycomb lattice is in a semimetallic state. At half-filling the low-energy physics is well described by massless Dirac fermionic quasiparticles. At zero temperature, strong short-range interactions drive continuous quantum semimetal-insulator phase transitions. Broken symmetries, such as the sublattice inversion, cause electronic insulating states in which the Dirac fermions are massive. Even at the mean-field level it is clear that the gapless Dirac fermions are pivotal in determining the critical behaviour.

2.1 Introduction

Single two-dimensional layers of carbon atoms arranged on a honeycomb lattice, known as graphene, were successfully synthesised in 2004 [59]. Since then a number of amazing properties, such as its flexibility and strength, have been discovered, but here the focus is on the electronic properties. The have opened and inspired new frontiers in condensed matter physics including topological insulators [36], Dirac and Weyl topological semimetals [43], and the search for further two-dimensional materials [60]. The remarkable electronic properties [15, 61] of undoped graphene, and more generally the honeycomb lattice, occur at the Fermi energy. In this region the dispersion is conical, and vanishes linearly to a point right at the Fermi energy, making graphene a semimetal. At this half-filling value, the low-energy physics

is well described by emergent massless quasirelativistic Dirac fermionic quasiparticles [16, 17]. The linear dispersion with a corresponding vanishing density of states is distinct from a standard metal, with a typical quadratic dispersion and finite density of states. From the perspective of strongly correlated physics this suggests interesting quantum critical properties [19]. Furthermore, there is promising and rapid progress in capturing this Dirac physics with cold atomic optical lattices [62] and artificial graphene [63].

In this Chapter introductory remarks are provided on the honeycomb lattice. Section 2.2 introduces the non-interacting lattice Hamiltonian and tight-binding dispersion. It is then demonstrated that the low-energy physics of fermions hopping on the lattice are well described by Dirac fermions, and characterised by an isotropic linear dispersion in the vicinity of the Dirac points. Section 2.3 discusses the semimetal-sublattice charge density wave insulator transition driven by strong nearest neighbour repulsion V_1. Mean-field theory is used to obtain the effective Landau free energy. An equivalent formulation is presented using the path integral saddle point expansion. Section 2.4 concludes this Chapter. The key message is that even at the mean-field level, the universality is not of the standard Ginzburg-Landau-Wilson mean-field variety, and the gapless Dirac fermions play a crucial role.

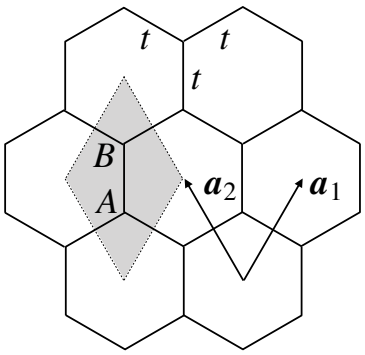

Figure 2.1: The two-dimensional honeycomb lattice is a bipartite (A, B) triangular lattice, with primitive lattice vectors $\boldsymbol{a}_{1,2}$. The primitive unit cell (grey area) contains a single A and B site. The fermionic hopping t is between nearest neighbour sites.

2.2 Non-Interacting Fermions on the Honeycomb Lattice

The two-dimensional honeycomb lattice with $2L$ lattice sites is bipartite with L two site unit cells on a triangular lattice, and is show in Fig. 2.1. The sites are labelled by A and B. The primitive lattice vectors are $\boldsymbol{a}_1 = \frac{\sqrt{3}a}{2}(1, \sqrt{3})$, $\boldsymbol{a}_2 = \frac{\sqrt{3}a}{2}(-1, \sqrt{3})$, and $a(1, 0)$ connects A and B sites with the lattice constant a. The symmetry of the honeycomb lattice belongs to the crystallographic point group C_{6v}, which contains sixfold rotational symmetry and mirror symmetries in the x and y planes. Throughout this Thesis units where $a = 1$, Planck's constant $\hbar = 1$ and Boltzmann's constant $k_B = 1$ are used.

The simplest non-interacting tight-binding Hamiltonian is described by the hopping between nearest neighbour sites

$$H_t = -t \sum_{\langle i,j \rangle} (c_i^\dagger c_j + \text{h.c.}), \tag{2.1}$$

where $t > 0$ is the hopping amplitude, c_i denotes the fermion annihilation operator on site i, likewise $c_i^\dagger$ denotes the creation operator, and h.c. stands for Hermitian conjugate. For simplicity spinless fermions are considered. The fermion operators have the following anticommutation relations $\{c_i, c_j^\dagger\} = \delta_{ij}$, $\{c_i, c_j\} = 0$, $\{c_i^\dagger, c_j^\dagger\} = 0$. To obtain the spectrum of H_t it is convenient to use the Fourier transform to momentum space $\boldsymbol{k} = (k_x, k_y)$,

$$c_{\boldsymbol{r}\sigma} = \frac{1}{\sqrt{L}} \sum_{\boldsymbol{k}}^{\text{BZ}} e^{i\boldsymbol{k}\cdot\boldsymbol{r}} c_{\boldsymbol{k}\sigma}, \tag{2.2}$$

as the eigenstates are Block waves. Here $\boldsymbol{r} = (x, y)$ is the spatial position, and the pseudospin index $\sigma = A, B = \pm$. The sum is over all momentum modes within the first hexagonal Brillouin zone (BZ), which is defined by the reciprocal lattice vectors

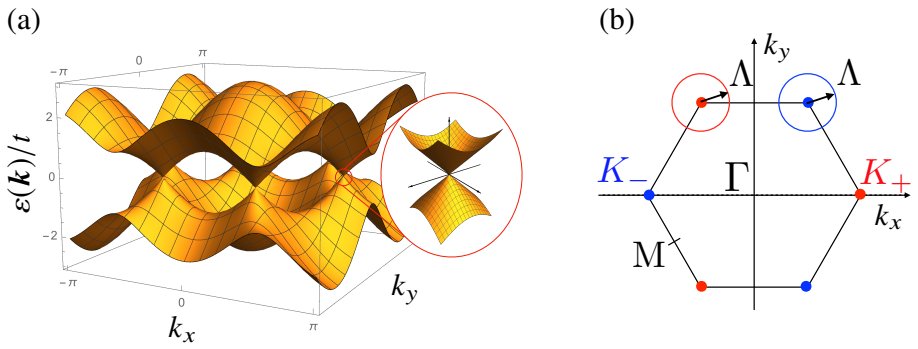

Figure 2.2: (a) The tight-binding dispersion. The key feature is the conical dispersion at half-filling located at the corners of the Brillouin zone. At these Dirac points the low-energy physics is well described by Dirac fermions. (b) The hexagonal Brillouin Zone. There are two distinct Dirac valleys $\boldsymbol{K}_\pm$ at opposite momenta. The effective theory is defined up to the ultraviolet cutoff Λ.

$\boldsymbol{b}_1 = \frac{2\pi}{3a}(\sqrt{3}, 1)$, $\boldsymbol{b}_2 = \frac{2\pi}{3a}(-\sqrt{3}, 1)$. Then (up to an inessential phase factor)

$$H_t = -t \sum_{\boldsymbol{k}}^{\mathrm{BZ}} \begin{pmatrix} c^\dagger_{\boldsymbol{k}A} \\ c^\dagger_{\boldsymbol{k}B} \end{pmatrix}^T \begin{pmatrix} 0 & 1 + e^{-i\boldsymbol{k}\cdot\boldsymbol{a}_1} + e^{i\boldsymbol{k}\cdot\boldsymbol{a}_2} \\ 1 + e^{i\boldsymbol{k}\cdot\boldsymbol{a}_1} + e^{-i\boldsymbol{k}\cdot\boldsymbol{a}_2} & 0 \end{pmatrix} \begin{pmatrix} c_{\boldsymbol{k}A} \\ c_{\boldsymbol{k}B} \end{pmatrix}, \tag{2.3}$$

where T is the transpose, and the Dirac delta function $\delta(\boldsymbol{k}_1 - \boldsymbol{k}_2) = L^{-1} \sum_{\boldsymbol{r}} e^{i(\boldsymbol{k}_1 - \boldsymbol{k}_2)\cdot\boldsymbol{r}}$ has been used. The eigenvalues provide the electronic dispersion

$$\varepsilon(\boldsymbol{k}) = \pm t \sqrt{3 + 4\cos\left(\frac{3}{2}k_x\right)\cos\left(\frac{\sqrt{3}}{2}k_y\right) + 2\cos\left(\sqrt{3}k_y\right)}, \tag{2.4}$$

and from this it can be concluded that the non-interacting honeycomb lattice is neither a metal, nor an insulator. Instead it is a semimetal with a vanishing density of states at half-filling $D(\varepsilon) \propto |\varepsilon|$. The dispersion is displayed in Fig. 2.2(a). It is worth noting that additional hoppings between extended neighbours does not qualitatively change the low-energy physics at half-filling [15].

2.2.1 Massless Dirac Fermions on the Honeycomb Lattice

The feature of the dispersion that is central to this Thesis is located at the corners of the hexagonal Brillouin zone. At these Dirac points (although arguably Weyl points, the convention in the "graphene" literature [15] is followed in this Thesis) the

dispersion vanishes linearly about the half-filling value $\varepsilon = 0$. Remarkably the low-energy, long wavelength physics is well described by massless Dirac fermions [16, 17]. This is evident from expanding around the two inequivalent Dirac points $\boldsymbol{K}_\tau = \frac{4\pi}{3\sqrt{3}}(\tau, 0)$ $(\tau = \pm)$, shown in Fig. 2.2(b). By doing so the Dirac Hamiltonian is obtained

$$\mathcal{H}_t = v_F \int^{\Lambda} \frac{d^2\boldsymbol{k}}{(2\pi a)^2} \Psi^\dagger(\boldsymbol{k})\, \boldsymbol{k} \cdot \boldsymbol{\alpha}\, \Psi(\boldsymbol{k}), \tag{2.5}$$

where $v_F = 3ta/2$ is the Fermi velocity, and the low-energy theory is defined up to the ultraviolet cut-off $\Lambda \sim 1/a$. $\Lambda \geq |\boldsymbol{k}|$ defines the momentum integration regime up to which $\varepsilon(\boldsymbol{k}) = \pm v_F\, |\boldsymbol{k}|$ is a good approximation to the lattice dispersion. For compactness, the 4-component spinor $\Psi = (\psi_{A+}, \psi_{A-}, \psi_{B+}, \psi_{B-})$ and tensor products $\alpha_x = \sigma_x \otimes \tau_z$, $\alpha_y = \sigma_y \otimes \tau_0$, are introduced. Here σ_μ, τ_μ $(\mu = 0, x, y, z)$ are the 4-vectors of identity and Pauli matrices acting respectively on the sublattice $\sigma = A, B$ and valley $\tau = \pm$ pseudospins.

2.3 The Sublattice Charge Density Wave Instability

At zero temperature, strong repulsive interactions drive continuous quantum semimetal-insulator phase transitions [19, 64], see Fig. 2.3. Here the instability to sublattice charge density wave (CDW) order driven by strong nearest neighbour repulsion V_1 is considered in a mean-field treatment of the low-energy model.

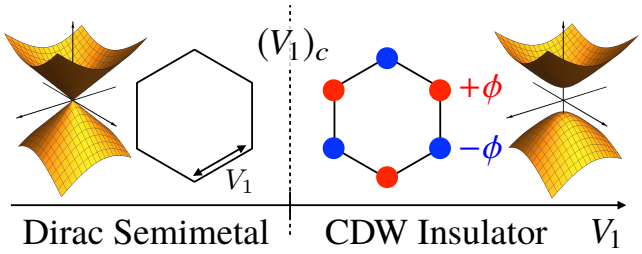

Figure 2.3: Zero temperature phase diagram as a function of the nearest neighbour interaction V_1 on the honeycomb lattice. At $(V_1)_c$ the system undergoes a continuous transition from the Dirac semimetal into the sublattice charge density wave (CDW) insulator phase. The charge modulation is shown relative to the half-filling value.

The lattice Hamiltonian is

$$H = -t \sum_{\langle i,j \rangle} (c_i^\dagger c_j + \text{h.c.}) + V_1 \sum_{\langle i,j \rangle} \hat{n}_i \hat{n}_j, \tag{2.6}$$

where $\hat{n}_i = c_i^\dagger c_i$ denotes the density operator. From consideration of the classical limit $t \longrightarrow 0$, it is clear that there is an energy cost V_1 for nearest neighbour A and B sites to be occupied. Therefore at half-filling in the large V_1 limit, it is energetically favourable for only a single sublattice (either A or B) to be occupied. This phase is the sublattice, or inversion, symmetry breaking charge density wave (CDW), shown in Fig. 2.3.

2.3.1 Mean-Field Theory of the Charge Density Wave Transition

The phase transition into the CDW state may be analysed with a mean-field approximation to the many body interaction Eq. (2.6). This proceeds in the charge channel by re-expressing the fermion bilinear $\hat{n}$ in terms of the sum of the expectation value $\langle \hat{n} \rangle$ and the fluctuations around this $\delta \hat{n}$. Then the mean-field decoupled interaction is

$$\begin{aligned} \hat{n}_i \hat{n}_j &= (\langle \hat{n}_i \rangle + \delta \hat{n}_i)(\langle \hat{n}_j \rangle + \delta \hat{n}_j), \\ &\approx \langle \hat{n}_i \rangle \langle \hat{n}_j \rangle + \langle \hat{n}_i \rangle \delta \hat{n}_j + \langle \hat{n}_j \rangle \delta \hat{n}_i, \\ &\approx \langle \hat{n}_i \rangle \hat{n}_j + \langle \hat{n}_j \rangle \hat{n}_i - \langle \hat{n}_i \rangle \langle \hat{n}_j \rangle. \end{aligned} \tag{2.7}$$

The mean-field approximation has been applied in the second line, and amounts to neglecting second order terms in the fluctuations $\delta \hat{n}_i \delta \hat{n}_j$. The substitution $\delta \hat{n}_i = \hat{n}_i - \langle \hat{n}_i \rangle$ has been used in the third line. Naturally, the mean-field approximation fails if the quadratic fluctuation term is not negligible, which is typically the case in the regime of a quantum critical point unless the number of spatial dimensions is large. Nevertheless, the mean-field approximation is an instructive first step in analysing criticality and identifying broken symmetry states. Finally, it is worth noting that an unbiased decoupling of interacting spinless fermions would include the bond order

channel $c_i^\dagger c_j$

$$\hat{n}_i\hat{n}_j \approx \langle\hat{n}_i\rangle\hat{n}_j + \langle\hat{n}_j\rangle\hat{n}_i - \langle\hat{n}_i\rangle\langle\hat{n}_j\rangle - \langle c_i^\dagger c_j\rangle c_j^\dagger c_i - \langle c_j^\dagger c_i\rangle c_i^\dagger c_j + \langle c_i^\dagger c_j\rangle\langle c_j^\dagger c_i\rangle, \quad (2.8)$$

but for now this is neglected.

For the nearest neighbour interaction

$$H_{V_1} = V_1 \sum_{\langle ij\rangle} \hat{n}_i\hat{n}_j = V_1 \sum_{\boldsymbol{r}} \left(\hat{n}_{\boldsymbol{r}A} + \hat{n}_{\boldsymbol{r}+\boldsymbol{a}_1 A} + \hat{n}_{\boldsymbol{r}+\boldsymbol{a}_2 A}\right) \hat{n}_{\boldsymbol{r}B}, \quad (2.9)$$

where $\sum_{\boldsymbol{r}}$ represents the sum over all unit cells (or lattice sites of the triangular lattice). Under the assumption that the charge order is spatially uniform $\langle\hat{n}_{\boldsymbol{r}\sigma}\rangle = \langle\hat{n}_\sigma\rangle$

$$H_{V_1} \approx \sum_{\boldsymbol{r}} \langle\hat{n}_A\rangle\hat{n}_{\boldsymbol{r}B} + \langle\hat{n}_B\rangle\hat{n}_{\boldsymbol{r}A} - 3V_1\langle\hat{n}_A\rangle\langle\hat{n}_B\rangle. \quad (2.10)$$

Following the argument in the classical limit, the CDW *ansatz* $\langle\hat{n}_A\rangle = \rho_0 - \phi$, $\langle\hat{n}_B\rangle = \rho_0 + \phi$ is made. Here ϕ is the CDW order parameter describing the charge imbalance between the A and B sublattices, and ρ_0 is the average charge occupation, which for the half-filled lattice is fixed to $\rho_0 = 1/2$. In the following ρ_0 is neglected, as it only acts to linearly shift the free energy. Expanding around the Dirac points, the low-energy mean-field CDW Hamiltonian is obtained

$$\mathcal{H}_{\mathrm{CDW}} = 3V_1\phi^2 + \int^\Lambda \frac{d^2\boldsymbol{k}}{(2\pi)^2}\, \Psi^\dagger(\boldsymbol{k})\left(v_F\boldsymbol{k}\cdot\boldsymbol{\alpha} + 3V_1\phi\sigma_z\otimes\tau_0\right)\Psi(\boldsymbol{k}). \quad (2.11)$$

The anticommutation $\{\boldsymbol{k}\cdot\boldsymbol{\alpha}, \phi\sigma_z\otimes\tau_0\} = 0$ indicates that ϕ couples to the Dirac fermions like a mass, and opens an insulating band gap, which can be seen from the low-energy dispersion ($\nu = \pm$)

$$\varepsilon_\nu(\boldsymbol{k}) = \nu\sqrt{v_F^2\,|\boldsymbol{k}|^2 + (3V_1\phi)^2}. \quad (2.12)$$

The excitations in the CDW ordered state are therefore described by massive Dirac fermions.

To analyse the broken symmetry state, the free energy is calculated and min-

imised. The zero temperature free energy density is obtained by integrating over the occupied fermionic spectrum

$$f = 3V_1\phi^2 + \sum_{\tau=\pm}\sum_{\nu=\pm}\int^{\Lambda}\frac{d^2\boldsymbol{k}}{(2\pi)^2}\,\varepsilon_\nu(\boldsymbol{k})\theta(\mu-\varepsilon_\nu(\boldsymbol{k})). \tag{2.13}$$

Here the sum τ is over the two Dirac points, θ is the Heaviside step function and μ is the chemical potential. This standard form of the free energy will be derived using a path integral approach in the next section.

2.3.2 Path Integral Approach to Mean-Field Theory

Here the mean-field free energy is obtained by means of the coherent state path integral representation of the fermionic partition function

$$Z = \int D[\Psi^\dagger,\Psi]e^{-\mathcal{S}_0-\mathcal{S}_{V_1}}. \tag{2.14}$$

A detailed discussion of many-body path integration can be found by following chapters 3, 4 and 6 of the textbook by Altland and Simons [65].

The starting point here is the effective field theory of Dirac fermions The non-interacting local action of free Dirac fermions, in imaginary time τ, is

$$\mathcal{S}_0 = \int_0^\beta d\tau\int_{\boldsymbol{r}}\Psi^\dagger(\tau,\boldsymbol{r})(\partial_\tau\alpha_0 + iv_F\alpha_x\partial_x + iv_F\alpha_y\partial_y)\Psi(\tau,\boldsymbol{r}), \tag{2.15}$$

where $\alpha_0 = \sigma_0\otimes\tau_0$ is the identity and $\beta = 1/T$ is the inverse temperature. Here

$$\Psi(\tau,\boldsymbol{r}) = T\sum_n\int^{\Lambda}\frac{d^2\boldsymbol{k}}{(2\pi a)^2}\,e^{-i\omega_n\tau - i\boldsymbol{k}\cdot\boldsymbol{r}}\Psi(\omega_n,\boldsymbol{k}), \tag{2.16}$$

where $\omega_n = (2n+1)\pi T$ is the fermionic Matsubara frequency. In addition there is the local interacting action

$$\mathcal{S}_{V_1} = 4V_1\int_0^\beta d\tau\int_{\boldsymbol{r}}(\Psi_A^\dagger\tau_0\Psi_A)(\Psi_B^\dagger\tau_0\Psi_B), \tag{2.17}$$

where $\Psi_\sigma = (\psi_{\sigma+},\psi_{\sigma-})$.

In general, only the path integrals of Gaussian (quadratic) actions are known

$$\int D[\psi^\dagger, \psi] e^{-\sum_{ij} \psi_i^\dagger A_{ij} \psi_j} = [\det(A)]^{-\zeta}, \tag{2.18}$$

where $\zeta = 1$ for bosonic ψ and $\zeta = -1$ for fermionic (Grassmann) ψ. One procedure to deal with the quartic interaction terms is the Hubbard-Stratonovich transformation [66, 67], which is essentially the generalisation of the mean-field decoupling. This transformation is effectively the field theoretic analogue of completing the square, but in reverse, for the exponent of the Gaussian integral

$$\exp\left(-x^2\right) = (4\pi)^{-\frac{1}{2}} \int dy \, \exp\left(-y^2 - 2ixy\right), \tag{2.19}$$

$$\text{or } \exp\left(x^2\right) = (4\pi)^{-\frac{1}{2}} \int dy \, \exp\left(-y^2 - 2xy\right). \tag{2.20}$$

The idea is to decouple the interaction x^2 (where $x \sim \psi^\dagger \psi$ is bilinear in the fields of interest) at the expense of introducing the auxiliary y. It is now possible to perform Gaussian integrals over the initial fields, which now enter at quadratic order.

The sublattice CDW has a finite expectation value $\langle \Psi^\dagger \sigma_z \otimes \tau_0 \Psi \rangle$. This motivates rewriting the interaction using the decomposition

$$4(\Psi_A^\dagger \tau_0 \Psi_A)(\Psi_B^\dagger \tau_0 \Psi_B) = (\Psi^\dagger \alpha_0 \Psi)^2 - (\Psi^\dagger \sigma_z \otimes \tau_0 \Psi)^2. \tag{2.21}$$

The first term is the uniform density and will be neglected. The transformation introduces the real auxiliary field $\hat{\phi}(\tau, \boldsymbol{r})$ conjugate to $\Psi^\dagger \sigma_z \otimes \tau_0 \Psi$,

$$e^{\int V_1 (\Psi^\dagger \sigma_z \otimes \tau_0 \Psi)^2} = \int D[\hat{\phi}] e^{-\int \left(V_1 \hat{\phi}^2 + 2 V_1 \hat{\phi} \Psi^\dagger \sigma_z \otimes \tau_0 \Psi\right)}. \tag{2.22}$$

Consequently the action is Gaussian in the fermions. Integrating out the fermions and using the identity $\mathrm{tr} \ln \hat{A} = \ln \det \hat{A}$ (obvious in the eigenbasis of $\hat{A}$), the partition function is

$$Z = \int D[\hat{\phi}] e^{\mathrm{tr} \ln(\hat{\partial}_\tau + i v_F \hat{\partial}_x + i v_F \hat{\partial}_y + V_1 \hat{\phi}) - V_1 \int \hat{\phi}^2}. \tag{2.23}$$

This result is exact, but to proceed an approximation must be made. The standard

procedure is to expand around the saddle point defined by $\delta\mathcal{S}[\hat{\phi}]/\delta\hat{\phi} = 0$, where the zeroth order expansion reduces to the mean-field result, as will now be demonstrated. As is generally the case, the action is extremised for the constant uniform field $\hat{\phi}(\tau, \boldsymbol{r}) = \phi$, and produces the mean-field self consistent solution

$$\begin{aligned}
\frac{\delta\mathcal{S}[\phi]}{\delta\phi} &= \frac{\delta}{\delta\phi}\left[\mathrm{tr}\ln(\hat{\partial}_\tau + iv_F\hat{\partial}_x + iv_F\hat{\partial}_y + V_1\phi) + V_1\phi^2\right], \\
\Rightarrow V_1\phi &= 2\sum_n \int \frac{d^2\boldsymbol{k}}{(2\pi)^2}\frac{V_1\phi}{\omega_n^2 + v_F^2\,|\boldsymbol{k}|^2 + (V_1\phi)^2}, \\
&= \sum_{\nu=\pm}\int \frac{d^2\boldsymbol{k}}{(2\pi)^2}\frac{V_1\phi n_F(\varepsilon_\nu(\boldsymbol{k}))}{|\varepsilon_\nu(\boldsymbol{k})|}.
\end{aligned} \tag{2.24}$$

In the zero temperature limit this reduces to the same result that would be obtained from the mean-field free energy Eq. (2.13).

With the saddle point solution, the mean-field free energy can be obtained directly from $f = -T\ln Z$,

$$\begin{aligned}
f &= V_1\phi^2 - T\sum_n \int \frac{d^2\boldsymbol{k}}{(2\pi)^2}\ln\det[\beta(-i\hat{\omega}_n + v_F\hat{\boldsymbol{k}}\cdot\boldsymbol{\alpha} + V_1\phi\sigma_z\otimes\tau_0)], \\
&= V_1\phi^2 - T\sum_{\tau=\pm}\sum_{\nu=\pm}\int \frac{d^2\boldsymbol{k}}{(2\pi)^2}\ln\left(1 + e^{-\beta\varepsilon_\nu(\boldsymbol{k})}\right).
\end{aligned} \tag{2.25}$$

As claimed, in the zero temperature limit this reduces to Eq. (2.13). The final result has been obtained following standard procedures. First it can be verified that $\det(-i\hat{\omega}_n + \hat{H}) = \prod_a(-i\hat{\omega}_n + \hat{\varepsilon}_a)$ by diagonalising $\hat{H}$ to obtain the matrix of energy eigenvalues $\hat{\varepsilon}_a$ (with the correct unitary transformation). Then the properties of the logarithm allows for $\log[\prod_a(-i\hat{\omega}_n + \hat{\varepsilon}_a)] = \sum_a \log(-i\hat{\omega}_n + \hat{\varepsilon}_a)$. Finally the Matsubara sum is evaluated using complex integration involving an auxiliary function with poles at $z = i\omega_n$. This is a standard result whose lengthy step-by-step calculation can be found in Chapter 4 of [65].

2.3.3 Analysis of the Effective Free Energy

At half-filling ($\mu = 0$) and zero temperature, only the negative energies ε_- are integrated over in Eq. (2.13). Therefore

$$\begin{aligned} f &= 3V_1\phi^2 - 2\int^{\Lambda} \frac{d^2\boldsymbol{k}}{(2\pi)^2}\sqrt{v_F^2\,|\boldsymbol{k}|^2 + (3V_1\phi)^2}, \\ &= 3V_1\phi^2 - \frac{\left[(v_F k)^2 + (3V_1\phi)^2\right]^{\frac{3}{2}}}{3\pi v_F^2}\Bigg|_0^{\Lambda}, \\ &= 3V_1\phi^2 + \frac{9V_1^3\,|\phi|^3}{\pi v_F^2} - \frac{\left[(v_F\Lambda)^2 + (3V_1\phi)^2\right]^{\frac{3}{2}}}{3\pi v_F^2}. \end{aligned} \tag{2.26}$$

It is crucial to recognise that the non-analytic cubic term $|\phi|^3$ has been generated from the gapless nature of the Dirac fermions in the infrared limit $\boldsymbol{k} \to 0$, and the vanishing density of states [1]. This is unusual, and would not appear in the standard symmetry based Landau expansion of the free energy, which assumes that the free energy is an *analytic* function of the order parameter.

From the expansion in the critical region $v_F\Lambda \gg V_1\phi$, the bounded Landau free energy is

$$f = \frac{a}{2}\phi^2 + \frac{b}{3}\,|\phi|^3 + O(\phi^4), \tag{2.27}$$

with

$$a = 6V_1\left(1 - \frac{3V_1\Lambda}{2\pi v_F}\right) \text{ and } b = \frac{27V_1^3}{\pi v_F^2}. \tag{2.28}$$

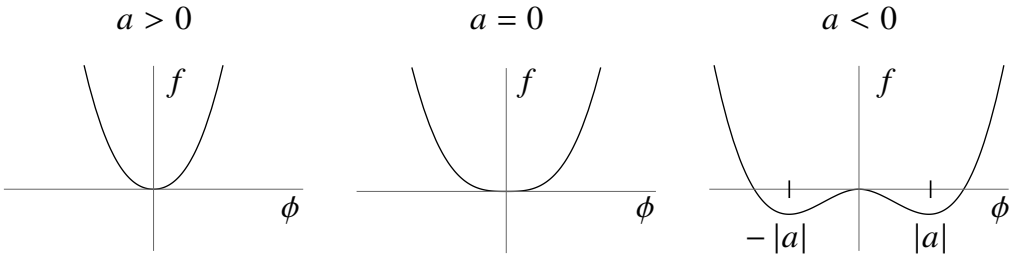

Figure 2.4: A sketch of the Landau free energy $f = \frac{a}{2}\phi^2 + \frac{1}{3}\,|\phi|^3$ for: $a > 0$, where the system is in the high symmetry state with the minimum $(\phi)_c = 0$; $a = 0$, where the system is critical; $a < 0$ where the system has undergone a continuous transition into the broken symmetry state with minima $\pm(\phi)_c = \mp a$.

The free energy is sketched in Fig. 2.4. The free energy is critical when

$$\left.\frac{\partial^2 f}{\partial \phi^2}\right|_{\phi=0} = 0 \Rightarrow a = 0 \Rightarrow (V_1)_c = \frac{2\pi v_F}{3\Lambda}. \tag{2.29}$$

The minimisation of the free energy determines the properties of the order parameter and it's scaling

$$\frac{\partial f}{\partial \phi} = 0 \Rightarrow (\phi)_c = -\frac{a}{b} \propto V_1 - (V_1)_c \Rightarrow \beta = 1. \tag{2.30}$$

Here the standard definition $(\phi)_c \propto (V_1 - (V_1)_c)^\beta$ has been used to extract the critical exponent $\beta = 1$.

2.4 Discussion

The conclusion is that the mean-field semimetal-insulator transition does not belong to the standard Ginzburg-Landau-Wilson mean-field universality class with $\beta = 1/2$. This would correspond to $f = a\phi^2 + c\phi^4$. Instead it suggests that the universality is beyond the Ginzburg-Landau-Wilson order-parameter paradigm, and that the gapless fermions play an important role. In fact, this result can be thought of as the "mean-field" of the Gross-Neveu-Yukawa universality class, which is perhaps the best understood example of fermionic quantum criticality. This will be discussed in detail in Chapter 4.

Chapter 3

The Fate of the Topological Mott Insulator

The topological chiral nature of the Dirac fermions in a semimetal allows for topologically non-trivial insulating states. Remarkably, extended repulsive interactions on the honeycomb lattice can dynamically induce such quantum Hall states, dubbed topological Mott insulators. However these phases turn out to be in competition with novel charge order. Naturally, quantum fluctuations would play a crucial role in determining the exotic phase behaviour. In this Chapter the impact of collective Gaussian quantum fluctuations are self-consistently examined using a path integral approach. The results are convincingly consistent with the general consensus of numerical lattice calculations: charge order is favoured over the topological Mott insulator. In the vicinity of the quantum critical point, the low-energy excitations of the charge ordered state are found to be massless semi-Dirac quasiparticles. The original work in this Chapter was published in *Hidden Charge Order of Interacting Dirac Fermions on the Honeycomb Lattice*, E. Christou, B. Uchoa, F. Krüger, Physical Review B, **98**, 161120 (Rapid Communications) (2018) [68]

3.1 Introduction

The extended, half-filled Hubbard model on the honeycomb lattice exhibits a rich phase diagram, even at mean-field level [57, 69, 70]. The low-energy Dirac excitations [61] couple to the order-parameter fluctuations, and are known to change

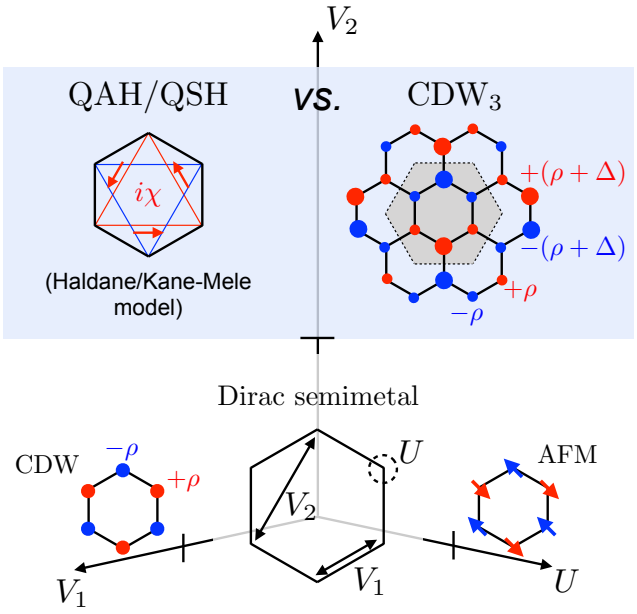

Figure 3.1: Schematic phase diagram of the half-filled Hubbard model on the honeycomb lattice. The on-site and nearest neighbour repulsions U and V_1 induce antiferromagnetic (AFM) and charge-density wave (CDW) states, respectively. At large next-nearest neighbour interactions V_2, there is phase competition between a topological Mott insulator and charge-ordered states with enlarged unit cell (CDW$_3$). The charge modulation is shown relative to half filling.

the universal critical behaviour to that of the Gross-Neveu-Yukawa (GNY) [21, 22] variety. For the transitions from the Dirac semimetal to the antiferromagnetic Mott insulator (see Fig. 3.1), driven by the on-site Hubbard repulsion (U), and to the sublattice charge density wave (CDW) Mott insulator, driven by nearest neighbour repulsion (V_1), this has been well understood through a combination of the renormalisation group studies of the low-energy theories [19, 20, 71, 72], and sign-free quantum Monte Carlo simulations on the lattice [26, 64, 73–77].

Remarkably, topological phases appear to be favourable for strong next-nearest neighbour interactions V_2 [57], which can stabilise Haldane's quantum anomalous Hall state in the spinless model [37], as well as the Kane-Mele quantum spin Hall phase in the spinful case [38, 39]. Those topological Mott insulating states nevertheless compete with unconventional CDW$_3$ charge order, see Fig. 3.1, that extends beyond the honeycomb unit cell [70]. Note that in the literature this phase is sometimes referred to as the sublattice charge modulated (CMs) phase. Due to this competition, it is natural to expect that quantum fluctuations will play a crucial role

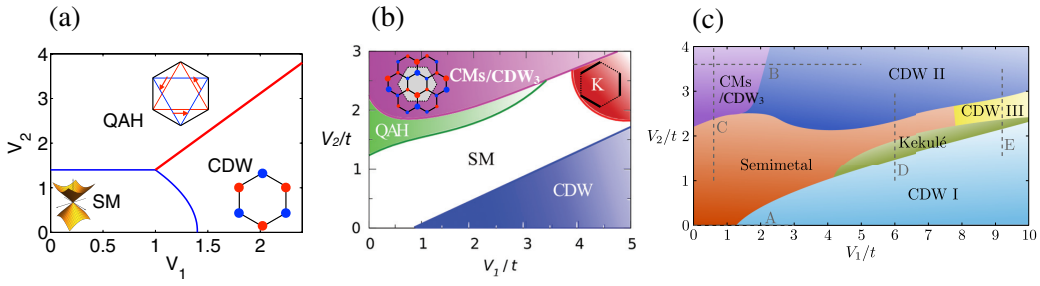

Figure 3.2: The evolution of the phase diagram of spinless fermions on the honeycomb lattice interacting with nearest neighbour V_1 and next-nearest neighbour V_2 repulsions. Phases include: Dirac semimetal (SM), sublattice charge density wave insulator (CDW/CDW I), Haldane's quantum anomalous Hall insulator (QAH), translational and rotational symmetry breaking charge order (CDW$_3$/CMs), bond ordered Kekulé valence bond solid insulator (K). The phase diagrams are for: (a) Mean-field theory in the standard $A-B$ sublattice basis, adapted from Raghu *et al.* [57]. (b) Unbiased numerical mean-field theory on the enlarged unit cell, indicating competing CDW$_3$ order, adapted from Grushin *et al.* [70]. (c) Infinite density matrix renormalisation group, as a representative for beyond mean-field numerical simulations, adapted from Motruk *et al.* [83]. The key point is the absence of the QAH phase. Note that the phases marked CDW II and CDW III break additional translational symmetries, but are not discussed here.

in determining the fate of the topological phases. In particular, there are additional soft fluctuations associated with the breaking of continuous spin rotational symmetry in the QSH phase. Unfortunately, the sign problem for large V_2 prevents the use of quantum Monte Carlo methods [78]. Extensive numerical research into spinless [79–84] and spinful [85–88] models using exact diagonalisation, variational Monte Carlo, infinite density matrix renormalisation group, and functional renormalisation group have been pivotal to determine the phase behaviour. Fig. 3.2 illustrates the evolution of the numerical phase diagram for the spinless case. Mean-field and some early numerical simulations supported the existence of the topological phases, but simulations with increased resolution supported the charge order. Further details are covered in the recent review article on this subject [89].

In this chapter the role of beyond mean-field collective quantum fluctuations for the phase competition along the V_2 axis is analytically examined. As a preliminary discussion, Section 3.2 introduces Haldane's model of quantum anomalous Hall insulators. The original work begins in Section 3.3 (topological Mott insulator)

and Section 3.4 (CDW_3 charge order), where the effective low-energy description of the broken symmetry states is derived, and analysed at the mean-field level. In Section 3.5 the leading instabilities are analysed in the presence of long-wavelength order parameter fluctuation fields via a path integral approach. The analytic results presented in Section 3.6 are convincingly consistent with the general consensus of numerical lattice calculations, which suggest that CDW_3 order is favoured over topological Mott insulating phases. The low-energy excitations of this CDW_3 ground-state are massless semi-Dirac quasiparticles [45, 47], which disperse linearly in one direction and parabolically in the other.

This chapter ends with a discussion in Section 3.7. It is concluded that the onset of CDW_3 order does not produce a many-body Mott gap, but rather a novel "hidden" metallic order. Naturally, this suggests the transition is not of the typical Gross-Neveu-Yukawa variety, and motivates a study of the quantum critical point, which appears in Chapter 4 of this Thesis.

3.2 Haldane's Model: Quantum Hall Effect Without Landau Levels

In a strong magnetic field, the two dimensional electron gas exhibits the integer quantum Hall effect [34]. A strong magnetic field induces Landau level quantisation into macroscopically degenerate electronic energy levels with $\varepsilon_n = (n+1/2)\hbar eB/mc$. Naively the Hall conductivity $\sigma_{\mathrm{H}} = Ce^2/h$ is found to depend on the number C of filled Landau levels. However this quantisation persists against perturbations such as disorder. It was realised by Thouless *et al.*[35] that this quantisation can be explained by a topological property of the electronic wavefunction. More so, that quantum Hall states are characterised by a topological invariant as opposed to the spontaneous symmetry breaking of a local order parameter. This topological invariant is known as the TKNN integer, or more generally the Chern invariant. Following this, Haldane [37] realised that the integer quantum Hall state could exist without Landau level quantisation. Rather the system had to break time reversal symmetry. Remarkably, Haldane's idea has been experimentally verified

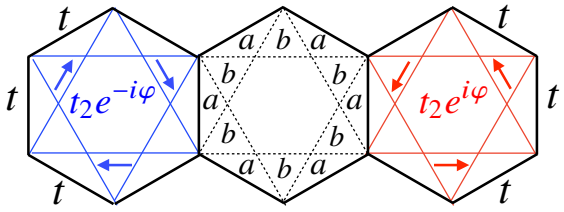

Figure 3.3: Haldane's model with a staggered a, b flux pattern that is used to break time reversal symmetry. The flux pattern is constructed such that there is no net flux through the honeycomb plaquette. Fermions hopping between next-nearest neighbours t_2 gain a Berry phase φ from anticlockwise hops around the plaquette, and $-\varphi$ from clockwise hops. Where as for nearest neighbour hopping t there is no additional phase, as there is no net flux through the plaquette.

with ultracold fermions on an optical honeycomb lattice [90].

Haldane proposed a model of non-interacting spinless fermions on the half-filled honeycomb lattice, in the presence of a staggered magnetic field. The field was constructed with zero net flux per plaquette, as is shown in Fig. 3.3, and this implies a periodic magnetic vector potential. Due to the field a fermion would gain an additional Berry phase [91] $\exp(\pm i\varphi)$ upon hopping to a next-nearest neighbour. The sign of the phase is dependent on whether the fermion made a left or right turn. This is related to the Aharanov-Bohm effect [92], where an electron state gains an additional relative phase $\frac{e}{\hbar}\oint d\boldsymbol{r}\cdot\boldsymbol{A}$ on orbiting a solenoid with associated magnetic vector potential $\boldsymbol{A}$. In the case of Fig. 3.3, the additional phase factor for a next-nearest neighbour hop is $\varphi = 2\pi(2\Phi_a + \Phi_b)/\Phi_0$, where $\Phi_{a,b}$ are the fluxes through the unit cell and $\Phi_0 = h/e$ is the magnetic flux quantum.

3.2.1 The Haldane Model

This phenomena is encapsulated by the Haldane model

$$H_{\mathrm{H}} = -t\sum_{\langle ij\rangle}\left(c_i^\dagger c_j + \mathrm{h.c.}\right) - \sum_{\langle\langle ij\rangle\rangle}\left(t_2 e^{i\varphi_{ij}} c_i^\dagger c_j + \mathrm{h.c.}\right), \tag{3.1}$$

with *complex* chiral next-nearest neighbour hoppings $t_2 e^{i\varphi_{ij}}$. Here $\varphi_{ij} = \varphi$ if the hopping is in the anti-clockwise direction around a plaquette, and $\varphi_{ij} = -\varphi$ if it is clockwise. It is evident that the complex hopping breaks time reversal symmetry

(for $\varphi \neq n\pi$ with integer n): a fermion hopping in the clockwise direction is no longer equivalent to a fermion hopping in the anticlockwise direction (or a fermion hopping backwards in time).

Here the case of $\varphi = \pi/2$ is discussed. Deviation from this introduces a real part to the hopping that breaks the particle-hole symmetry, but does not change the conclusions. In the momentum representation

$$H_{\mathrm{H}} = -\sum_{\boldsymbol{k}}^{\mathrm{BZ}} \begin{pmatrix} c^{\dagger}_{\boldsymbol{k}A} \\ c^{\dagger}_{\boldsymbol{k}B} \end{pmatrix}^{T} \begin{pmatrix} t_2 s(\boldsymbol{k}) & t(1+e^{-i\boldsymbol{k}\cdot\boldsymbol{a}_1}+e^{i\boldsymbol{k}\cdot\boldsymbol{a}_2}) \\ t(1+e^{i\boldsymbol{k}\cdot\boldsymbol{a}_1}+e^{-i\boldsymbol{k}\cdot\boldsymbol{a}_2}) & -t_2 s(\boldsymbol{k}) \end{pmatrix} \begin{pmatrix} c_{\boldsymbol{k}A} \\ c_{\boldsymbol{k}B} \end{pmatrix}, \quad (3.2)$$

where $s(\boldsymbol{k}) = 2[\sin \boldsymbol{k}\cdot\boldsymbol{a}_1 - \sin \boldsymbol{k}\cdot\boldsymbol{a}_2 - \sin \boldsymbol{k}\cdot(\boldsymbol{a}_1-\boldsymbol{a}_2)]$. The spectrum is

$$\varepsilon(\boldsymbol{k}) = \pm t\sqrt{3+4\cos\left(\frac{3}{2}k_x\right)\cos\left(\frac{\sqrt{3}}{2}k_y\right)+2\cos\left(\sqrt{3}k_y\right)+\left[\frac{t_2}{t}s(\boldsymbol{k})\right]^2}. \quad (3.3)$$

Similar to the CDW, breaking the time-reversal symmetry with finite t_2 opens a gap in the spectrum at the Dirac points. Although the CDW and Haldane dispersions look similar, the fermionic wavefunction and topological properties are different.

These properties are transparent in the low-energy theory, in which the Haldane term $m_{\mathrm{H}} = 3\sqrt{3}t_2$ also couples like a mass to the Dirac fermions

$$\mathcal{H} = \int^{\Lambda} \frac{d^2\boldsymbol{k}}{(2\pi)^2}\, \Psi^{\dagger}(\boldsymbol{k})\left[v_F \boldsymbol{k}\cdot\boldsymbol{\alpha} + \sigma_z \otimes (m_{\mathrm{CDW}}\tau_0 + m_{\mathrm{H}}\tau_z)\right]\Psi(\boldsymbol{k}). \quad (3.4)$$

The valley (τ) dependence of the mass $m_{\mathrm{H}}\sigma_z \otimes \tau_z$ is a manifestation of the time reversal symmetry breaking, as under time reversal $\boldsymbol{k} \to -\boldsymbol{k}$ implying that the Dirac points are time reversed pairs with $\boldsymbol{K}_+ \to \boldsymbol{K}_-$. More formally, the time reversal operation is the antiunitary operator $\mathcal{T} = \sigma_0 \otimes \tau_x \mathcal{K}$ (along with $\boldsymbol{k} \to -\boldsymbol{k}$), where $\mathcal{K}$ is complex conjugation [93]. Then it is evident that under $\mathcal{T}$

$$m_{\mathrm{H}}\sigma_z \otimes \tau_z \to \mathcal{T}^{-1} m_{\mathrm{H}}\sigma_z \otimes \tau_z \mathcal{T} = -m_{\mathrm{H}}\sigma_z \otimes \tau_z, \quad (3.5)$$

hence time reversal symmetry is broken. In contrast, the CDW term preserves time

reversal symmetry with $m_{\mathrm{CDW}}\sigma_z \otimes \tau_0 \rightarrow m_{\mathrm{CDW}}\sigma_z \otimes \tau_0$. Ultimately, Haldane's state with broken time reversal symmetry is topologically non-trivial, as is shown in the following.

3.2.2 Calculation of the Topological Chern Invariant

It is convenient to analyse the two Dirac points ($\tau = \pm$) separately (temporarily working in units with $v_F = 1$) with Hamiltonian

$$\mathcal{H}_\tau(\boldsymbol{k}) = \tau k_x \sigma_x + k_y \sigma_y + (m_{\mathrm{CDW}} + \tau m_{\mathrm{H}})\sigma_z. \tag{3.6}$$

This can be mapped from $\boldsymbol{k}$ to a three dimensional space $\mathcal{H}_\tau(\boldsymbol{k}) = \boldsymbol{h}_\tau(\boldsymbol{k}) \cdot \boldsymbol{\sigma}$ with the unit vector field [36, 91]

$$\boldsymbol{h}_\tau(\boldsymbol{k}) = \frac{\left(k_x, k_y, m_{\mathrm{CDW}} + \tau m_{\mathrm{H}}\right)}{\sqrt{|\boldsymbol{k}|^2 + m_{\mathrm{CDW}}^2 + m_{\mathrm{H}}^2}}, \tag{3.7}$$

and $\boldsymbol{\sigma} = (\sigma_x, \sigma_y, \sigma_z)$. For a two level system the Berry flux Ω_τ, perpendicular to the two dimensional $\boldsymbol{k}$ surface, is defined as

$$\Omega_\tau(\boldsymbol{k}) = \frac{1}{2}(\partial_{k_x}\boldsymbol{h}_\tau \times \partial_{k_y}\boldsymbol{h}_\tau) \cdot \boldsymbol{h}, \tag{3.8}$$

and is equal to half the solid angle element of the mapping $\boldsymbol{h}_\tau$. Therefore the integral of the total Berry flux $\Omega_+ + \Omega_-$ is an integer multiple of 2π, and this integer is the topological Chern invariant

$$\begin{aligned} C &= \sum_{\tau=\pm} \int^{\Lambda\rightarrow\infty} \frac{d^2\boldsymbol{k}}{2\pi} \Omega_\tau(\boldsymbol{k}), \\ &= \sum_{\tau=\pm} \int^{\Lambda\rightarrow\infty} \frac{d^2\boldsymbol{k}}{4\pi} \frac{\tau\left(m_{\mathrm{CDW}} + \tau m_{\mathrm{H}}\right)}{\left(|\boldsymbol{k}|^2 + m_{\mathrm{CDW}}^2 + m_{\mathrm{H}}^2\right)^{\frac{3}{2}}}, \\ &= \sum_{\tau=\pm} \frac{\tau m_{\mathrm{CDW}} + m_{\mathrm{H}}}{2\sqrt{m_{\mathrm{CDW}}^2 + m_{\mathrm{H}}^2}}. \end{aligned} \tag{3.9}$$

Clearly, each gapped Dirac point contributes half a Chern number, but whether or not this results in a finite Chern number depends on the symmetry that is broken.

The CDW insulator $m_{\mathrm{CDW}} \neq 0$, $m_{\mathrm{H}} = 0$ is topologically trivial with $C = 0$. Where as when $m_{\mathrm{CDW}} = 0$, $m_{\mathrm{H}} \neq 0$ the state is topologically non-trivial with $C = \mathrm{sign}(m_{\mathrm{H}})$. Haldane's quantum Hall state from time-reversal symmetry breaking is known as the Chern insulator.

3.2.3 Topologically Non-Trivial Insulators

The Chern insulator exhibits the quantum anomalous Hall effect: quantised Hall conductance in the absence of a magnetic field. This is analogous to the anomalous Hall effect observe by Hall in ferromagnetic materials with no external magnetic field [94]. The quantised conductance is transported by a single topologically protected gapless chiral edge mode. This can be understood as a consequence of the bulk-boundary correspondence: metallic states must exist at the interface between topologically distinct insulating states. This edge mode can be seen in the spectrum of a tight-binding model solved on a finite strip geometry.

Some time later, Haldane's idea was generalised to include spin by Kane and Mele [38, 39]. In this case intrinsic spin-orbit coupling, or helical (spin dependent chiral) next-nearest neighbour hopping, generates a mass term $m_{\mathrm{KM}} \boldsymbol{s} \otimes \sigma_z \otimes \tau_z$, where $\boldsymbol{s} = (s_x, s_y, s_z)$ are the Pauli matrices acting in real spin space $s = \uparrow, \downarrow$. A finite m_{KM} corresponds to a state with $C = 0$, but a finite Z_2 topological invariant [36]. This state is known as the two dimensional topological insulator or quantum spin Hall insulator that exhibits the quantum spin Hall effect. Assuming spin is a conserved quantity, the quantised spin Hall conductance is transported by counter-propagating spin-polarised helical edge states. The spin-polarised Chern number $C_{\mathrm{QSH}} = C_{\uparrow} - C_{\downarrow}$ in the same vein as the standard definition of spin-current $j_{\mathrm{spin}} = j_{\uparrow} - j_{\downarrow}$.

The following discussion is concerned with the possibility that strong interactions can dynamically generate complex chiral/helical hopping and spontaneously break the symmetry into states with non-trivial topological classifications.

3.3 Topological Mott Insulator

Raghu *et al.* [57] devised a mean-field decoupling of the next-nearest neighbour repulsive interaction on the honeycomb lattice that dynamically generated the Hal-

dane and Kane-Mele terms. Here this is reviewed and the effective mean-field theory derived for these topological Mott insulating states.

3.3.1 Bond Order Decoupling

To begin, the next-nearest neighbour interaction V_2 is mean-field decoupled in the bond order channel $\langle c_i^\dagger c_j \rangle$ as follows

$$\begin{aligned} H_{V_2} &= V_2 \sum_{\langle\langle i,j \rangle\rangle} \hat{n}_i \hat{n}_j \,, \\ &= -V_2 \sum_{\mu} \sum_{\langle\langle i,j \rangle\rangle} (c_i^\dagger s_\mu c_j)(c_j^\dagger s_\mu c_i) \,, \\ &\approx \frac{V_2}{2} \sum_{\mu} \sum_{\langle\langle i,j \rangle\rangle} \langle c_i^\dagger s_\mu c_j \rangle \langle c_j^\dagger s_\mu c_i \rangle - \langle c_i^\dagger s_\mu c_j \rangle (c_j^\dagger s_\mu c_i) - \langle c_j^\dagger s_\mu c_i \rangle (c_i^\dagger s_\mu c_j) \,. \end{aligned} \tag{3.10}$$

Here $s_\mu = (s_0, \boldsymbol{s})$ is the 4-vector acting on $c_i = (c_{i\uparrow}, c_{i\downarrow})$, s_0 is the identity in spin space and μ-sums are over $\mu = 0, x, y, z$. It is expedient to apply the translationally invariant, sublattice dependent, and purely imaginary *ansatz* $\langle c_i^\dagger s_\mu c_j \rangle = i \chi^\mu \sigma_z$, with χ^μ a real valued 4-vector order parameter. This *ansatz* for the bond order is known to minimise the free energy [57], as it was found that there is an associated energetic cost to any real part of $\langle c_i^\dagger s_\mu c_j \rangle$, which breaks the particle-hole symmetry. Notice that this maps the $\mu = 0$ directly onto Haldane's model Eq. (3.1) with $t_2 \leftrightarrow V_2 \chi^0$ for $\varphi = \pi/2$. Likewise, the $\mu = x, y, z$ maps onto the Kane-Mele hopping.

3.3.2 Effective Theory and Landau Free Energy

The effective mass terms are obtained by expanding around the Dirac points

$$\mathcal{H}_\chi = \sum_\mu 3 V_2 \chi^\mu \chi^\mu + \frac{3\sqrt{3} V_2}{2} \int^\Lambda \frac{d^2 \boldsymbol{k}}{(2\pi)^2} \Psi^\dagger(\boldsymbol{k}) \chi^\mu s_\mu \otimes \sigma_z \otimes \tau_z \Psi(\boldsymbol{k}), \tag{3.11}$$

with the eight component spinor

$$\Psi = (\psi_{\uparrow A+}, \psi_{\uparrow A-}, \psi_{\uparrow B+}, \psi_{\uparrow B-}, \psi_{\downarrow A+}, \psi_{\downarrow A-}, \psi_{\downarrow B+}, \psi_{\downarrow B-}). \tag{3.12}$$

The singlet ($\mu = 0$) component of χ^μ describes the order parameter of Haldane's quantum anomalous Hall (QAH) or Chern insulator phase, which spontaneously

breaks time reversal symmetry, opening a Mott gap at the Dirac points. Similarly, a non-zero triplet component ($\mu \neq 0$) describes the Kane-Mele quantum spin Hall (QSH) or topological insulator state, which spontaneously breaks $SU(2)$ spin-rotational symmetry but preserves time reversal symmetry. The electron mean-field dispersion takes the same form in both phases,

$$\varepsilon_{s\tau}(\boldsymbol{k}) = \pm\sqrt{v_F^2\,|\boldsymbol{k}|^2 + \sum_{\mu}\left(3\sqrt{3}V_2\chi^{\mu}/2\right)^2}. \tag{3.13}$$

The dispersion is degenerate for both spin and valley pseudospin flavours. Of course, there is no coexistence between QAH and QSH because they have distinct topological properties. In the following it is assumed that the spin bond order is spontaneously polarised in the z direction with $\chi^x = 0$ and $\chi^y = 0$. The resulting Landau mean-field free energy density is

$$f_{\mathrm{mf}}(\chi) = \alpha_{\mathrm{mf}}\chi^2 + \beta_{\mathrm{mf}}\,|\chi|^3 \tag{3.14}$$

with $\chi = \chi^0$ and $\chi = \chi^z$ in the QAH and QSH phases respectively. The mean-field coefficients do not depend on the channel in which the symmetry is broken, indicating that at this level, the QAH and QSH phases are degenerate. The quadratic coefficient $\alpha_{\mathrm{mf}} = 3V_2(1 - 9v_2)$ with $v_2 = \Lambda V_2/4\pi v_F$ is obtained, whilst the cubic coefficient is positive definite with $\beta_{\mathrm{mf}} = 27\sqrt{3}V_2^3/16\pi v_F^2$. This supports a continuous phase transition between the semimetal and topological Mott insulators at a critical coupling $(v_2)_c = 1/9$.

3.3.3 Motivation to Include Quantum Fluctuations

In the spinful case it is natural to expect that quantum fluctuations play a crucial role in determining the fate of the topological phases. Raghu *et al.* [57] argued that the soft fluctuations associated with breaking of continuous spin rotational symmetry would favour the QSH phase, which they confirmed with numerical functional renormalisation group analysis. Here this will be demonstrated analytically. More importantly, quantum fluctuations are paramount to determining the phase behaviour

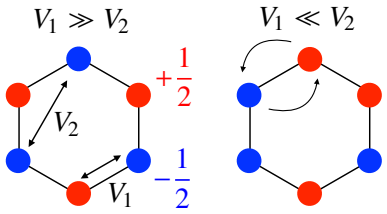

Figure 3.4: Classical (fermionic hopping $t = 0$) charge instabilities from nearest neighbour V_1 and next-nearest neighbour V_2 repulsive interactions on a honeycomb plaquette. $V_1 \gg V_2$ favours the sublattice CDW state. $V_2 \gg V_1$ favours the translational and rotational lattice symmetry breaking CDW_3 charge order. The charge occupation is inverted on a single $A - B$ bond of the plaquette, relative to the sublattice CDW.

between topological phases and the competing CDW_3 charge order discussed in the following.

3.4 CDW_3 Lattice Symmetry Breaking Charge Order

Using unbiased numerical mean-field theory on the honeycomb with an enlarged unit cell, Grushin *et al.* [70] discovered that there was competing CDW_3 charge order at large next-nearest neighbour V_2. This order that spontaneously breaks translational and rotational symmetries is motivated in the classical limit for large V_2. Then the effective theory is derived, and the Landau free energy analysed.

3.4.1 Classical Limit

The CDW_3 or sublattice charge modulated order can be motivated from the classical limit $t \to 0$ of the V_1, V_2 Hamiltonian [70, 79]. The classical free energy density is

$$f_{\text{cl}} = \frac{1}{3}\Big[V_1(n_{A_1} + n_{A_2} + n_{A_3})(n_{B_1} + n_{B_2} + n_{B_3}) + 3V_2(n_{A_1}n_{A_2} + n_{A_2}n_{A_3} + n_{A_3}n_{A_1} + n_{B_1}n_{B_2} + n_{B_2}n_{B_3} + n_{B_3}n_{B_1})\Big], \tag{3.15}$$

where the index $(A_1, \ldots, B_3)$ runs over the six sites of the honeycomb plaquette. Note the factor of $1/3$ because there are $L/3$ plaquettes for 2L sites. Here it is clear that there is an energy cost V_2 for neighbouring sites on the same sublattice (next-nearest neighbours) to both be occupied. Considering one sublattice only, this problem maps onto the classical frustrated triangular lattice Ising antiferromagnet.

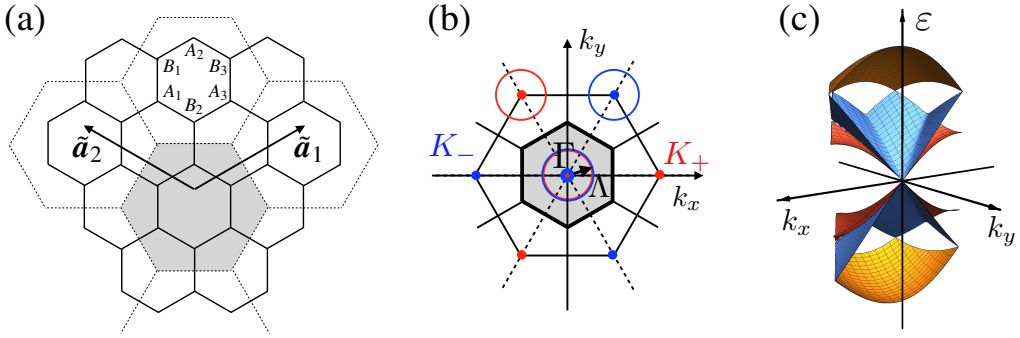

Figure 3.5: (a) The threefold enlarged unit cell (grey area) of the honeycomb lattice. Further unit cells are outlined by the dashed lines. Also, the basis $A_1, \ldots, B_3$ of the plaquette is defined. (b) The corresponding reduced Brillouin zone (grey area). Dirac valleys in the normal state (red and blue dots) fold into the center of the zone. (c) A cut through the non-interacting tight-binding dispersion on the enlarge unit cell.

However with the charge ordering on an entire honeycomb plaquette there is also the constraint on charge conservation. At half-filling the energetically favourable state is no longer the sublattice CDW but rather the CDW_3, where the occupation has been inverted between one A and one B site relative to the CDW, as is illustrated in Fig. 3.4. Overall there is still one frustrated bond on the plaquette, and there is an associated 18-fold degenerate classical ground state, which was confirmed by exact diagonalisation [79]. In the following, these states are enumerated by Eq. (3.30) and in Fig. 3.6, and are related by $2\pi/3$ rotations, translations and charge occupation inversion.

3.4.2 Derivation of the Effective Theory

In the following the effective theory of CDW_3 order is derived from the lattice model

$$H = -t \sum_{\langle i,j \rangle} c_i^\dagger c_j + V_1 \sum_{\langle i,j \rangle} \hat{n}_i \hat{n}_j + V_2 \sum_{\langle\langle i,j \rangle\rangle} \hat{n}_i \hat{n}_j, \tag{3.16}$$

at half-filling and zero temperature. For brevity the trivial spin dependence s_0 (from decoupling in the charge channel) is temporarily suppressed. The CDW_3 phase is characterised by an enlarged six-site unit cell covering an entire honeycomb plaquette, see Fig. 3.1 and Fig. 3.5(a). In this case the lattice vectors are $\tilde{\boldsymbol{a}}_1 =$

$\frac{3a}{2}(\sqrt{3}, 1)$ and $\tilde{\boldsymbol{a}}_2 = \frac{3a}{2}(-\sqrt{3}, 1)$ (with $\tilde{\boldsymbol{a}}_3 = -(\tilde{\boldsymbol{a}}_1 + \tilde{\boldsymbol{a}}_2)$), as opposed to the primitive lattice vectors $\boldsymbol{a}_1 = \frac{\sqrt{3}a}{2}(1, \sqrt{3})$, $\boldsymbol{a}_2 = \frac{\sqrt{3}a}{2}(-1, \sqrt{3})$. Also the basis is increased to

$$\boldsymbol{c} = (c_{A_1}, c_{A_2}, c_{A_3}, c_{B_1}, c_{B_2}, c_{B_3}). \tag{3.17}$$

The corresponding reciprocal lattice vectors of the down-folded Brillouin zone (see Fig. 3.5(b)) are $\tilde{\boldsymbol{b}}_{1,2} = \frac{2\pi}{3\sqrt{3}a}(\pm 1, \sqrt{3})$, as opposed to $\boldsymbol{b}_{1,2} = \frac{2\pi}{3a}(\pm\sqrt{3}, 1)$. The non-interacting tight-binding Hamiltonian is

$$H_t = \sum_{\boldsymbol{k}} \boldsymbol{c}^\dagger(\boldsymbol{k}) H_t(\boldsymbol{k}) \boldsymbol{c}(\boldsymbol{k}), \tag{3.18}$$

$$H_t(\boldsymbol{k}) = \begin{pmatrix} 0 & T^\dagger(\boldsymbol{k}) \\ T(\boldsymbol{k}) & 0 \end{pmatrix}, \tag{3.19}$$

$$T(\boldsymbol{k}) = -t \begin{pmatrix} 1 & 1 & e^{i\boldsymbol{k}\cdot\tilde{\boldsymbol{a}}_2} \\ 1 & e^{i\boldsymbol{k}\cdot\tilde{\boldsymbol{a}}_3} & 1 \\ e^{i\boldsymbol{k}\cdot\tilde{\boldsymbol{a}}_1} & 1 & 1 \end{pmatrix}. \tag{3.20}$$

The resultant down-folding of the bands increases the number of energy levels at a given momentum threefold. This gives rise to six bands with an additional 2-fold degeneracy in the spinful model, and maps the Dirac points onto the Γ point ($\boldsymbol{k} = \boldsymbol{0}$), as shown in Fig. 3.5(b,c). High energy modes are integrated out by projecting into the low-energy Dirac subspace $\Psi = \mathcal{P}\boldsymbol{c}$, and this obtains the non-interacting Dirac Hamiltonian

$$\mathcal{H}_t(\boldsymbol{p}) = \mathcal{P}\{H_t(\boldsymbol{0}) + [\nabla_{\boldsymbol{k}} H_t(\boldsymbol{k})]_{\boldsymbol{k}=\boldsymbol{0}} \cdot \boldsymbol{p}\}\mathcal{P}^\dagger = v_F \boldsymbol{p} \cdot \boldsymbol{\alpha}. \tag{3.21}$$

The projection $\mathcal{P}$ is formulated from the low energy (row) eigenvectors of $H_t(\boldsymbol{k} = \boldsymbol{0})$

$$P_0 = \frac{1}{\sqrt{6}} \begin{pmatrix} -1 & -1 & 2 & 0 & 0 & 0 \\ \sqrt{3} & -\sqrt{3} & 0 & 0 & 0 & 0 \\ 0 & 0 & 0 & -\sqrt{3} & \sqrt{3} & 0 \\ 0 & 0 & 0 & -1 & -1 & 2 \end{pmatrix}. \tag{3.22}$$

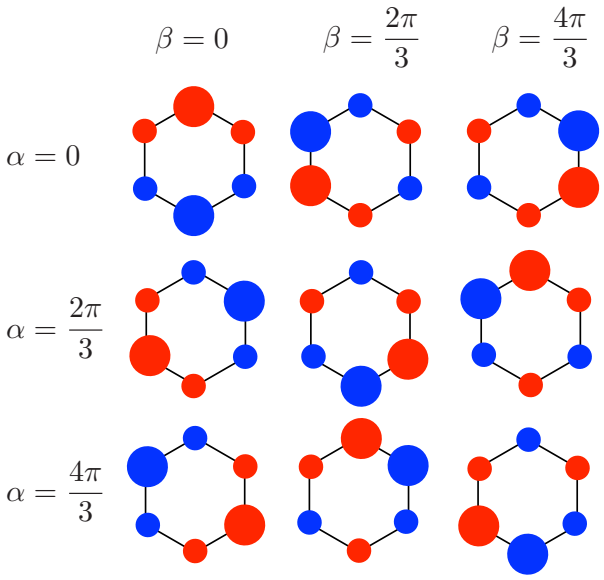

Figure 3.6: All 9 (18 with charge inversion) degenerate CDW_3 charge patterns. Charge modulation is shown relative to half-filling, with red for positive modulation, and blue for negative modulation. The charge patterns are parameterised by α and β, see Eq. (3.30). Different α correspond to translational shifts of the unit cell, whilst β correspond to C_3 ($2\pi/3$) spatial rotations.

It is useful to apply the additional unitary transformation, such that the projection is

$$\mathcal{P} = e^{-i\frac{\pi}{4}\sigma_z\otimes\tau_z} e^{-i\frac{2\pi}{3}\sigma_0\otimes\tau_z} e^{-i\frac{\pi}{4}\sigma_0\otimes\tau_x} P_0. \tag{3.23}$$

The first exponential transforms into the basis $\boldsymbol{\alpha} = (\sigma_x \otimes \tau_z, \sigma_y \otimes \tau_0)$. The second enacts a coordinate transformation. The third translates the unit cell into the form displayed in Fig. 3.6. Decoupling in the charge channel

$$H_V = \sum_{\boldsymbol{k}} \boldsymbol{c}^\dagger(\boldsymbol{k}) H_V(\boldsymbol{k}) c(\boldsymbol{k}) + E_{V;\mathrm{cl}}, \tag{3.24}$$

$$\begin{aligned} E_{V;cl} = \frac{L}{3}\Big[& V_1(\langle\hat{n}_{A_1}\rangle + \langle\hat{n}_{A_2}\rangle + \langle\hat{n}_{A_3}\rangle)(\langle\hat{n}_{B_1}\rangle + \langle\hat{n}_{B_2}\rangle + \langle\hat{n}_{B_3}\rangle) \\ & + 3V_2 \sum_{\sigma=A,B} \langle\hat{n}_{\sigma_1}\rangle\langle\hat{n}_{\sigma_2}\rangle + \langle\hat{n}_{\sigma_2}\rangle\langle\hat{n}_{\sigma_3}\rangle + \langle\hat{n}_{\sigma_3}\rangle\langle\hat{n}_{\sigma_1}\rangle\Big]. \end{aligned} \tag{3.25}$$

$$\begin{aligned} H_V(\boldsymbol{k}) = V_1 \sum_{i=1}^{3} & \mathrm{diagonal}(\langle\hat{n}_{B_i}\rangle, \langle\hat{n}_{B_i}\rangle, \langle\hat{n}_{B_i}\rangle, \langle\hat{n}_{A_i}\rangle, \langle\hat{n}_{A_i}\rangle, \langle\hat{n}_{A_i}\rangle) \\ & + V_2\, \mathrm{diagonal}(\langle\hat{n}_{A_2}\rangle + \langle\hat{n}_{A_3}\rangle, \langle\hat{n}_{A_1}\rangle + \langle\hat{n}_{A_3}\rangle, \langle\hat{n}_{A_1}\rangle + \langle\hat{n}_{A_2}\rangle, \end{aligned}$$

$$\langle \hat{n}_{B_2} \rangle + \langle \hat{n}_{B_3} \rangle, \langle \hat{n}_{B_1} \rangle + \langle \hat{n}_{B_3} \rangle, \langle \hat{n}_{B_1} \rangle + \langle \hat{n}_{B_2} \rangle), \tag{3.26}$$

where diagonal( ) are the diagonal entries of a matrix. The half-filling condition is satisfied by

$$\langle \hat{n}_{A_1} \rangle + \langle \hat{n}_{A_2} \rangle + \langle \hat{n}_{A_3} \rangle + \langle \hat{n}_{B_1} \rangle + \langle \hat{n}_{B_2} \rangle + \langle \hat{n}_{B_3} \rangle = 0. \tag{3.27}$$

The effective low-energy Hamiltonian is obtained from the projection $\mathcal{H}_V = \mathcal{P} H_V \mathcal{P}^\dagger$. To leading order

$$\begin{aligned}
\mathcal{H}_V = \int^{\Lambda} \frac{d^2\boldsymbol{k}}{(2\pi)^2} \Psi^\dagger(\boldsymbol{k}) \Big\{ & \\
& (V_2 - V_1/2)[\langle \hat{n}_{A_1} \rangle + \langle \hat{n}_{A_2} \rangle + \langle \hat{n}_{A_3} \rangle - \langle \hat{n}_{B_1} \rangle - \langle \hat{n}_{B_2} \rangle - \langle \hat{n}_{B_3} \rangle]\, \sigma_z \otimes \tau_0 \\
& + \frac{V_2}{4}[\langle \hat{n}_{A_1} \rangle - 2\langle \hat{n}_{A_2} \rangle + \langle \hat{n}_{A_3} \rangle - \langle \hat{n}_{B_1} \rangle + 2\langle \hat{n}_{B_2} \rangle - \langle \hat{n}_{B_3} \rangle](-\sigma_z \otimes \tau_x) \\
& + \frac{\sqrt{3}V_2}{4}[-\langle \hat{n}_{A_1} \rangle + \langle \hat{n}_{A_3} \rangle - \langle \hat{n}_{B_1} \rangle + \langle \hat{n}_{B_3} \rangle](-\sigma_0 \otimes \tau_y) \\
& + \frac{\sqrt{3}V_2}{4}[-\langle \hat{n}_{A_1} \rangle + \langle \hat{n}_{A_3} \rangle + \langle \hat{n}_{B_1} \rangle - \langle \hat{n}_{B_3} \rangle](-\sigma_z \otimes \tau_y) \\
& + \frac{V_2}{4}[-\langle \hat{n}_{A_1} \rangle + 2\langle \hat{n}_{A_2} \rangle - \langle \hat{n}_{A_3} \rangle - \langle \hat{n}_{B_1} \rangle + 2\langle \hat{n}_{B_2} \rangle - \langle \hat{n}_{B_3} \rangle]\, \sigma_0 \otimes \tau_x \\
& + (V_2 + V_1/2)[\langle \hat{n}_{A_1} \rangle + \langle \hat{n}_{A_2} \rangle + \langle \hat{n}_{A_3} \rangle + \langle \hat{n}_{B_1} \rangle + \langle \hat{n}_{B_2} \rangle + \langle \hat{n}_{B_3} \rangle]\, \sigma_0 \otimes \tau_0 \Big\} \Psi(\boldsymbol{k}).
\end{aligned} \tag{3.28}$$

This is simplified by making the CDW_3 plaquette *ansatz* for the charge occupation $\langle \hat{n}_i \rangle = \rho_0 + \rho_i$ with the deviation

$$(\rho_{A_1}, \rho_{A_2}, \rho_{A_3}, \rho_{B_1}, \rho_{B_2}, \rho_{B_3}) = (\rho, -\rho - \Delta, \rho, -\rho, \rho + \Delta, -\rho), \tag{3.29}$$

from the half filling value $\rho_0 = N_s/2$ (where $N_s = 1$ or 2 is the number of fermionic spin flavours). The constraints $0 \leq \Delta \leq \rho \leq \rho_0$ and $\rho + \Delta \leq \rho_0$ ensure the filling is devoid of pathology. This *ansatz* satisfies the half-filling condition. The *ansatz* is motivated by the discussed classical analysis, and was also obtained from unbiased numerical mean-field theory on the honeycomb lattice with an enlarged

unit cell [70]. Such a phase spontaneously breaks translational symmetry and keeps only one mirror: $C_{6v} \to C_{1v}$.

Finally, the effective mean-field term is

$$\begin{aligned}\mathcal{H}_\rho = \int^{\Lambda} \frac{d^2\boldsymbol{k}}{(2\pi)^2} \Psi^\dagger(\boldsymbol{k})\, s_0 \otimes \Big\{ \\ 2V_2(\rho+\Delta/2)[S_\alpha\sigma_0 \otimes (S_\beta\tau_x - C_\beta\tau_y) - C_\alpha\sigma_z \otimes (C_\beta\tau_x + S_\beta\tau_y)] \\ + (2V_2 - V_1)(\rho-\Delta)\sigma_z \otimes \tau_0\Big\}\Psi(\boldsymbol{k}) + 2V_2\rho(\rho+2\Delta) + \frac{V_1}{3}(\rho-\Delta)^2, \end{aligned} \tag{3.30}$$

where $C_\alpha = \cos\alpha$, $S_\alpha = \sin\alpha$ and $\alpha, \beta = 2n\pi/3$ for $n = 0, 1, 2$. Here α encodes translations and β rotations, which together enumerate the 9 possible charge configurations in Fig. 3.6, which is doubled with charge inversion ($\rho, \Delta < 0$).

3.4.3 Effective Dispersion and Landau Free Energy

The effective mean-field CDW_3 dispersion

$$\begin{aligned}\varepsilon(\boldsymbol{k}) = \pm\Big\{ v_F\,|\boldsymbol{k}|^2 + [2V_2(\rho+\Delta/2)]^2 + [(2V_2 - V_1)(\rho-\Delta)]^2 \\ \pm 2\,|2V_2(\rho+\Delta/2)|\sqrt{(k_xC_\alpha + k_yS_\alpha)^2 + [(2V_2 - V_1)(\rho-\Delta)]^2}\Big\}^{\frac{1}{2}}, \end{aligned} \tag{3.31}$$

is rotated relative to the k_x by α, but is otherwise invariant. This implies that the free energy of the CDW_3 broken symmetry states are degenerate. Therefore, it is sufficient to analyse the charge pattern $\alpha = \beta = 0$, which is displayed in Fig. 3.1. Collective fluctuations will be considered about this particular broken symmetry state. It is noted that the dispersion is not of the putative massive Dirac form $\sqrt{k^2 + m^2}$. Underlying this is that certain charge order parameter combinations couple as emergent non-Abelian gauge fields to the Dirac fermions, and have an impact on the criticality. This is discussed in detail in Chapter 4.

Integrating over the occupied dispersion obtains the mean-field Landau free energy

$$\tilde{f}_{\rm mf}(\rho, x) = \tilde{\alpha}_{\rm mf}(x)\rho^2 + \tilde{\beta}_{\rm mf}(x)\,|\rho|^3\,, \tag{3.32}$$

with the parameterisation $\Delta = x\rho$ for $0 \leq x \leq 1$, and

$$\tilde{\alpha}_{\mathrm{mf}}(x) = 2V_2(1+2x) + \frac{V_1}{3}(x-1)^2 + \\ - \frac{N_s\Lambda}{4\pi v_F}\left[2(2V_2 - V_1)^2(1-x)^2 + (2V_2)^2(1+x/2)^2\right], \tag{3.33}$$

$$\tilde{\beta}_{\mathrm{mf}}(x) = \frac{4-\pi}{2\pi v_F^2} N_s V_2 (2V_2 - V_1)^2 (1-x)^2 (1+x/2). \tag{3.34}$$

Along the V_2 phase axis ($V_1 = 0$)

$$\tilde{\alpha}_{\mathrm{mf}}(x) = 2V_2[1 + 2x - 6N_s v_2(1 - x + \frac{3}{4}x^2)], \tag{3.35}$$

$$\tilde{\beta}_{\mathrm{mf}}(x) = \frac{4-\pi}{\pi v_F^2} 2N_s V_2^3 (1-x)^2 (1+x/2), \tag{3.36}$$

with $N_s = 1, 2$ the spin degeneracy and $v_2 = \Lambda V_2/4\pi v_F$. By inspection, the state with $x = 0$ ($\Delta = 0$) is the leading instability within the CDW_3 state manifold. This state is critical at $(\tilde{v}_2)_c = 1/(6N_s)$. In the ordered phase, the $\Delta = 0$ state remains energetically favourable until large values of V_2 outside the range of applicability of the model.

3.4.4 Summary and Competition with the Topological Mott Phase

To summarise, for the spinless case ($N_s = 1$), the topological QAH Mott insulator is the leading instability at a critical coupling $(v_2)_c = 1/9$. On the other hand, in the spinful model ($N_s = 2$) the transition into the CDW_3 phase occurs at a critical value $(\tilde{v}_2)_c = 1/12$, pre-empting the transition into the QSH phase. These findings are in qualitative agreement with previous mean-field studies on the lattice [70, 87, 88]. The competing order and the similarity of the critical couplings indicate that beyond mean-field quantum fluctuations will play a crucial role.

3.5 Self-Consistent Collective Quantum Fluctuations

The corrections to the Landau mean-field free energy from order parameter quantum fluctuations are self-consistently calculated to quadratic order using a path integral

approach. The aim is to determine the leading order instability from the semimetal along the V_2 axis of the phase diagram. The conclusions are expected to hold in the regime of the critical line extending out to finite V_1. The cases of spinless and spinful fermions are calculated and contrasted.

3.5.1 Topological Mott Insulator Fluctuations

The collective quantum fluctuation corrections $\delta\alpha^\mu$ to the free energy

$$f^\mu(\chi) = (\alpha_{\mathrm{mf}} + \delta\alpha^\mu)(\chi^\mu)^2 + \beta_{\mathrm{mf}}\,|\chi^\mu|^3\,, \tag{3.37}$$

are self-consistently calculated to quadratic order around the topological Mott insulating states. The fermionic lattice action in the bond order channel is

$$S[c^\dagger, c] = \int_0^\beta d\tau\{\sum_{s=\uparrow,\downarrow}[\sum_i c_{is}^\dagger \partial_\tau c_{is} + t\sum_{\langle i,j\rangle} c_{is}^\dagger c_{js}] - \frac{V_2}{2}\sum_{\mu=0}^{3}\sum_{\langle\langle i,j\rangle\rangle}(c_i^\dagger s_\mu c_j)(c_j^\dagger s_\mu c_i)\}. \tag{3.38}$$

From here on the Einstein summation convention over the repeated index $\mu = 0, x, y, z$ will be employed.

The interaction is decoupled in the bond order channel using the Hubbard-Stratonovich transformation, which introduces the auxiliary bosonic fields $\hat{\chi}_{ij}^\mu$ conjugate to $c_i^\dagger s_\mu c_j$. The purpose of this is to expand around the topological Mott insulator broken symmetry states. The most general transformation would be to introduce four complex fields, which is equivalent to introducing eight real fields. Yet each additional field introduces a new source of error if not evaluated exactly [95]. Anticipating a truncation at Gaussian order, and following the mean-field analysis, it is only necessary to introduce four real fields. These are the imaginary components of the more general complex fields.

To formulate the self-consistent expansion, static and uniform components of the Hubbard-Stratonovich fields $\hat{\chi}^\mu(\omega = 0, \boldsymbol{k} = 0) = \chi^\mu$ are separated from the finite frequency quantum fluctuations $\hat{\chi}^\mu(\omega \neq 0, \boldsymbol{k}) = \tilde{\chi}^\mu(\omega, \boldsymbol{k})$. The static fields χ^μ are to be identified as the mean-field order parameter fields that solve the saddle

point equations. The self-consistent expansion is equivalent to working with the renormalised propagator $\hat{G}^{-1} = \hat{G}_0^{-1} + \hat{\Sigma}$. After expanding around the Dirac points, the bare propagator is $\hat{G}_0^{-1} = s_0 \otimes (-i\omega\alpha_0 + v_F \boldsymbol{k}\cdot\boldsymbol{\alpha})$ and the spin-resolved self energy is $\hat{\Sigma}_s = \frac{3\sqrt{3}}{2} V_2 \chi_s \sigma_z \otimes \tau_z$. Here $\chi_s = \chi^0$ or $\chi_s = s\chi^z$ for the QAH and QSH phases respectively, with $s = \pm$ indexing the spin. The spin resolved inverse propagator is then

$$\hat{G}_s^{-1} = -i\omega\alpha_0 + v_F \boldsymbol{k}\cdot\boldsymbol{\alpha} + \frac{3\sqrt{3}}{2} V_2 \chi_s \sigma_z \otimes \tau_z. \tag{3.39}$$

Inclusion of the finite frequency fluctuation fields $\tilde{\chi}^\mu$ amounts to the addition of a Yukawa coupling to the low-energy effective action, $\mathcal{S} = \mathcal{S}_\Psi + \mathcal{S}_{\tilde{\chi}} + \mathcal{S}_{\Psi\tilde{\chi}} + \mathcal{S}_\chi$, with

$$\mathcal{S}_\Psi = \int_{\vec{k}} \Psi^\dagger_{\vec{k}} \hat{G}^{-1}(\vec{k}) \Psi_{\vec{k}}, \tag{3.40}$$

$$\mathcal{S}_{\Psi\tilde{\chi}} = \frac{3\sqrt{3}}{2} V_2 \sum_{\sigma=A,B} \int_{\vec{k}_1\vec{k}_2} \Psi^\dagger_{\vec{k}_1\sigma} s_\mu \otimes \tau_z \Psi_{\vec{k}_2\sigma} \tilde{\chi}^\mu_{\vec{k}_1-\vec{k}_2\sigma}, \tag{3.41}$$

$$\mathcal{S}_{\tilde{\chi}} = \frac{3}{2} V_2 \sum_{\sigma=A,B} \int_{\vec{k}} \tilde{\chi}^\mu_{-\vec{k}\sigma} \tilde{\chi}^\mu_{\vec{k}\sigma}, \tag{3.42}$$

$$\mathcal{S}_\chi = 3V_2 \chi^\mu \chi^\mu. \tag{3.43}$$

Here $\vec{k} = (\omega, v_F\boldsymbol{k})$ and

$$\int_{\vec{k}} = \int^{|\vec{k}|\le v_F\Lambda} \frac{d\omega d^2\boldsymbol{k}}{(2\pi)^3 v_F^2}. \tag{3.44}$$

The fermions are integrated out to quadratic order in $\tilde{\chi}$ using the cumulant expansion and the linked cluster theorem [65]

$$\begin{aligned} Z &= \int D[\Psi^\dagger, \Psi, \tilde{\chi}] e^{-\mathcal{S}_\chi - \mathcal{S}_{\tilde{\chi}} - \mathcal{S}_\Psi} \sum_{n=0}^{\infty} \frac{(-\mathcal{S}_{\Psi\tilde{\chi}})^n}{n!}, \\ &= \int D[\tilde{\chi}] e^{-\mathcal{S}_\chi - \mathcal{S}_{\tilde{\chi}} + \int_{\vec{k}} \ln\det \hat{G}^{-1}(\vec{k})} \exp\left[\sum_{n=1}^{\infty} \frac{\langle(-\mathcal{S}_{\Psi\tilde{\chi}})^n\rangle}{n!}\right], \\ &\approx Z_{\mathrm{mf}} \int D[\tilde{\chi}] \exp\left[-\mathcal{S}_{\tilde{\chi}} - \langle \mathcal{S}_{\Psi\tilde{\chi}}\rangle + \frac{1}{2}\langle \mathcal{S}^2_{\Psi\tilde{\chi}}\rangle\right]. \end{aligned} \tag{3.45}$$

Here the fermionic contraction

$$\langle \cdots \rangle = \frac{\int D[\Psi^\dagger, \Psi] e^{-\mathcal{S}_\Psi} (\cdots)}{\int D[\Psi^\dagger, \Psi] e^{-\mathcal{S}_\Psi}}, \tag{3.46}$$

is implicitly over connected diagrams, and the mean-field free energy is $f_{\rm mf} = -\ln Z_{\rm mf}$. The goal is to calculate $\tilde{Z} = \int_{\tilde{\chi}} \exp(-\tilde{\mathcal{S}})$, where $\tilde{\mathcal{S}} = \mathcal{S}_{\tilde{\chi}} + \langle \mathcal{S}_{\Psi\tilde{\chi}} \rangle - \langle \mathcal{S}^2_{\Psi\tilde{\chi}} \rangle / 2$. Wick's theorem is used to evaluate the fermionic contractions with

$$\langle \Psi^{\tau s}_{\vec{k}_1\sigma} \Psi^{\dagger\tau' s'}_{\vec{k}_2\sigma'} \rangle = G^{\tau s}_{\sigma\sigma'}(\vec{k}_1) \delta(\vec{k}_1 - \vec{k}_2) \delta_{ss'} \delta_{\tau\tau'}, \tag{3.47}$$

as the propagator Eq. (3.39) is diagonal in momentum, as well as spin and valley spaces, but not the sublattice pseudospin. The term linear in $\tilde{\chi}$ vanishes under the contraction

$$\begin{aligned} \langle \mathcal{S}_{\Psi\tilde{\chi}} \rangle &= \frac{3\sqrt{3}}{2} V_2 \sum_\sigma \int_{\vec{k}_1 \vec{k}_2} \langle \Psi^\dagger_{\vec{k}_1\sigma} s_\mu \otimes \tau_z \Psi_{\vec{k}_2\sigma} \rangle \tilde{\chi}^\mu_{\vec{k}_1 - \vec{k}_2 \sigma}, \\ &= -\frac{3\sqrt{3}}{2} V_2 \sum_{s\sigma\tau} \int_{\vec{k}_1 \vec{k}_2} \delta(\vec{k}_1 - \vec{k}_2) \tau G^{\tau s}_{\sigma\sigma}(\vec{k}_1) (s_\mu)_{ss} \tilde{\chi}^\mu_{\vec{k}_1 - \vec{k}_2 \sigma} = 0, \end{aligned} \tag{3.48}$$

as $\tilde{\chi}^\mu_{\vec{0}\sigma} = 0$ by definition. The quadratic term is finite

$$\begin{aligned} \langle \mathcal{S}^2_{\Psi\tilde{\chi}} \rangle &= \left(\frac{3\sqrt{3}V_2}{2} \right)^2 \sum_{\sigma\sigma'} \int_{\vec{k}_{1,2,3,4}} \tilde{\chi}^\mu_{\vec{k}_1 - \vec{k}_2 \sigma} \tilde{\chi}^{\mu'}_{\vec{k}_3 - \vec{k}_4 \sigma'} \times \\ &\qquad \langle \left(\Psi^\dagger_{\vec{p}_1\sigma} s_\mu \otimes \tau_z \Psi_{\vec{p}_2\sigma} \right) \left(\Psi^\dagger_{\vec{p}_3\sigma'} s_{\mu'} \otimes \tau_z \Psi_{\vec{p}_4\sigma'} \right) \rangle, \\ &= -\left(\frac{3\sqrt{3}V_2}{2} \right)^2 \sum_{\sigma\sigma' ss'\tau} \int_{\vec{q}\vec{k}} \tilde{\chi}^\mu_{-\vec{q}\sigma} \tilde{\chi}^{\mu'}_{\vec{q}\sigma'} (s_\mu)_{ss'} (s_{\mu'})_{s's} G^{\tau s}_{\sigma\sigma'}(\vec{k} + \vec{q}) G^{\tau s'}_{\sigma'\sigma}(\vec{k}), \\ &= -\left(\frac{3\sqrt{3}V_2}{2} \right)^2 \sum_{\sigma\sigma' ss'} \int_{\vec{q}} \tilde{\chi}^\mu_{-\vec{q}\sigma} \tilde{\chi}^{\mu'}_{\vec{q}\sigma'} (s_\mu)_{ss'} (s_{\mu'})_{s's} \Pi^{ss'}_{\sigma\sigma'}(\vec{q}). \end{aligned} \tag{3.49}$$

Only the intra-valley long-wavelength bond order fluctuations survive.

The fluctuation action

$$\tilde{\mathcal{S}} = \int_{\vec{q}} \tilde{\chi}^{\mu}_{-\vec{q}\sigma} A^{s'}_{\vec{q}\sigma\sigma'} \tilde{\chi}^{\mu}_{\vec{q}\sigma'}, \tag{3.50}$$

decouples into the longitudinal $\tilde{\chi}^0$, $\tilde{\chi}^z$ ($s' = s$) and transverse $\tilde{\chi}^x$, $\tilde{\chi}^y$ ($s' = -s$) sectors, with the matrix elements

$$A^{s'}_{\sigma\sigma'}(\vec{q}) = \frac{3}{2} V_2 \left(\delta_{\sigma\sigma'} + \frac{9}{4} \gamma V_2 \sum_s \Pi^{ss'}_{\sigma\sigma'}(\vec{q}) \right). \tag{3.51}$$

In matrix form, the polarisation $\Pi^{ss'}(\vec{q}) = \Pi^{ss'}_{\mu}(\vec{q})\sigma_{\mu}$, where

$$\Pi^{ss'}_0(\vec{q}) \approx \frac{1}{32 v_F^2 q} \left(q^2 + \tilde{\omega}^2 + 4M^2 \frac{q^2 - \tilde{\omega}^2}{q^2} + 8 M_s M_{s'} \right), \tag{3.52}$$

$$\Pi^{ss'}_x(\vec{q}) \approx -\frac{1}{32 v_F^2 q} \left(2q^2 + v_F^2 |\mathbf{q}|^2 + 4M^2 \frac{v_F^2 |\mathbf{q}|^2 - 2q^2}{q^2} \right), \tag{3.53}$$

$$\Pi^{ss'}(\vec{q}) = 0, \tag{3.54}$$

$$\Pi^{ss'}_{\mu}(\vec{q}) = 0, \tag{3.55}$$

up to second order in $M_s = 3\sqrt{3}/2 V_2 \chi_s$, with $\vec{q} = (\tilde{\omega}, v_F \boldsymbol{q})$. Details of this calculation are presented in Appendix A.1.

The constant γ in Eq. (3.51) is a phenomenological parameter that has been included to account for renormalisation of the vertex $V_2 \tilde{\chi} \Psi^{\dagger} \Psi$ from: (i) coarse-graining the lattice in a Wilsonian sense; (ii) higher order $\tilde{\chi}$ terms; (iii) the Fermi velocity renormalisation as $\Pi \propto 1/v_F$. Both the theoretical and experimental evidence for graphene [96–98] suggests $\gamma < 1$. In addition, γ has the added benefit of smoothly interpolating between mean-field ($\gamma = 0$) and the bare coupling with fluctuations ($\gamma = 1$).

The Gaussian integrals over the fluctuation fields lead to the free-energy corrections $\delta f_{s'} = \mathrm{tr} \ln A^{s'}$, from which the fluctuation contributions to the quadratic coefficients of the Landau expansion are obtained to infinite order in the Gaussian

fluctuations,

$$\begin{aligned}
\delta\alpha^{\mu}_{s'} &= \frac{1}{2}\frac{\partial^2 \delta f_{s'}}{\partial(\chi^\mu)^2}\bigg|_{\chi=0}, \\
&= \frac{1}{2}\int_{\vec{q}} \mathrm{tr}\, \frac{\gamma V_2 \sum_s \partial^2_{\chi^\mu}\Pi^{ss'}(\vec{q})}{\sigma^0 + \gamma V_2 \sum_s \Pi^{ss'}(\vec{q})}\bigg|_{\chi^\mu=0}, \\
&= \gamma V_2 \int_{\vec{q}} \frac{(1+\gamma V_2 \sum_s \Pi_0^{ss'}(\vec{q}))\sum_s \partial^2_{\chi^\mu}\Pi_0^{ss'}(\vec{q})}{(1+\gamma V_2 \sum_s \Pi_0^{ss'}(\vec{q}))^2 - (2\gamma V_2 \Pi_x(\vec{q}))^2}\bigg|_{\chi=0} \\
&\quad - \gamma V_2 \int_{\vec{q}} \frac{4\gamma V_2 \Pi_x(\vec{q})\partial^2_{\chi^\mu}\Pi_x(\vec{q})}{(1+\gamma V_2 \sum_s \Pi_0^{ss'}(\vec{q}))^2 - (2\gamma V_2 \Pi_x(\vec{q}))^2}\bigg|_{\chi=0},
\end{aligned} \tag{3.56}$$

for $s' = \pm s$, and Π_x is independent s, s'. The form is reminiscent of the inverse susceptibility in the random phase approximation. Remarkably, by first evaluating the angular integral, it is possible to evaluate the expressions analytically using standard integration techniques. Finally, the quadratic coefficients of the QSH order parameter are

$$\delta\alpha^z_L = \frac{24 V_2}{\gamma\pi^2}\left(\mathrm{arccot}^2\Omega - \frac{1}{2}\ln\frac{\Omega^2+3}{\Omega^2+1}\right), \tag{3.57}$$

$$\delta\alpha^z_T = -\frac{54 v_2}{\pi} V_2 \left(1 - \Omega\,\mathrm{arccot}\Omega\right), \tag{3.58}$$

for the contributions from longitudinal (L) and transverse (T) fluctuations, where $\Omega = \sqrt{8/(9\pi\gamma v_2) - 1}$. For the QAH order $\delta\alpha^0_L = \delta\alpha^0_T = \delta\alpha^z_L$, and in this case the calculation breaks down for $v_2 \geq 8/9\pi\gamma$ due to the proximity to a pole.

3.5.2 CDW_3 Fluctuation Calculation

Here the fluctuation correction to the quadratic coefficient $\delta\tilde{\alpha}$ of the free energy

$$\tilde{f}(\rho, x) = [\tilde{\alpha}_{\mathrm{mf}}(x) + \delta\tilde{\alpha}(x)]\rho^2 + \tilde{\beta}_{\mathrm{mf}}(x)\,|\rho|^3, \tag{3.59}$$

is self-consistently calculated. The calculation presented here follows in the spirit of the bond order calculation above. The only difference is the increased basis, and the need to integrate out the high energy modes as discussed in the mean-field

treatment. Starting once more with the lattice action

$$S[c^\dagger, c] = \int_0^\beta d\tau \{ \sum_{s=\uparrow,\downarrow} [\sum_i c_{is}^\dagger \partial_\tau c_{is} + t \sum_{\langle i,j \rangle} c_{is}^\dagger c_{js}] + V_2 \sum_{\langle\langle i,j \rangle\rangle} \hat{n}_i \hat{n}_j \} \tag{3.60}$$

the interaction is rewritten and decoupled in the charge channel

$$e^{V_2 \sum_{\vec{q}} \sum_{ij=1}^{6} \hat{n}_{-\vec{q}i} U_{\vec{q}ij} \hat{n}_{\vec{q}j}} \rightarrow \int D[\hat{\rho}] \exp\{-V_2 \sum_{\vec{q}} [\sum_{ij=1}^{6} \hat{\rho}_{-\vec{q}i} U^{-1}_{\vec{q}ij} \hat{\rho}_{\vec{q}j} + 2 \sum_{i=1}^{6} \hat{n}_{-\vec{q}i} \hat{\rho}_{\vec{q}i}]\}, \tag{3.61}$$

using the density in momentum space

$$\hat{n}_{\vec{q}i} = \sum_s \sum_{\vec{k}} c^\dagger_{\vec{k}is} c_{\vec{k}+\vec{q}is} \text{ for } i \in \{A_1, \ldots, B_3\}. \tag{3.62}$$

Here the matrix (in the basis of (3.17))

$$U_{\vec{q}} = -\frac{1}{2} \begin{pmatrix} 0 & e_{\bar{1}3} & e_{\bar{1}2} & 0 & 0 & 0 \\ e_{1\bar{3}} & 0 & e_{2\bar{3}} & 0 & 0 & 0 \\ e_{1\bar{2}} & e_{\bar{2}3} & 0 & 0 & 0 & 0 \\ 0 & 0 & 0 & 0 & e_{2\bar{3}} & e_{\bar{1}2} \\ 0 & 0 & 0 & e_{\bar{2}3} & 0 & e_{\bar{1}3} \\ 0 & 0 & 0 & e_{1\bar{2}} & e_{1\bar{3}} & 0 \end{pmatrix}, \tag{3.63}$$

comes from the Fourier transform of the extended interaction, with

$$e_{xy} = 1 + e^{i\boldsymbol{q}\cdot\tilde{\boldsymbol{a}}_x} + e^{i\boldsymbol{q}\cdot\tilde{\boldsymbol{a}}_y} = 3 + \boldsymbol{q}\cdot(\tilde{\boldsymbol{a}}_x + \tilde{\boldsymbol{a}}_y) + O(|\boldsymbol{q}|^2), \tag{3.64}$$

$\tilde{\boldsymbol{a}}_{\bar{x}} = -\tilde{\boldsymbol{a}}_x$.

Once more, to formulate the self-consistent expansion, static and uniform components of the Hubbard-Stratonovich fields $\hat{\rho}_i(\omega = 0, \boldsymbol{k} = 0) = \rho_0 + \rho_i$ are separated from the finite frequency quantum fluctuations $\hat{\rho}_i(\omega \neq 0, \boldsymbol{k}) = \tilde{\rho}_i(\omega, \boldsymbol{k})$. The projec-

tion $\mathcal{P}$ is applied to the fermionic fields to obtain the low-energy effective action

$$\mathcal{S} = \int_{\vec{k}} \Psi^\dagger_{\vec{k}} s_0 \otimes [-i\omega\alpha_0 + v_F \boldsymbol{k}\cdot\boldsymbol{\alpha} + 2V_2(\rho-\Delta)\sigma_z\otimes\tau_0 - 2V_2(\rho+\Delta/2)\sigma_z\otimes\tau_x]\Psi_{\vec{k}} + 2V_2\sum_{ab=1}^{4}\sum_{i=1}^{6}\int_{\vec{k}_1\vec{k}_2}\Psi^\dagger_{\vec{k}_1 a}\mathcal{P}_{ai}s_0\mathcal{P}^\dagger_{ib}\Psi_{\vec{k}_2 b}\tilde{\rho}_{\vec{k}_1-\vec{k}_2 i} + V_2\sum_{ij=1}^{6}\int_{\vec{k}}\tilde{\rho}_{-\vec{k}i}U^{-1}_{\vec{k}ij}\tilde{\rho}_{\vec{k}j}. \quad (3.65)$$

The fluctuation action is obtained by integrating out the fermions to quadratic order in $\tilde{\rho}$

$$\tilde{\mathcal{S}} = V_2\sum_{ij=1}^{6}\int_{\vec{q}}\tilde{\rho}_{-\vec{q}i}[U^{-1}_{\vec{q}ij} + 2\gamma V_2 N_s\tilde{\Pi}_{\vec{q}ij}]\tilde{\rho}_{\vec{q}j}, \quad (3.66)$$

with the polarisation

$$\tilde{\Pi}_{\vec{q}ij} = \sum_{abcd=1}^{4}\int_{\vec{k}}\mathcal{P}^\dagger_{ia}G_{\vec{k}+\vec{q}ab}\mathcal{P}_{bj}\mathcal{P}^\dagger_{jc}G_{\vec{k}cd}\mathcal{P}_{di}. \quad (3.67)$$

Further details on evaluating $\tilde{\Pi}$ are presented in Appendix A.2.

Apart from the more complicated and larger matrix structure, the fluctuation action is of the same form as for bond order fluctuations. By integrating over the charge fluctuations the corrections to the free energy are

$$\delta f = \mathrm{tr}\log(\hat{U}^{-1} + 2\gamma V_2 N_s\hat{\tilde{\Pi}}). \quad (3.68)$$

The fluctuation corrections to the quadratic coefficient of the Landau expansion in ρ (with $\Delta = x\rho$, $0 \le x \le 1$) are most easily obtained by expanding the polarisation to quadratic order $\tilde{\Pi}_{\vec{q}} = \sum_{n=0}^{2}\tilde{\Pi}^{(n)}_{\vec{q}}(x)\rho^n$, and then expanding the logarithm to quadratic order in ρ, which results in

$$\delta\tilde{\alpha} = V_2\int_{\vec{q}}\mathrm{tr}\frac{2\gamma N_s\tilde{\Pi}^{(2)}_{\vec{q}}}{U^{-1}_{\boldsymbol{q}} + 2\gamma N_s\tilde{\Pi}^{(0)}_{\vec{q}}}. \quad (3.69)$$

This can be evaluated analytically if the zeroth order approximation in $\boldsymbol{q}$ of the Fourier transform matrix is taken, $U^{-1}_{\boldsymbol{q}} \approx U^{-1}_{\boldsymbol{0}}$. Further details are presented in

Appendix A.3. Then it is found that

$$\begin{aligned}\delta\tilde{\alpha} =& \frac{8V_2v_2}{\pi\tilde{\Omega}}\Bigg\{ \\ &\left[384(2+x)^2 + 8(28-68x+31x^2)\tilde{\Omega} + (12-20x+11x^2)\tilde{\Omega}^2\right]\frac{\arctan\left(\frac{\sqrt{\tilde{\Omega}}}{4}\right)}{4\sqrt{\tilde{\Omega}}} \\ &+ \frac{16}{3}\Bigg[-(1-x)^2\tilde{\Omega} - \frac{9}{2}(2+x)^2 + (62 - \frac{635}{2}x + \frac{883}{8}x^2)\log(2) \\ &- \frac{3}{2}(1+x)^2 \sum_{\sigma=\pm1} \mathrm{Li}_2\left(\frac{\sigma\sqrt{\tilde{\Omega}(4+\tilde{\Omega})} - \tilde{\Omega}}{2}\right) \\ &+ (2 - \frac{5}{2}x + \frac{13}{8}x^2)\log(2-\tilde{\Omega}) - 16(1 - 5x + \frac{7}{4}x^2)\log(16+\tilde{\Omega})\Bigg]\Bigg\}, \end{aligned} \tag{3.70}$$

where $\tilde{\Omega} = 2\pi\gamma N_s v_2$ and $\mathrm{Li}_2(z) = \sum_{n=1}^{\infty} z^n/n^2$ is the dilogarithm function. The series expansion in v_2 yields

$$\delta\tilde{\alpha} = -\frac{V_2}{\gamma N_s}\sum_{n\geq 0}(a_n - b_n x + c_n x^2)(\gamma N_s v_2)^{n+2}, \tag{3.71}$$

with the coefficients $b_n > a_n > c_n \geq 0$ that monotonically increase with n.

3.6 Results

The main results are summarised in Fig. 3.7. For the spinless model the leading instability at short-range ($\gamma = 0$) is to the topological QAH Mott insulator. Fluctuations favour CDW_3 order over the QAH state and are strong enough to cause a continuous phase transition from the Dirac semimetal to the CDW_3 phase for $\gamma \gtrsim 0.62$. This is precisely the nature of the transitions found within numerical approaches [80, 82–84]. Similar fluctuation-driven changes of the ground state have been recently discussed in terms of a fermionic quantum order-by-disorder mechanism [99–102]. In the spinful model the transverse fluctuations in the QSH phase stabilise the order, lifting the mean-field degeneracy of the QSH and QAH phases, $\delta\alpha_T^z < 0 < \delta\alpha_L^z = \delta\alpha_{T/L}^0$. The transverse fluctuations are not strong enough however to suppress the CDW_3 phase, which is the leading instability at mean-field. In the presence of fluctuations the leading CDW_3 instability remains as $\Delta = 0$, which is in

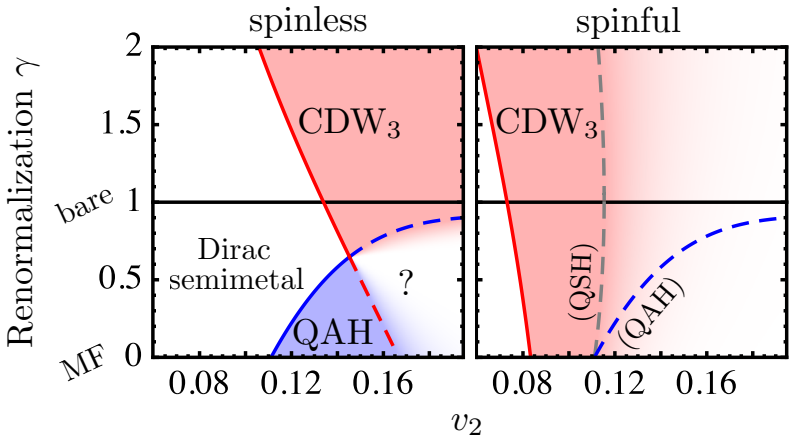

Figure 3.7: Lines of critical-instability along the $v_2 = \frac{\Lambda}{4\pi v_F} V_2$ axis in the presence of fluctuations, renormalised by the phenomenological parameter γ. The mean-field instabilities are at $\gamma = 0$, the cut $\gamma = 1$ indicates the phase behaviour without vertex renormalisation. While the critical interaction strengths depend on the momentum cut-off Λ, the order of instabilities does not. In the regime where the NN interactions are zero ($V_1 = 0$), the CDW$_3$ phases are gapless ($\Delta = 0$).

fact a *gapless* state with semi-Dirac fermionic quasiparticle excitations.

3.6.1 Semi-Dirac Excitations

In the absence of nearest neighbour repulsion, the favoured charge-ordered state with $\rho > 0$ and $\Delta = 0$ describes a smectic order with gapless excitations. This broken-symmetry state remains semimetallic, with one pair of bands opening a gap and another pair remaining gapless, as shown in Fig. 3.8. From the hybridisation of the down-folded Dirac valleys there is a condensation energy gain from the gap $\pm|2V_2\rho|$. This is to be compared with the topological Mott state with gaps $\pm|V_2\chi|$ at the two Dirac points. The effective Hamiltonian matrix of the two gapless bands in the CDW$_3$ phase is

$$\hat{\mathcal{H}}(\mathbf{k}) = v_F k_x \tau^x + v_F^2 k_y^2/(4V_2\rho)\tau^z, \tag{3.72}$$

with energy spectrum $|\varepsilon_\pm(\mathbf{k})| = v_F\sqrt{k_x^2 + v_F^2 k_y^4/(4V_2\rho)^2}$. The quasiparticles are *semi-Dirac* fermions, which disperse linearly (relativistically) along the x direction and have a quadratic (non-relativistic) touching along the y axis. Those touching points sit at the high symmetry Γ points of the folded Brillouin zone (see Fig. 3.8).

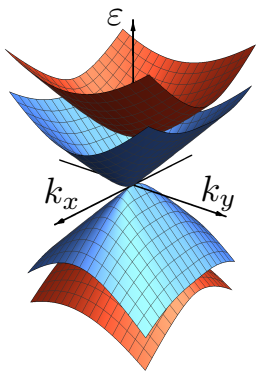

Figure 3.8: Low energy bands of the CDW_3 state, for $\alpha = 0, \beta = 0, \Delta = 0$, around the Γ point. At half filling, the system is gapless, with semi-Dirac quasiparticles that disperse linearly in the $k_y direction$, but quadratically in the k_x direction.

3.7 Discussion

The transition to the gapless CDW_3 state ($\rho > 0$, $\Delta = 0$) is highly unconventional since the ground state remains semimetallic with semi-Dirac quasiparticles. It does not belong to the class of putative Dirac semimetal-to-insulator transitions, with Gross-Neveu-Yukawa universality. This "hidden" charge order eluded previous numerical studies [79–88] that identified phase transitions through the opening of a Mott gap. The onset of semi-Dirac behaviour may be resolved in large-scale density matrix renormalisation group simulations on infinite cylinders, which are now capable of extracting the momentum-dependent excitation spectra of Dirac systems [103]. In addition, with the recent advent of "designer Hamiltonian" methods [26, 104] in quantum Monte Carlo it seems possible to engineer the unconventional self-energy terms of the CDW_3 state.

As was demonstrated, the hidden CDW_3 order is stable against Gaussian fluctuations. A small nearest neighbour repulsion V_1 is expected to lead to finite Δ when higher order and lattice terms are included in the free energy, and hence to the opening of a Mott gap. Closer inspection shows that the semi-Dirac mode splits into two massive Dirac cones along the quadratic touching direction. Unconventional critical properties are still expected due to the proximity to the unusual critical point at $V_1 = 0$.

It has been suggested [88] that the regime of dominant V_2 could become exper-

imentally accessible by using silicon adatoms or ultracold atoms in double-layers of triangular optical lattices. In the case of the optical lattice, the interaction strength for charged fermionic molecules will depend only on the distance between the sites, and so can be tuned to the $V_2 \gg V_1$ situation by spatially separating the layers. In this case the next-nearest neighbours (intra-triangular layer) in the honeycomb sense are spatially closer that the nearest neighbours (inter-triangular layer). The hopping amplitudes depend on several parameters, and in principle can be tuned to accommodate the layer separation.

In addition, it is interesting to note that a similar charge ordering has been experimentally observed (below $T \sim 340$K) in $YbFe_2O_4$ [105, 106]. Here the Fe are AB stacked on triangular layers, and can be mapped to the honeycomb lattice with comparable inter- and intra-layer distances implying $V_1 \sim V_2$. However, in this case the charge order is slightly incommensurate due to coupling between the bilayers in the z direction. Also magnetic order sets in at $T \sim 280$K [107].

Although the topological Mott insulator is not stable on the honeycomb lattice, the notion that interactions can spontaneously break symmetry into topological phases is still robust [58]. There are proposals to bias towards the topological phases using RKKY interactions [108], or extended hoppings [87]. Similarly the topological Mott insulator phase was also found at mean-field in the semimetallic π-flux square lattice model [69], but again there is numerical evidence indicating fluctuations stifle these states [109].

More promisingly, there is evidence to suggest that topologically non-trivial phases can be induced by interactions when the touching point is quadratic [110–112]. This is because interactions are marginally relevant in the renormalisation group sense, indicating that the non-interacting quadratic point, such as for bilayer graphene [113], will be gapped for weak interactions. These weak interactions are not able to stabilise competing phases like the charge order considered here. To this end, there is numerical evidence of stable topological Mott phases on the kagome [114, 115] and checkerboard [116, 117] lattices. However, it has been shown that if linear terms are allowed by symmetry, then they are always generated

by the weak interactions under the renormalisation group flow [118, 119]. In the process, the critical interaction strength is pushed back up to finite values. It is worth noting that this argument does not hold for the present semi-Dirac case, where the bare electron dispersion is already linear. Only because of the matrix structure of the Yukawa coupling for $V_1 = 0$, the symmetry breaking does not lead to the opening of a gap but instead to a quadratic touching along the CDW_3 order.

Motivated by the unconventional nature of the CDW_3 broken symmetry state, the critical properties are analysed in the next Chapter using the renormalisation group.

Chapter 4

Novel Criticality of Dirac Fermions from Lattice Symmetry Breaking

The role of spontaneous lattice symmetry breaking in strongly interacting two dimensional Dirac systems is considered. The fermion induced quantum (multi-)criticality is described by Dirac fermions coupled to a dynamical order parameter that is composed of mass and emergent gauge fields. This is illustrated for the example of translational and rotational symmetry breaking due to charge density wave order on the honeycomb lattice. Using a renormalisation group analysis it is found that the putative emergent Lorentz invariance is violated, resulting in unconventional universal behaviour. Finally, it is identified that topological phase transitions are well described by this effective field theory. The original work in this chapter was made available as a preprint in *Novel Criticality of Dirac Fermions from Lattice Symmetry Breaking*, E. Christou, F. de Juan, F. Krüger, arXiv:1906.03892 (2019) [120].

4.1 Introduction

Interacting Dirac fermions exhibit perhaps the simplest example of fermionic quantum criticality. In high energy physics this has been known for some time, and goes under the guise of spontaneous fermion mass generation and chiral symmetry breaking in the Gross-Neveu-Yukawa (GNY) model [21, 22]. The prototypical condensed matter examples are semimetal-insulator transitions on the half-filled honeycomb

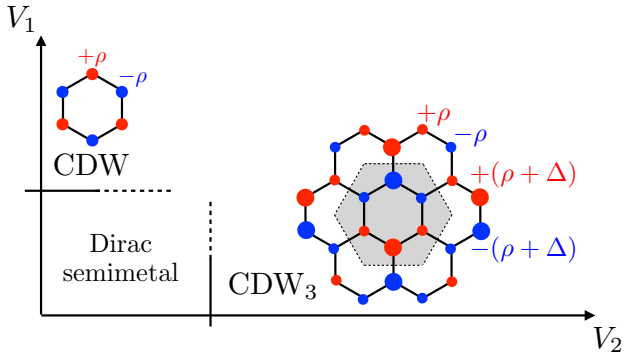

Figure 4.1: Schematic phase diagram of Dirac fermions on the half-filled honeycomb lattice with nearest and next-nearest neighbour repulsive interactions V_1 and V_2. Charge modulation is shown relative to half-filling. The CDW breaks sublattice inversion symmetry. The CDW_3 translation, rotation, mirror and inversion symmetries.

lattice [19, 20], which are driven by strong on-site and nearest neighbour repulsive interactions. The low-energy excitations are well described by Dirac fermions [17], which couple to the order-parameter fields and play a crucial role in determining the universal behaviour [1, 9]. In recent years GNY models and sign-free lattice Quantum Monte Carlo simulations have helped to push the understanding of fermionic criticality beyond the Ginzburg-Landau-Wilson (GLW) paradigm [14, 23–32].

Strong parallels can be drawn between the high energy and condensed matter settings. Remarkably, the quantum critical fixed point exhibits emergent Lorentz invariance with a characteristic terminal velocity and dynamical exponent $z = 1$ [18, 121–123]. Also, the emergent chiral symmetry is spontaneously broken in the ordered phase, opening a mass gap in the Dirac spectrum.

Yet it is precisely the reduction from Poincaré symmetry to the crystallographic space groups that allows the solid-state to host exotic fermionic quasiparticles [124]. An example are the recently discovered multifolds that are higher spin generalisations of Weyl fermions with no elementary particle analogs [125, 126]. More relevant to the current discussion are the semi-Dirac [45–47] fermions with relativistic and non-relativistic dynamics along orthogonal directions, which are known to exist at the critical point of topological phase transitions in two and three spatial dimensions [48].

In this Chapter Lorentz violating quantum critical points in Dirac fermion systems with spontaneously broken crystal symmetries are investigated. It is shown that the effective field theories contain order parameter fields that couple to the Dirac fermions as components of emergent gauge fields, in addition to the standard mass fields. This is illustrated for the honeycomb lattice where strong next-nearest neighbour repulsions induce charge density wave order (CDW_3) with a three fold increased unit cell [68, 70, 79–88] (see Fig. 4.1).

The fermion-induced (multi-)critical fixed point [23] is characterised using a perturbative renormalisation-group (RG) analysis. The results show that the broken symmetry state is in the vicinity of a topological critical point. This demonstrates that topological phase transitions in Dirac systems can be comprehensively described by effective field theories containing mass- and non-Abelian gauge fields.

The rest of this Chapter is organised as follows. Section 4.2 derives the low-energy theory of lattice symmetry breaking charge order on the honeycomb lattice. Section 4.3 presents an introduction to the renormalisation group. Section 4.4 presents the scaling of the low-energy theory. Section 4.5 discusses in detail the Gross-Neveu-Yukawa theory, which describes the sublattice CDW quantum critical point. The renormalisation group equations are derived in detail, and the critical properties of the ensuing non-trivial fixed point analysed. Section 4.6 presents the renormalisation group analysis of the lattice symmetry breaking effective field theory and the criticality is contrasted with Gross-Neveu-Yukawa theory. Section 4.7 analyses the broken symmetry state by minimising the free energy obtained from integrating out the fermions. Section 4.8 ends the chapter with a discussion of the results.

4.2 Lattice Symmetry Breaking Charge Order on the Honeycomb Lattice

As a concrete example of the effects of lattice symmetry breaking on fermionic quantum criticality the honeycomb lattice at half-filling and zero temperature, subject to nearest (V_1) and next-nearest (V_2) neighbour repulsive interactions are once more

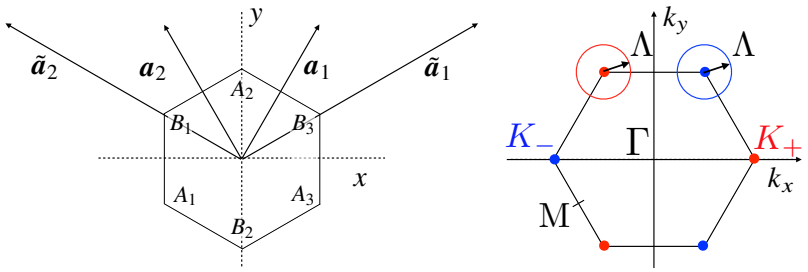

Figure 4.2: (Left) Honeycomb lattice with the primitive ($\boldsymbol{a}_{1,2}$) and plaquette ($\tilde{\boldsymbol{a}}_{1,2}$) lattice vectors, as well as the plaquette labelings $A_1, \ldots, B_3$. (Right) Brillouin zone corresponding to the $A-B$ unit cell. Low-energy Dirac fermion excitations are located at $\boldsymbol{K}_\pm$.

considered.

4.2.1 Dirac Fermions

In this discussion it is useful to highlight some algebraic properties of the effective field theory of Dirac fermions [20]

$$L_\Psi = \Psi^\dagger \left[\partial_\tau + i v_F \boldsymbol{\alpha}\cdot\boldsymbol{\partial}\right]\Psi = \Psi^\dagger\left[(-ik_0 + v_F \boldsymbol{k}\cdot\boldsymbol{\alpha}\right]\Psi, \tag{4.1}$$

where $\boldsymbol{\alpha} = (\sigma_x\otimes\tau_z, \sigma_y\otimes\tau_0)$ and $\boldsymbol{\partial} = (\partial_x, \partial_y)$. With $\alpha_z = \sigma_z\otimes\tau_z$, $\boldsymbol{\alpha}$ form an $SU(2)$ pseudospin algebra $[\alpha_i, \alpha_j] = 2i\sum_{k=x}^{z}\epsilon_{ijk}\alpha_k$ and $\{\alpha_i, \alpha_j\} = 2\delta_{ij}\alpha_0$, with the (implicit) identity $\alpha_0 = \sigma_0\otimes\tau_0$. Here ϵ_{ijk} is the antisymmetric Levi-Civita tensor.

Eq. (4.1) is endowed with emergent intravalley spatial rotational symmetry $\Psi \to e^{i\theta\alpha_z/2}\Psi$ $[\boldsymbol{k} \to (k_x\cos\theta - k_y\sin\theta, k_x\cos\theta + k_y\sin\theta)]$ and emergent global $SU(2)$ chiral/gauge symmetry $\Psi \to e^{i\sum_{a=1}^{3}\theta^a T^a}\Psi$ that is generated by $T^1 = -\sigma_y\otimes\tau_y$, $T^2 = \sigma_y\otimes\tau_x$ and $T^3 = \sigma_0\otimes\tau_z$. (T^1, T^2, T^3) also form a pseudospin algebra with identity T^0, and commute with α_i. In addition, Eq. (4.1) has emergent pseudo-relativistic invariance where the "speed of light" is v_F. This Lorentz invariance is exposed using the Dirac gamma matrices γ, in which covariant form is achieved, $L_\Psi = \sum_{\mu=\tau,x,y}(\Psi^\dagger\gamma_0)\gamma_\mu\partial_\mu\Psi$ (temporarily setting $v_F = 1$). The γ matrices are defined in Section 4.4.

4.2.2 Symmetries from the Honeycomb Lattice

The low-energy effective Hamiltonian

$$H = \int_{\boldsymbol{k}}^{\Lambda} \Psi_{\boldsymbol{k}}^{\dagger} H(\boldsymbol{k}) \Psi_{\boldsymbol{k}}, \text{ with } H(\boldsymbol{k}) = v_F \boldsymbol{k} \cdot \boldsymbol{\alpha}, \tag{4.2}$$

also inherits the symmetries of the non-interacting honeycomb lattice Hamiltonian $H_t = -t \sum_{\langle i,j \rangle} c_i^{\dagger} c_j$ (and Eq. (2.3)) that was discussed in Section 2.2 [20, 127]. There are the reflection symmetries in the x and y planes, which respectively are $R_x = \alpha_x T^3 = \sigma_x \otimes \tau_0$ $[k_y \to -k_y]$ and $R_y = \alpha_y T^2 = \sigma_0 \otimes \tau_x$ $[k_x \to -k_x]$ such that

$$R_x H(k_x, -k_y) R_x^{-1} = H(k_x, k_y) \text{ and } R_y H(-k_x, k_y) R_y^{-1} = H(k_x, k_y). \tag{4.3}$$

R_x interchanges the sublattices, as can be seen from the lattice in Fig. 4.2. R_y interchanges the Dirac valleys, as can be seen from the Brillouin zone in Fig. 4.2. Together $R_x R_y = \alpha_z T^1 = \sigma_x \otimes \tau_x$ $[\boldsymbol{k} \to -\boldsymbol{k}]$ defines spatial inversion, equivalent to a C_2 π rotation. The honeycomb lattice also has three-fold rotational symmetry $C_3 = e^{\pm 2\pi i \alpha_z/3}$ $[\boldsymbol{k} \to (-k_x \mp \sqrt{3}k_y, \pm\sqrt{3}k_x - k_y)/2]$, which is constructed such that [127]: it is diagonal in valley and sublattice, $(C_3)^3 = 1$ (hence $2\pi/3$), and it commutes with C_2. The translation symmetry under the primitive lattice vectors $\boldsymbol{a}_1 = \frac{\sqrt{3}}{2}(1, \sqrt{3})$, $\boldsymbol{a}_2 = \frac{\sqrt{3}}{2}(-1, \sqrt{3})$ is enacted by $t_{\boldsymbol{a}_{1,2}} = e^{i\boldsymbol{K}_+ \cdot \boldsymbol{a}_{1,2} T^3} = e^{\pm 2\pi i T^3/3}$, where $\boldsymbol{K}_\tau = 4\pi/3\sqrt{3}(\tau, 0)$ is the location of the Dirac points. That $T^3 = \sigma_0 \otimes \tau_z$ is the generator of translations follows from the action of a primitive translation on Ψ, where it is clear it must be valley dependent. From the properties of Bloch waves it is the case that under primitive translations $c_{\boldsymbol{k}} \to e^{i\boldsymbol{k} \cdot \boldsymbol{a}_{1,2}} c_{\boldsymbol{k}}$. It then follows that

$$(\psi_{\boldsymbol{k}}^{A+}, \psi_{\boldsymbol{k}}^{A-}, \psi_{\boldsymbol{k}}^{B+}, \psi_{\boldsymbol{k}}^{B-}) \to (e^{i\boldsymbol{K}_+ \cdot \boldsymbol{a}_{1,2}} \psi_{\boldsymbol{k}}^{A+}, e^{i\boldsymbol{K}_- \cdot \boldsymbol{a}_{1,2}} \psi_{\boldsymbol{k}}^{A-}, e^{i\boldsymbol{K}_+ \cdot \boldsymbol{a}_{1,2}} \psi_{\boldsymbol{k}}^{B+}, e^{i\boldsymbol{K}_- \cdot \boldsymbol{a}_{1,2}} \psi_{\boldsymbol{k}}^{B-}), \tag{4.4}$$

where it is understood that $\psi_{\boldsymbol{k}}^{\sigma\tau} = \psi^{\sigma}(\boldsymbol{k} + \boldsymbol{K}_\tau)$ is the small $\boldsymbol{k}$ expansion around the Dirac point $\boldsymbol{K}_\tau$.

In addition, the theory has the discrete time reversal $\mathcal{T}$, chiral $\mathcal{S}$ and particle-hole $\mathcal{C}$ symmetries [93], $\mathcal{X} H \mathcal{X}^{-1} = H$ for $\mathcal{X} = \mathcal{T}, \mathcal{S}, \mathcal{C}$, and with $\mathcal{T}\mathcal{S} = \mathcal{C}$. Time

reversal is the antiunitary operation $\mathcal{T} = \alpha_y T^2 \mathcal{K} = \sigma_0 \otimes \tau_x \mathcal{K}\,[\boldsymbol{k} \to -\boldsymbol{k}]$, where $\mathcal{K}$ is complex conjugation, from which it follows that $\mathcal{T} H^*(-\boldsymbol{k})\mathcal{T}^{-1} = H(\boldsymbol{k})$. Also, it is evident that $\mathcal{T}$ interchanges the Dirac valleys. Chiral symmetry $\mathcal{S}$ is a property of any nearest neighbour hopping fermionic model on a bipartite lattice $H_{AB} = \sum_{\langle ij \rangle} t_{ij} c_i^\dagger c_j$. It is the operation under which $c_A \to c_B^\dagger$, $c_B \to -c_A^\dagger$, or equivalently $(c_A, c_B) \to \sigma_z (c_A, c_B)^\dagger$, where the minus sign accounts for fermion anticommutation. Following this, here the chiral operation $\mathcal{S} = \alpha_z T^3 = \sigma_z \otimes \tau_0$, and is sometimes known as the energy reflection symmetry because $\mathcal{S} H(\boldsymbol{k}) \mathcal{S}^{-1} = -H(\boldsymbol{k})$. Finally, the particle-hole (or charge conjugation) operation is the combination of the two, leading to $C = \alpha_x T^1 \mathcal{K} = -\sigma_z \otimes \tau_x \mathcal{K}\,[\boldsymbol{k} \to -\boldsymbol{k}]$, from which it follows that $C H^*(-\boldsymbol{k}) C^{-1} = -H(\boldsymbol{k})$. Additional real hopping terms, such as the next-nearest neighbour t_2 would break the particle-hole symmetry, but particle-hole would still be an emergent symmetry of the low-energy Dirac theory. In contrast, a finite chemical potential that deviates from half-filling breaks the particle-hole symmetry.

4.2.3 Hubbard-Stratonovich Decoupling

Sufficiently strong V_2 stabilises CDW_3 order (Fig. 4.1). The steps discussed previously to obtain the general effective field theory of charge order are repeated for clarity. (1) The interaction is decoupled in the charge channel with the Hubbard-Stratonovich transformation

$$e^{-\int_\tau (V_1 \sum_{\langle i,j \rangle} \hat{n}_i \hat{n}_j + V_2 \sum_{\langle\langle i,j \rangle\rangle} \hat{n}_i \hat{n}_j)} = \int D[\boldsymbol{\rho}] \exp\left\{ -\int_\tau \sum_{\boldsymbol{k}} [\boldsymbol{\rho}_{\boldsymbol{k}}^\dagger(\tau) \cdot \boldsymbol{V}_{\boldsymbol{k}} \cdot \boldsymbol{\rho}_{\boldsymbol{k}}(\tau) + 2\hat{\boldsymbol{n}}_{\boldsymbol{k}}^\dagger(\tau) \cdot \boldsymbol{V}_{\boldsymbol{k}} \cdot \boldsymbol{\rho}_{\boldsymbol{k}}(\tau)] \right\}. \tag{4.5}$$

This introduces six auxiliary charge fields $\boldsymbol{\rho} = (\rho_{A_1}, \rho_{A_2}, \rho_{A_3}, \rho_{B_1}, \rho_{B_2}, \rho_{B_3})$, which are conjugate to the density $\hat{n}$ on each site of the plaquette. In addition, the transfor-

mation matrix is introduced

$$\boldsymbol{V_k} = -\frac{1}{2}\begin{pmatrix} 0 & V_2 e_{\bar{1}3} & V_2 e_{\bar{1}2} & V_1 & V_1 & V_1 e^{i\boldsymbol{k}\cdot\tilde{\boldsymbol{a}}_{\bar{1}}} \\ V_2 e_{1\bar{3}} & 0 & V_2 e_{2\bar{3}} & V_1 & V_1 e^{i\boldsymbol{k}\cdot\tilde{\boldsymbol{a}}_{\bar{3}}} & V_1 \\ V_2 e_{1\bar{2}} & V_2 e_{\bar{2}3} & 0 & V_1 e^{i\boldsymbol{k}\cdot\tilde{\boldsymbol{a}}_{\bar{2}}} & V_1 & V_1 \\ V_1 & V_1 & V_1 e^{i\boldsymbol{k}\cdot\tilde{\boldsymbol{a}}_2} & 0 & V_2 e_{2\bar{3}} & V_2 e_{\bar{1}2} \\ V_1 & V_1 e^{i\boldsymbol{k}\cdot\tilde{\boldsymbol{a}}_3} & V_1 & V_2 e_{\bar{2}3} & 0 & V_2 e_{\bar{1}3} \\ V_1 e^{i\boldsymbol{k}\cdot\tilde{\boldsymbol{a}}_1} & V_1 & V_1 & V_2 e_{1\bar{2}} & V_2 e_{1\bar{3}} & 0 \end{pmatrix}, \tag{4.6}$$

with $e_{nm} = 1 + e^{i\boldsymbol{k}\cdot\tilde{\boldsymbol{a}}_n} + e^{i\boldsymbol{k}\cdot\tilde{\boldsymbol{a}}_m}$ and $\tilde{\boldsymbol{a}}_{\bar{n}} = -\tilde{\boldsymbol{a}}_n$, $n = 1, 2, 3$. Here $\tilde{\boldsymbol{a}}_1 = \frac{3}{2}(\sqrt{3}, 1)$ and $\tilde{\boldsymbol{a}}_2 = \frac{3a}{2}(-\sqrt{3}, 1)$ are the lattice vectors of the enlarged plaquette unit cell lattice. (2) The high energy modes are integrated out, with the projection $\mathcal{P}$. This obtains the location interaction

$$\begin{aligned} L_V = \Psi^\dagger \Big\{ & (V_2 - V_1/2)[\rho_{A_1} + \rho_{A_2} + \rho_{A_3} - \rho_{B_1} - \rho_{B_2} - \rho_{B_3}]\alpha_z T^3 \\ & + \frac{V_2}{4}[\rho_{A_1} - 2\rho_{A_2} + \rho_{A_3} - \rho_{B_1} + 2\rho_{B_2} - \rho_{B_3}]\alpha_x T^1 \\ & + \frac{\sqrt{3}V_2}{4}[-\rho_{A_1} + \rho_{A_3} - \rho_{B_1} + \rho_{B_3}]\alpha_y T^1 \\ & + \frac{\sqrt{3}V_2}{4}[-\rho_{A_1} + \rho_{A_3} + \rho_{B_1} - \rho_{B_3}]\alpha_x T^2 \\ & + \frac{V_2}{4}[-\rho_{A_1} + 2\rho_{A_2} - \rho_{A_3} - \rho_{B_1} + 2\rho_{B_2} - \rho_{B_3}]\alpha_y T^2 \\ & + (V_2 + V_1/2)[\rho_{A_1} + \rho_{A_2} + \rho_{A_3} + \rho_{B_1} + \rho_{B_2} + \rho_{B_3}]\alpha_0 T^0 \Big\} \Psi \\ & + V_1(\rho_{A_1} + \rho_{A_2} + \rho_{A_3})(\rho_{B_1} + \rho_{B_2} + \rho_{B_3}) \\ & + 3V_2(\rho_{A_1}\rho_{A_2} + \rho_{A_2}\rho_{A_3} + \rho_{A_3}\rho_{A_1} + \rho_{B_1}\rho_{B_2} + \rho_{B_2}\rho_{B_3} + \rho_{B_3}\rho_{B_1}), \end{aligned} \tag{4.7}$$

where the Yukawa coupling matrices between fermions and dynamical order parameter fields have been expressed in terms of the α and T matrices. Here the gradient terms have been suppressed in the interest of brevity. The relevant gradient terms are systematically included by the one-loop fermion bubbles, and are discussed in more detail below. The half-filling condition is $\rho_{A_1} + \rho_{A_2} + \rho_{A_3} + \rho_{B_1} + \rho_{B_2} + \rho_{B_3} = 0$.

4.2.4 Low-Energy Theory

To analyse the criticality the charge order symmetry must not be broken by hand, as it was in Chapter 3. It is convenient to introduce the dynamical order parameter fields ρ_0, ϕ, $\boldsymbol{A}^1 = (A^1_x, A^1_y)$, $\boldsymbol{A}^2 = (A^2_x, A^2_y)$ with

$$\begin{pmatrix} \rho_0 \\ \phi \\ A^1_x \\ A^1_y \\ A^2_x \\ A^2_y \end{pmatrix} = \frac{1}{6} \begin{pmatrix} \sqrt{6} & \sqrt{6} & \sqrt{6} & \sqrt{6} & \sqrt{6} & \sqrt{6} \\ \sqrt{6} & \sqrt{6} & \sqrt{6} & -\sqrt{6} & -\sqrt{6} & -\sqrt{6} \\ \sqrt{3} & -2\sqrt{3} & \sqrt{3} & -\sqrt{3} & 2\sqrt{3} & -\sqrt{3} \\ -3 & 0 & 3 & 3 & 0 & -3 \\ -3 & 0 & 3 & -3 & 0 & 3 \\ -\sqrt{3} & 2\sqrt{3} & -\sqrt{3} & -\sqrt{3} & 2\sqrt{3} & -\sqrt{3} \end{pmatrix} \begin{pmatrix} \rho_{A_1} \\ \rho_{A_2} \\ \rho_{A_3} \\ \rho_{B_1} \\ \rho_{B_2} \\ \rho_{B_3} \end{pmatrix}, \tag{4.8}$$

and $\rho_0 = 0$ at half-filling. The corresponding charge patterns on the hexagonal unit cell that are induced by $\phi, \boldsymbol{A}^{1,2}$ are shown in Fig. 4.3. In fact, the terms obtained are precisely the irreducible representations of the point group $C''_{6v} = (1 + t_{\boldsymbol{a}_1} + t_{\boldsymbol{a}_1})C_{6v}$ containing primitive translations $t_{\boldsymbol{a}_{1,2}}$ [127, 128]. Here ϕ transforms as the B_2 irreducible representation and $(\boldsymbol{A}^1, \boldsymbol{A}^2)$ transform like the 4-components of G. The components mix into each other under primitive translations $\Psi \rightarrow e^{\pm 2\pi i T^3/3}\Psi$, thereby breaking the translational symmetry of C_{6v} (the primitive unit cell). Also, it is important to note that $(A^1_x, A^1_y, A^2_x, A^2_y)$ are (even, odd, odd, even) under reflections in the x axis (R_x), and (odd, even, odd, even) under reflections in the y axis (R_y). This can be seen by inspection of Fig. 4.3 and distinguishes each of the components.

Finally, the effective local Yukawa Lagrangian that couples Dirac fermions and dynamical order parameter fields has the compact form

$$L_g = \Psi^\dagger \left(g_\phi \phi \alpha_z T^3 + g_A \boldsymbol{\alpha} \cdot \boldsymbol{A}^a T^a \right) \Psi, \tag{4.9}$$

where the summation over repeated $a = 1, 2$ is used throughout. The bare effective couplings are related to the lattice couplings $(g_\phi)_0 = \sqrt{3/2}(V_1 - 2V_2)$ and $(g_A)_0 = \sqrt{3}/2V_2$. Note that L_g preserves emergent spatial rotational and $U(1)$ chiral symmetry, but breaks breaks Lorentz invariance. In addition, the bare Hubbard-

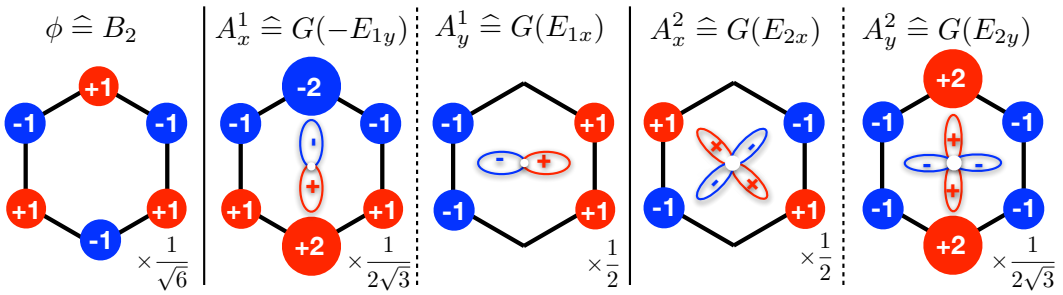

Figure 4.3: All possible charge instabilities in the 6-site unit cell on the half-filled honeycomb lattice. Charge modulation is shown relative to half-filling. They are labelled with the order parameter fields that couple to the Dirac fermions in the effective field theory, as well as the corresponding elements in symmetry groups C_{6v}'' and C_{6v} in parentheses.

Stratonovich bosonic mass term is

$$L_{\text{HS}} = \sqrt{3/2}(g_\phi)_0\phi^2 + \sqrt{3}(g_A)_0 A^2. \tag{4.10}$$

4.2.4.1 Mass Sector

In the regime $V_1 \gg V_2$ the order parameter ϕ describes the quantum phase transition from the semimetal into the CDW insulator that spontaneously breaks sublattice exchange symmetry, $\Psi \to R_x\Psi, \phi \to -\phi$. This corresponds to Z_2 chiral symmetry breaking in the low energy effective field theory [129], where the dynamics of ϕ are encapsulated by the Lagrangian

$$L_\phi = \frac{1}{2}\phi\left(-\partial_\tau^2 - c_\phi^2\partial^2 + m_\phi^2\right)\phi, \tag{4.11}$$

with $\partial^2 = \partial_x^2 + \partial_y^2$. At the bare level of the Hubbard-Stratonovich (prior to integrating out any fermionic or bosonic modes) the bosonic mass $(m_\phi^2)_0 = 3/2(V_1 - 2V_2)$. The convention in this Thesis is to always redefine the bosonic order parameter masses by their fixed point values $m_\phi^2 \to m_\phi^2 - (m_\phi^2)_*$. Then the fermionic quantum critical point $m_\phi^2 = 0$ belongs to the Z_2 GNY or chiral Ising universality class. The properties of this critical fixed point have been intensively studied with a variety of techniques, see Refs. [130, 131] for a review. The basic properties are discussed at length in Section 4.5.

The anticommutation $\{H_0, \Psi^\dagger \alpha_z T^3 \Psi\} = 0$ identifies ϕ as a mass field that opens a gap $\langle g_\phi \phi \rangle$ [132, 133]. All possible mass terms of 4-component Dirac fermions are enumerated by $M^\mu \alpha_z T^\mu$ for $\mu = 0, 1, 2, 3$. Only the sublattice CDW mass [17] ($M^3 = \phi$) is considered here. The other terms arise from bond order $\langle c_i^\dagger c_j \rangle$ on the honeycomb lattice. The Haldane quantum anomalous Hall mass $M^0 \alpha_z T^0$ [37] was discussed in Chapter 3. Additionally, $(M^1 \alpha_z T^1, M^2 \alpha_z T^2)$ correspond to the mass fields of the Kekulé valence bond solid phase (shown in Fig. 3.2(b)), which form an XY order parameter [23, 24, 134].

4.2.4.2 Emergent Gauge Sector

In the low-energy $\boldsymbol{A}^{1,2}$ minimally couple as components of an emergent $SU(2)$ non-Abelian local gauge theory generated by T^a. This is revealed by the local Lagrangian

$$L_\Psi + L_{g_A} = \Psi^\dagger \left[\partial_\tau + i\boldsymbol{\alpha} \cdot (v_F \boldsymbol{\partial} - i g_A \boldsymbol{A}^a T^a) \right] \Psi, \tag{4.12}$$

with $\boldsymbol{\partial} = (\partial_x, \partial_y)$. To avoid integrating over the emergent gauge redundancies, the theory is gauge fixed in the R_ξ gauge by following the Fadeev-Popov procedure, which is discussed in further detail in Appendix B.1. The result is the gauge fixed Lagrangian of the critical low-energy theory is

$$L_A = \sum_{i,j=x,y} \frac{1}{2} A_i^a \left(-\delta_{ij} (\partial_\tau^2 + \partial^2 + m_A^2) - \frac{1-\xi}{\xi} \partial_i \partial_j \right) A_j^a, \tag{4.13}$$

which is invertible for all finite ξ. It is convenient to use the Feynman-'t Hooft gauge $\xi = 1$, where the Lagrangian is isotropic

$$L_A = \frac{1}{2} \boldsymbol{A}^a \cdot \left(-\partial_\tau^2 - c_A^2 \partial^2 + m_A^2 \right) \boldsymbol{A}^a. \tag{4.14}$$

The universal behaviour should not depend on the choice of gauge.

The bosonic mass m_A^2 is finite from the lattice Hubbard-Stratonovich transformation with the bare mass $(m_A^2)_0 = 3/2V_2$. This implies that $\boldsymbol{A}^{1,2}$ can have finite order parameter expectation values [135–137], which is expected from the lattice model where A are linear combinations of charge order parameters. This is in

contrast to the standard Yang-Mills theory, where $m_A^2 = 0$ is enforced by a Ward identity.

4.2.4.3 Bosonic Self-Interactions

From symmetry considerations, or alternatively by integrating out high energy fermionic modes, one obtains the bosonic self-interaction

$$L_\lambda = \lambda_\phi \phi^4 + \lambda_A A^4 + \lambda_{\phi A} \phi^2 A^2 + \lambda_{\mathrm{YM}} (\boldsymbol{A}^1 \times \boldsymbol{A}^2)^2, \tag{4.15}$$

where $A = \sqrt{\boldsymbol{A}^a \cdot \boldsymbol{A}^a}$. The Yang-Mills term λ_{YM} reflects the underlying emergent non-Abelian gauge structure.

4.2.4.4 Bosonic Cubic Terms and Particle-Hole Symmetry

In the low-energy theory there is the symmetry allowed cubic term $\tilde{b}\phi(\boldsymbol{A}^1 \times \boldsymbol{A}^2)$. This is because $\boldsymbol{A}^1 \times \boldsymbol{A}^2$ preserves the emergent global chiral symmetry $\Psi \to e^{i\theta T^3}\Psi$, under which $\boldsymbol{A}^1 \to \boldsymbol{A}^1 \cos\theta - \boldsymbol{A}^2 \sin\theta$ and $\boldsymbol{A}^2 \to \boldsymbol{A}^1 \sin\theta + \boldsymbol{A}^2 \cos\theta$. Spatial rotational symmetry $\Psi \to e^{i\theta\alpha_z}\Psi$ is also preserved, under which $A_x^a \to A_x^a \cos\theta - A_y^a \sin\theta$ and $A_y^a \to A_x^a \sin\theta + A_y^a \cos\theta$. Note the useful double-complex representation $G = G_1 + jG_2$ with $G_a = A_x^a + iA_y^a$, in which spatial rotations are implemented by $e^{i\theta}$ and chiral transformations are implemented by $e^{j\theta}$. Yet, the non-interacting theory is particle-hole symmetric, see Section 4.2.2, where as the Yukawa terms in L_g, Eq. (4.9), are all particle-hole odd $CL_gC^{-1} = -L_g$. Therefore the cubic terms are forbidden as all loop corrections vanish by symmetry

$$\langle \Psi^\dagger \alpha_z T^3 \Psi \Psi^\dagger \alpha_i T^a \Psi \Psi^\dagger \alpha_j T^b \Psi \rangle \to -\langle \Psi^\dagger \alpha_z T^3 \Psi \Psi^\dagger \alpha_i T^a \Psi \Psi^\dagger \alpha_j T^b \Psi \rangle = 0. \tag{4.16}$$

This is in accordance with Furry's theorem [9], which states that odd-legged fermion loops that are odd under a discrete Z_2 symmetry of the non-interacting theory must vanish.

Similarly, the reduced lattice symmetry group C_{6v}'' allows for the lattice cubic term $b\mathrm{Im}[G_2^3 - 3G_1^2 G_2]$, where $G_a = A_x^a + iA_y^a$. This term is not generated by the Dirac fermion loops, as they possess the higher continuous spatial rotational

symmetry, which is discrete on the lattice. One way to identify this term is using the double complex representation. The cubic term is identified by first decomposing G^3 into the real (R) and imaginary (I) parts in complex i and j

$$G^3 = (G^3)_{\mathrm{RR}} + j(G^3)_{\mathrm{IR}} + i(G^3)_{\mathrm{RI}} + ij(G^3)_{\mathrm{II}}. \tag{4.17}$$

Each of the four terms is individually invariant under primitive translations $G \to e^{j2\pi/3}G$ and C_3 rotations $G \to e^{i2\pi/3}G$. However, only $(G^3)_{\mathrm{II}} = \mathrm{Im}[G_2^3 - 3G_1^2G_2]$ is invariant under reflections $R_{x,y}$ in x and y planes. This can be checked by inspecting

$$\mathrm{Im}[G_2^3 - 3G_1^2G_2] = -6A_x^1A_x^2A_y^1 + 3\left[(A_y^1)^2 - (A_x^1)^2 + (A_x^2)^2\right]A_y^2 - (A_y^2)^3, \tag{4.18}$$

where $(A_x^1, A_y^1, A_x^2, A_y^2)$ transform as $(+,-,-,+)$ in R_x and $(-,+,-,+)$ and in R_y. Repeating this type of analysis the symmetry allowed lattice quartic term is found ϕG^3 results in $\phi\,\mathrm{Re}[G_1^3 - 3G_1G_2^2]$.

However, even if the particle-hole symmetry is relaxed, these analytic low-energy and lattice cubic terms vanish at the fermionic critical point, which is an example of fermion-induced quantum criticality [23]. These terms will be neglected in the main renormalisation group analysis, but this topic is addressed in Section 4.6.4.

Finally, an important clarification is in order, as it may appear that finite order parameter expectation values are forbidden by this symmetry. This is of course not the case. Instead it indicates that spontaneous symmetry breaking is a non-perturbative effect, and that it requires expectation values to be self-consistently calculated with respect to the broken symmetry state. This is achieved in Chapter's 2 and 3 with the saddle-point expansion where the order parameter explicitly enters the fermionic self-energy, and is equivalent to an infinite order resummation of diagrams. This feature is present but somewhat hidden in the coupled renormalisation group equations.

4.3 Introduction to the Renormalisation Group

Relevant aspects of the renormalisation group are introduced. A more complete description can be found in the following selection of textbooks and review articles [1, 5, 8, 9, 138, 139]. Quantum (multi-)critical points are described by scale invariant fixed points of the renormalisation group (RG) transformation $k_i' = k_i e^{\ell}$, $k_0' = k_0 e^{z\ell}$. Here z is the dynamical exponent indicating discrepancies in the scaling of space $x' = x^{-\ell}$ and imaginary time $\tau' = \tau e^{-z\ell}$. This allows for a mapping of a d-spatial dimensional quantum field theory to a $d+z$ classical field theory. Then the perturbative Wilson momentum shell scheme [6] can be used to identify universal features of the action $S = \int_{\tau,\boldsymbol{r}} L$, with

$$L = L_\Psi + L_\phi + L_A + L_g + L_\lambda. \tag{4.19}$$

The Wilson momentum shell formulation of the renormalisation group is essentially a three step procedure. (1) Integrate over the infinitesimal fraction of "fast" modes in the momentum shell $\Lambda e^{-\delta\ell} \leq |\boldsymbol{k}| \leq \Lambda$ (and all frequency modes $-\infty \leq k_0 \leq \infty$) corresponding to the highest energies. Here $\delta\ell$ is used to emphasise the transformation is infinitesimal. (2) Rescale the "slow" modes $k \rightarrow k_i' = k_i e^{\delta\ell}$, such that the resulting theory has the same integration region as the original theory $\int_k^{\Lambda e^{-\delta\ell}} \rightarrow \int_k^{\Lambda}$. (3) Identify the set of renormalised coupling constants $x_i(\ell + \delta\ell) = x_i(\ell) + F_i(\{x_j(\ell)\})\delta\ell$, where F_i are the set of renormalisation corrections that depend on the couplings. In the current case $x_i = (g_\phi^2, g_A^2, \lambda_\phi, \lambda_A, \lambda_{\rm YM}, \lambda_{\phi A}, m_\phi^2, m_A^2)$. Steps (1-3) are repeated in a self-consistent manner until no new couplings x_i are generated. This iterative procedure is encapsulated by the set of renormalisation group equations (coupled differential equations, or recursion relations)

$$\frac{d}{d\ell} x_i(\ell) = F_i(\{x_j(l)\}). \tag{4.20}$$

The solutions of Eq. (4.20) define scale invariant fixed points $(x_i)_*$ in the coupling parameter space. Scale invariance implies that there is no defining length scale, as is the case at a critical point of a continuous phase transition where the

correlation length diverges, $\xi \to \infty$. Fixed points can be characterised by the linearised RG flow in their vicinity

$$\frac{d}{d\ell}x_i = \sum_j M_{ij}(x_j - (x_j)_*), \tag{4.21}$$

with the stability matrix

$$M_{ij} = \frac{\partial}{\partial x_j}\frac{d}{d\ell}x_i\bigg|_{x_i=(x_i)_*}. \tag{4.22}$$

Negative eigenvalues of the stability matrix corresponds to eigendirections in the parameter space whose couplings converge to their respective fixed point values under the RG flow. These define *irrelevant* perturbations at the fixed point. In contrast, positive eigenvalues correspond to eigendirections where the couplings diverge from the fixed point values. These define *relevant* perturbations at the fixed point.

A critical fixed point is defined by a single relevant eigenperturbation m^2, with θ_{m^2} the single positive eigenvalue of M, and which corresponds to the tuning parameter of the continuous phase transition $m^2 \sim |V - V_c|$. This is related to the correlation length exponent ν

$$\xi \sim |V - V_c|^{-\nu} \Rightarrow \xi \sim \left|m^2\right|^{-\nu}. \tag{4.23}$$

In addition, the correlation length is identified as the characteristic scale $\xi = e^{l_*}$ of the flow at which $m^2 e^{\theta_{m^2} l_*} = 1$ [1]. Thus $m^2 = \xi^{-\theta_{m^2}}$ and therefore $\theta_{m^2} = 1/\nu$. However, in the current context, there are two tuning parameters V_1, V_2 of the lattice model, which defines a quantum multicritical point. These corresponds to the two relevant perturbations of L which are the bosonic masses $m^2_{\phi,A}$.

The correlation length exponent ν, the dynamical exponent z, and the anomalous dimension η can be extracted from RG analysis of the critical fixed point. Assuming that the system satisfies hyperscaling, the standard scaling relations obtain the remaining critical exponents [140]. The Josephson hyperscaling relation $2 - \alpha = \nu(d + z)$ gives the specific heat exponent $C = -T\partial_T^2 f \sim |T - T_c|^\alpha$. The

Fisher scaling relation $\gamma = \nu(2-\eta)$ gives the order parameter susceptibility exponent $\chi = \partial_h^2 f \sim (-m^2)^{-\gamma}$, where h is the symmetry breaking field conjugate to the order parameter ϕ_0. The Rushbrooke scaling relation $\alpha + 2\beta + \gamma = 2$ gives the order parameter critical exponent $\phi_0 = \partial_h f \sim (-m^2)^{\beta}$. Finally, the Widom scaling relation $\gamma = \beta(\delta - 1)$ gives the field exponent $\phi_0 \sim |h|^{1/\delta}$.

4.3.1 Perturbative Renormalisation Group

In the following the renormalisation group equations of L will be obtained to one-loop order, the (multi-)critical fixed points identified and their universal properties analysed. The one-loop corrections are obtained to all one-particle irreducible vertex functions. This procedure can be formulated with the cumulant expansion. The action is split $S = S_0 + S_{\text{int}}$ into non-interacting S_0 and interacting S_{int} parts

$$S_0 = \int L_\Psi + L_\phi + L_A \text{ and } S_{\text{int}} = \int L_g + L_\lambda. \tag{4.24}$$

Each field is split into slow $(\Psi^<, \phi^<, A^<)$ and fast $(\Psi^>, \phi^>, A^>)$ fields where, for example, $\phi^<$ contains only the slow Fourier components $0 \leq |\boldsymbol{k}| \leq \Lambda e^{-\delta\ell}$, whilst $\phi^>$ contains the fast Fourier components $\Lambda e^{-\delta\ell} \leq |\boldsymbol{k}| \leq \Lambda$. The cumulant expansion is

$$\begin{aligned}
Z &= \int D[\Psi^\dagger, \Psi, \phi, A] e^{-(S_0 + S_{\text{int}})}, \\
&= \left[\int D[\Psi^\dagger, \Psi, \phi, A] e^{-S_0}\right]_< \left[\int D[\Psi^\dagger, \Psi, \phi, A] e^{-S_0}\right]_> \sum_{n=0}^{\infty} \left(-\frac{S_{\text{int}}}{n!}\right)^n, \\
&= \left[\int D[\Psi^\dagger, \Psi, \phi, A] e^{-S_0}\right]_< \left\langle \sum_{n=0}^{\infty} \left(-\frac{S_{\text{int}}}{n!}\right)^n \right\rangle_>, \\
&= \left[\int D[\Psi^\dagger, \Psi, \phi, A] e^{-S_0}\right]_< e^{\left\langle \sum_{n=1}^{\infty} \left(-\frac{S_{\text{int}}}{n!}\right)^n \right\rangle_>^{\text{1PI, con}}}.
\end{aligned} \tag{4.25}$$

Here $\langle \cdots \rangle_>$ represents functional averages with respect to the fast modes of the non-interacting action, and therefore only fields over fast modes can be contracted. In the last line the linked-cluster theorem has been used to replace the logarithm over all possible diagrams with the sum over connected diagrams. In addition, the diagrams considered are restricted to the one-particle irreducible (1PI) vertex

functions, as these correspond to the renormalisation corrections to the bare action. In the following it assumed that all contractions are restricted to this variety, and the notation "1PI, con" will be suppressed. At one-loop order the contributions are from

$$-\left\langle \sum_{n=1}^{\infty} \left(-\frac{S_{\text{int}}}{n!}\right)^n \right\rangle_{>} = \langle S_\lambda \rangle_> - \frac{1}{2}\langle S_g^2 \rangle_> - \frac{1}{2}\langle S_\lambda^2 \rangle_> + \frac{1}{6}\langle S_g^3 \rangle_> - \frac{1}{24}\langle S_g^4 \rangle_> + O(\text{two-loop}). \tag{4.26}$$

4.3.2 Tree-Level Scaling of ϕ^4 Theory

Before obtaining the one-loop corrections, the zeroth order is analysed, which is also known as tree-level scaling. This procedure is illustrated in detail for the d-dimensional generalisation of the non-interacting ϕ action

$$S_\phi = \frac{1}{2}\int_{-\infty}^{\infty} dk_0 \int^{\Lambda} d^d\boldsymbol{k}\,\phi(k_0^2 + c_\phi^2\,|\boldsymbol{k}|^2 + m_\phi^2)\phi, \tag{4.27}$$

where $\boldsymbol{k} = (k_1, \ldots, k_d)$ is the d-dimensional momentum vector. Integrating out the high energy modes produces an unimportant multiplicative constant to the partition function. What remains is the action of the slow modes

$$(S_\phi)_< = \frac{1}{2}\int_{-\infty}^{\infty} dk_0 \int^{\Lambda e^{-\delta\ell}} d^d\boldsymbol{k}\,\phi(k_0^2 + c_\phi^2\,|\boldsymbol{k}|^2 + m_\phi^2)\phi. \tag{4.28}$$

Enacting the rescaling transformation $k_i \to k_i' = k_i e^{\delta\ell}$, $k_0 \to k_0' = k_0 e^{z\delta\ell}$

$$(S_\phi)_< = \frac{1}{2}\int_{-\infty}^{\infty} dk_0' \int^{\Lambda} d^d\boldsymbol{k}'\, e^{(d+z)\delta\ell}\phi(k_0'^2 e^{2z\delta\ell} + c_\phi^2\,|\boldsymbol{k}'|^2\, e^{2\delta\ell} + m_\phi^2)\phi. \tag{4.29}$$

The rescaling of the ϕ fields, $\phi \to \phi' = \phi e^{-\frac{(d+3z)}{2}\delta\ell}$, ensures that the frequency term k_0 is scale invariant

$$(S_\phi)_< = \frac{1}{2}\int_{-\infty}^{\infty} dk_0' \int^{\Lambda} d^d\boldsymbol{k}'\phi'(k_0'^2 + c_\phi^2\,|\boldsymbol{k}'|^2\, e^{2(1-z)\delta\ell} + m_\phi^2 e^{2z\delta\ell})\phi'. \tag{4.30}$$

Clearly if $z = 1$ then c_ϕ is dimensionless and an invariant of the flow, but the mass term $m_\phi'^2(\ell+\delta\ell) = m_\phi^2(\ell)e^{2z\delta\ell}$ grows under the flow. The non-interacting (Gaussian)

fixed point is situated at $m_\phi^2 = 0$, and m_ϕ^2 is a relevant perturbation at the fixed point.

The role of dimensionality is important when considering interactions. This is illustrated for the λ_ϕ term

$$\lambda_\phi \int \phi^4 \to \lambda_\phi e^{(d-3z)\delta\ell} \int' (\phi')^4, \tag{4.31}$$

and therefore $\lambda'_\phi(\ell + \delta\ell) = \lambda_\phi(\ell) e^{(3z-d)\delta\ell}$. Taking $z = 1$ at tree-level, such that the non-interacting action is scale invariant, it is evident that λ_ϕ is relevant (grows) for $d < 3$ at the non-interacting fixed point, but is irrelevant for $d > 3$. This defines $d = 3$ as the upper-critical dimension of the Lagrangian $L_\phi + \lambda_\phi \int \phi^4$, where λ_ϕ is scale invariant. The implication is that interactions are important below the upper critical dimension, and render the non-interacting fixed point at $\lambda_\phi = 0$ unstable. Beyond tree-level it is well understood that the system flows to the Wilson-Fisher fixed point. Where as, above the upper critical dimension the non-interacting fixed point is stable, and Landau mean-field theory exactly describes the universal behaviour.

The cumulant expansion truncated in the number of loops is an expansion around the non-interacting fixed point - averages are all taken with respect to S_ϕ. Below the upper critical dimension λ_ϕ grows

$$\frac{d}{d\ell}\lambda_\phi = (3 - d)\lambda_\phi, \tag{4.32}$$

and so this truncation cannot be controlled by assuming $\lambda_\phi \ll 1$. Instead, analytic control of quantum fluctuations can be obtained by expanding around the upper critical dimension with the small parameter $\epsilon = 3 - d$. Here ϵ allows for a systematic expansion in the number of loops.

4.4 Scaling of L in $d = 3 - \epsilon$ Spatial Dimensions

The scaling of the Lagrangian $L = L_\Psi + L_\phi + L_A + L_g + L_\lambda$ is presented. Under the spacetime rescaling the fermion and boson fields rescale as

$$\Psi'(k') = \Psi(k) e^{-(2z+d-\eta_\Psi)\frac{\delta\ell}{2}} \tag{4.33}$$

$$\phi'(k') = \phi(k) e^{-(3z+d-\eta_\phi)\frac{\delta\ell}{2}} \tag{4.34}$$

$$\boldsymbol{A}^{a\prime}(k') = \boldsymbol{A}^{a}(k) e^{-(3z+d-\eta_A)\frac{\delta\ell}{2}} \tag{4.35}$$

where $\eta_{\Psi,\phi,A}$ are the anomalous dimensions that account for the beyond tree-level corrections to the field rescaling, and $k = (k_0, \boldsymbol{k})$ with the d-dimensional $\boldsymbol{k}$. The field rescalings impose scale invariance on the frequency components.

The non-interacting part of the action must be invariant under the spacetime rescaling. At tree-level the velocities are invariant for $z = 1$

$$v_F \to v_F e^{(z-1)\delta\ell},\ c^2_{\phi,A} \to c^2_{\phi,A} e^{2(z-1)\delta\ell} \tag{4.36}$$

Criticality is accessed by tuning the relevant bosonic masses with scaling $m^2_{\phi,A} \to m^2_{\phi,A} e^{2z\delta\ell}$. The Yukawa and self-interactions are relevant perturbations at the non-interacting fixed point for $d < 3$ spatial dimensions

$$(g^2_{\phi,A}, \lambda_{\phi,A,\phi A,\mathrm{YM}}) \to e^{(3z-d)\delta\ell}(g^2_{\phi,A}, \lambda_{\phi,A,\phi A,\mathrm{YM}}). \tag{4.37}$$

This motivates an $\epsilon = 3 - d$ expansion. Further control is exerted by generalising to a large number N of fermionic flavours

$$\Psi^\dagger\Psi \to \sum_{n=1}^{N} \Psi^\dagger_n \Psi_n\,,\ (g^2_{\phi,A}, \lambda_{\phi,A,\phi A,\mathrm{YM}}) \to \frac{8\pi^2\Lambda^\epsilon}{N}(g^2_{\phi,A}, \lambda_{\phi,A,\phi A,\mathrm{YM}}), \tag{4.38}$$

which is known to favourably reorganise the perturbative expansion, and also enables perturbative RG directly in $d = 2$ [141]. Physically, N could be a generalisation of the number of spin flavours, which works well for charge ordering.

The dimensional continuation to $d = 3 - \epsilon$ dimensions (for $\epsilon > 0$ or $d < 3$) is best formulated with the anticommuting Dirac γ matrices

$$\gamma_0 = \alpha_z T^3,\ \gamma_1 = i\gamma_0\alpha_x,\ \gamma_2 = i\gamma_0\alpha_y,\ \gamma_3 = T^1,\ \gamma_5 = T^2, \gamma_{35} = -i\gamma_3\gamma_5 = T^3, \tag{4.39}$$

with $\{\gamma_\mu, \gamma_\nu\} = 2\delta_{\mu,\nu}\alpha_0$ for $\mu, \nu = 0, 1, 2, 3, 5$. The Lagrangian in continuous $d < 3$

spatial dimensions is

$$\begin{aligned} L = \sum_{n=1}^{N} \bar{\Psi}_n \Big[& \partial_\tau \gamma_0 + v_F \partial_i \gamma_i + \frac{g_\phi}{\sqrt{\tilde{N}}} \phi \\ & - \frac{i g_A}{\sqrt{\tilde{N}}} \left(\gamma_1 \gamma_3 A_x^1 + \gamma_2 \gamma_3 A_y^1 + \gamma_1 \gamma_5 A_x^2 + \gamma_2 \gamma_5 A_y^2 \right) \Big] \Psi_n \\ & + \frac{1}{2} \phi \left(-\partial_\tau^2 - c_\phi^2 \partial_i \partial_i + m_\phi^2 \right) \phi + \frac{1}{2} \boldsymbol{A}^a \cdot \left(-\partial_\tau^2 - c_A^2 \partial_i \partial_i + m_A^2 \right) \boldsymbol{A}^a \\ & + \frac{1}{\tilde{N}} \left[\lambda_\phi \phi^4 + \lambda_A A^4 + \lambda_{\phi A} \phi^2 A^2 + \lambda_{\mathrm{YM}} (\boldsymbol{A}^1 \times \boldsymbol{A}^2)^2 \right], \end{aligned} \tag{4.40}$$

where $\bar{\Psi} = \Psi^\dagger \gamma_0$ and the repeated summation over $i = 1, \ldots, d$, such that $\mathrm{tr} \gamma_i \gamma_i = 4d$. Also $\tilde{N} = N/8\pi^2 \Lambda^\epsilon$ is defined for brevity. Here and in the following the identity matrix α_0 is implicit $\bar{\Psi}\Psi = \bar{\Psi}\alpha_0\Psi$. Finally, the corresponding propagators are

$$G_\Psi(k_0, \boldsymbol{k}) = \frac{i(k_0 \gamma_0 + v_F k_i \gamma_i)}{k_0^2 + v_F^2 |\boldsymbol{k}|^2} \text{ and } G_{\phi,A}(k_0, \boldsymbol{k}) = \frac{1}{k_0^2 + c_{\phi,A}^2 |\boldsymbol{k}|^2 + m_{\phi,A}^2}. \tag{4.41}$$

4.5 Gross-Neveu-Yukawa Theory and CDW Criticality

In this and the following sections it will be demonstrated that the Yukawa couplings $g_{\phi,A}$ between Dirac fermions and dynamical order parameter bosons are relevant perturbations at the putative Wilson-Fisher fixed points ($\{\lambda_i\} \neq \{0\}$, $g_{\phi,A} = 0$), owing to the gapless nature of the fermion excitations. At the ensuing fermionic critical fixed points ($\{\lambda_i, g_{\phi,A}\} \neq \{0\}$) both the boson $\eta_{\phi,A}$ and fermion η_Ψ anomalous dimensions are finite, which indicates the breakdown of the quasiparticle picture and the onset of a non-Fermi liquid.

However, the coupling to a particular fluctuating order parameter field can be rendered irrelevant if the related bosonic mass is tuned far from critical [22, 29]. In this case the bosonic field can be integrated out and the corresponding fermion-fermion interaction, $V \sim O(g^2/m^2)$, will be vanishingly small. This is now schematically demonstrated for the scenario $m_A^2 \gg (m_A^2)_*$ and $m_\phi^2 = (m_\phi^2)_*$. With no loss of generality, in the following the linear shift $m_{\phi,A}^2 \to m_{\phi,A}^2 - (m_{\phi,A}^2)_*$ is made

such that $(m^2_{\phi,A})_* = 0$ by definition. Then in the large m_A^2 limit,

$$\begin{aligned} S_A + S_{g_A} + S_\lambda &= \int \frac{m_A^2}{2}\left[\frac{2ig_A}{m_A^2}\bar{\Psi}A\Psi + A\left(1-\frac{\partial^2}{m_A^2}\right)A + O\left(\frac{\lambda}{m_A^2}\right)\right] \\ &= \int \frac{g_A^2}{m_A^2}(\bar{\Psi}\Psi)^2 + \frac{m_A^2}{2}\left[\left(A+\frac{ig_A}{m_A^2}\right)^2 + O\left(\frac{\lambda}{m_A^2},\frac{\partial^2}{m_A^2}\right)\right], \end{aligned} \tag{4.42}$$

where in the second line the square has been completed and the A fields can be integrated out. The result is the Gross-Neveu model [22] with a vanishing four-fermion interaction $g_A^2/m_A^2\bar{\Psi}\Psi\bar{\Psi}\Psi$. This corresponds to $V_1 = (V_1)_c$ and $V_2 \ll (V_2)_c$ of the lattice model, where the system undergoes a continuous phase transition into the sublattice CDW phase with $\langle\phi\rangle \neq 0$.

The criticality is described by the the Gross-Neveu-Yukawa theory

$$\begin{aligned} L_{\mathrm{GNY}} = &\sum_{n=1}^{N}\bar{\Psi}_n\left(\partial_\tau\gamma_0 + v_F\partial_i\gamma_i + \frac{g_\phi}{\sqrt{\tilde{N}}}\phi\right)\Psi_n \\ &+ \frac{1}{2}\phi\left(-\partial_\tau^2 - c_\phi^2\partial_i\partial_i + m_\phi^2\right)\phi + \frac{\lambda_\phi}{\tilde{N}}\phi^4, \end{aligned} \tag{4.43}$$

which more generally describes Dirac fermions coupled to a dynamical Ising order parameter field, and has a non-trivial GNY or chiral Ising fermionic quantum critical fixed point, outside of the GLW paradigm. Here the one-loop RG equations of the GNY theory are calculated in detail, and the scaling properties of the fermionic critical point are discussed. Following this, the full set of RG equations for L defined in Eq. (4.40) are presented.

4.5.1 One-Loop Corrections

The one-loop corrections to the bare action

$$\hat{S}^<_{\mathrm{GNY}} = S^<_{\mathrm{GNY}} + \langle S_{\lambda_\phi}\rangle_> - \frac{1}{2}\langle S^2_{g_\phi}\rangle_> - \frac{1}{2}\langle S^2_{\lambda_\phi}\rangle_> + \frac{1}{6}\langle S^3_{g_\phi}\rangle_> - \frac{1}{24}\langle S^4_{g_\phi}\rangle_>, \tag{4.44}$$

amount to calculating the diagrams displayed in Fig. 4.4. The fields are split into slow and fast modes $\Psi = \Psi^< + \Psi^>$, $\phi = \phi^< + \phi^>$, and the fast modes are integrated

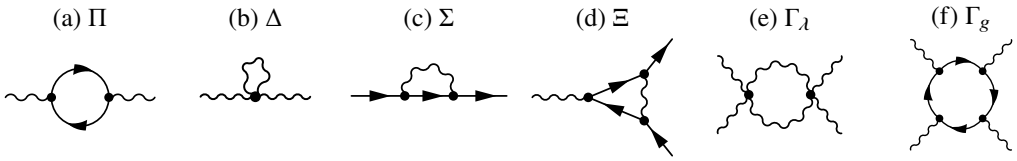

Figure 4.4: One-loop Feynman diagrams used to calculate the renormalisation group equations. Internal lines are contractions over fast modes. External lines are slow modes. The fermion propagator is denoted by the arrowed line. The boson propagators are denoted by the wavy line.

out.

4.5.1.1 Renormalisation to the Dynamical Order Parameter Field S_ϕ

The renormalisation to the ϕ propagator comes from contractions with two remaining external slow ϕ legs

$$\begin{aligned}\hat{S}_\phi^< &= S_\phi^< - \frac{1}{2}\langle S_{g_\phi}^2\rangle_> + \langle S_{\lambda_\phi}\rangle_>, \\ &= S_\phi^< + \frac{1}{2}\int_k^< \phi^<(-k)[\frac{N}{N}\Pi(k) + \frac{1}{N}\Delta]\phi^<(k). \end{aligned} \tag{4.45}$$

Here the factors of N have been extracted from the fermion loop diagrams Fig. 4.4(a) and 4.4(e), as well as the $g_\phi^2/N, \lambda_\phi/N$ terms. This fermionic N is shown explicitly for the fermion polarisation bubble/boson self-energy Π, shown in Fig. 4.4(a),

$$\begin{aligned}-\langle S_{g_\phi}^2\rangle_> &= -\frac{g_\phi^2}{\tilde{N}}\int_{k_1,k_2,k_4,k_5}^> \int_{k_3,k_6}^< \delta_{k_1-k_2-k_3}\delta_{k_4-k_5-k_6}\times \\ &\quad \sum_{n,m=1}^N \langle\bar{\Psi}_n^>(k_1)\Psi_n^>(k_2)\phi^<(k_3)\bar{\Psi}_m^>(k_4)\Psi_m^>(k_5)\phi^<(k_6)\rangle_>, \\ &= \frac{g_\phi^2}{\tilde{N}}\int_{k_1,k_2,k_4,k_5}^> \int_{k_3,k_6}^< \delta_{k_1-k_2-k_3}\delta_{k_4-k_5-k_6}\times \\ &\quad \sum_{n,m=1}^N \langle\Psi_m^>(k_5)\bar{\Psi}_n^>(k_1)\rangle_>\langle\Psi_n^>(k_2)\bar{\Psi}_m^>(k_4)\rangle_>\phi^<(k_3)\phi^<(k_6), \\ &= \frac{g_\phi^2}{\tilde{N}}\int_{k_1,k_2,k_4,k_5}^> \int_{k_3,k_6}^< \delta_{k_1-k_2-k_3}\delta_{k_4-k_5-k_6}\times \\ &\quad \sum_{n,m=1}^N \delta_{mn}\delta_{k_1-k_5}\delta_{k_2-k_4}\,\mathrm{tr}\,G\Psi(k_1)G\Psi(k_2)\phi^<(k_3)\phi^<(k_6), \end{aligned} \tag{4.46}$$

where $\langle \Psi_n \bar{\Psi}_m \rangle = G_\Psi \delta_{mn}$ as the propagator is diagonal in the fermion flavour. It is clear that an additional factor of N is obtained. In general, the loop contraction of M Yukawa vertices, constrains $M-1$ of the flavour sums, and the final free sum produces the factor of N

$$\begin{aligned}
\langle \prod_{m=1}^{M} \sum_{n_m=1}^{N} \bar{\Psi}_{n_m} \Psi_{n_m} \rangle &= -\left(\prod_{m=1}^{M} \sum_{n_m=1}^{N} \right) \langle \Psi_{n_1} \bar{\Psi}_{n_2} \rangle \langle \Psi_{n_2} \bar{\Psi}_{n_3} \rangle \cdots \langle \Psi_{n_M} \bar{\Psi}_{n_1} \rangle, \\
&= -\left(\prod_{m=1}^{M} \sum_{n_m=1}^{N} \right) \delta_{n_1 n_2} \delta_{n_2 n_3} \cdots \delta_{n_M n_1} \mathrm{tr}\, G_\Psi^M, \\
&= -\sum_{n_1=1}^{N} \mathrm{tr}\, G_\Psi^M = -N \mathrm{tr}\, G_\Psi^M. \qquad (4.47)
\end{aligned}$$

Then the bubble is

$$\begin{aligned}
\Pi(q) &= 8\pi^2 \Lambda^\epsilon g_\phi^2 \int_k^> \mathrm{tr} G_\Psi(k+q) G_\Psi(k), \\
&= -32\pi^2 \Lambda^\epsilon g_\phi^2 \int_{-\infty}^{\infty} \frac{dk_0}{2\pi} \int^> \frac{d^d \boldsymbol{k}}{(2\pi)^d} \frac{(k_0+q_0)k_0 + v_F^2 (\boldsymbol{k}+\boldsymbol{q})\cdot \boldsymbol{k}}{[(k_0+q_0)^2 + v_F^2 |\boldsymbol{k}+\boldsymbol{q}|^2][k_0^2 + v_F^2 |\boldsymbol{k}|^2]}, \\
&= \Pi_0 q_0^2 + c_\phi^2 \Pi_i q_i^2 + \Pi_{m_\phi^2}, \qquad (4.48)
\end{aligned}$$

where the identity $\mathrm{tr}\gamma_i \gamma_j = 4\delta_{ij}$ is used. In the final line the expansion to quadratic (relevant) order in q is made, such that

$$\begin{aligned}
\Pi_0 &= \frac{32\pi \Lambda^\epsilon g_\phi^2}{(4\pi)^{d/2}\Gamma(d/2)} \int_{-\infty}^{\infty} dk_0 \int_{\Lambda e^{-\delta\ell}}^{\Lambda} d\,|\boldsymbol{k}|\,|\boldsymbol{k}|^{d-1} \frac{-k_0^2 + v_F^2 |\boldsymbol{k}|^2}{(k_0^2 + v_F^2 |\boldsymbol{k}|^2)^3}, \\
&= \frac{2}{v_F^3} g_\phi^2 \delta\ell, \qquad (4.49) \\
\Pi_i &= \frac{v_F^2}{c_\phi^2} \frac{32\pi \Lambda^\epsilon g_\phi^2}{(4\pi)^{d/2}\Gamma(d/2)} \int_{-\infty}^{\infty} dk_0 \int_{\Lambda e^{-\delta\ell}}^{\Lambda} d\,|\boldsymbol{k}|\,|\boldsymbol{k}|^{d-1} \frac{k_0^2 + v_F^2 |\boldsymbol{k}|^2 (1-\frac{2}{d})}{(k_0^2 + v_F^2 |\boldsymbol{k}|^2)^3}, \\
&= \frac{2}{v_F c_\phi^2} g_\phi^2 \delta\ell, \qquad (4.50) \\
\Pi_{m_\phi^2} &= -\frac{32\pi \Lambda^\epsilon g_\phi^2}{(4\pi)^{d/2}\Gamma(d/2)} \int_{-\infty}^{\infty} dk_0 \int_{\Lambda e^{-\delta\ell}}^{\Lambda} d\,|\boldsymbol{k}|\,|\boldsymbol{k}|^{d-1} \frac{1}{k_0^2 + v_F^2 |\boldsymbol{k}|^2}, \\
&= -\frac{8\Lambda^2}{v_F} g_\phi^2 \delta\ell. \qquad (4.51)
\end{aligned}$$

Here the expansion to leading order in $\delta\ell \ll 1$ and $\epsilon = 3-d$ is made. The $\boldsymbol{k}$ integral is radially symmetric, in which case

$$\int d^d\boldsymbol{k}\, k_i k_j f(|\boldsymbol{k}|) = \delta_{ij} \int d^d\boldsymbol{k}\, \frac{|\boldsymbol{k}|^2}{d} f(|\boldsymbol{k}|), \tag{4.52}$$

$$\int^> \frac{d^d\boldsymbol{k}}{(2\pi)^d} = \int_{\Lambda e^{-\delta\ell}}^{\Lambda} d\,|\boldsymbol{k}|\,|\boldsymbol{k}|^{d-1}\, \frac{2}{(4\pi)^{d/2}\Gamma(d/2)}. \tag{4.53}$$

Here $f(|\boldsymbol{k}|)$ is an isotropic function of $\boldsymbol{k}$, and $2\pi^{d/2}/\Gamma(d/2)$ is the surface area of a d-dimensional sphere. The identity $k_i k_j \to \delta_{ij}\,|\boldsymbol{k}|^2/d$ is obvious, but can be determined systematically by conjecturing that $k_i k_j = \delta_{ij}\,|\boldsymbol{k}|^2\, x$ based on symmetry, where x is unknown. Then acting with δ_{ij} on both sides $\delta_{ij}k_i k_j = d\,|\boldsymbol{k}|^2\, x$ implying $x = 1/d$. This systematic approach is useful for dealing with higher order numerators, for example

$$\int d^d\boldsymbol{k}\, k_a k_b k_c k_d f(|\boldsymbol{k}|) = \int d^d\boldsymbol{k}\, \frac{\delta_{ab}\delta_{cd} + \delta_{ac}\delta_{bd} + \delta_{ad}\delta_{bc}}{d(d+2)}\, |\boldsymbol{k}|^4\, f(|\boldsymbol{k}|). \tag{4.54}$$

The δ's in the numerator can be conjectured by symmetry, and following this the $d(d+2)$ factor is found by acting on both sides with $\delta_{ij}\delta_{kl}$.

The tadpole diagram, shown in Fig. 4.4(b), is

$$\begin{aligned}
\Delta &= 16\pi^2\Lambda^\epsilon \lambda_\phi \int_k^> G_\phi(k) \\
&= 16\pi^2\Lambda^\epsilon \lambda_\phi \int_k^> \frac{1}{k_0^2 + c_\phi^2\,|\boldsymbol{k}|^2 + m_\phi^2} \\
&= 16\pi^2\Lambda^\epsilon \lambda_\phi \int_k^> \frac{1}{k_0^2 + c_\phi^2\,|\boldsymbol{k}|^2} - \frac{m_\phi^2}{(k_0^2 + c_\phi^2\,|\boldsymbol{k}|^2)^2} + O(m_\phi^4) \\
&= \frac{2}{c_\phi^3}\left(2\Lambda^2 c_\phi^2 - m_\phi^2\right)\lambda_\phi \delta\ell.
\end{aligned} \tag{4.55}$$

Note the combinatorial factor of 2. The linear shift of m_ϕ^2 such that $(m_\phi^2)_* = 0$ amounts to neglecting the constant (m_ϕ^2 independent) contribution to $\Pi_{m_\phi^2}$ and Δ.

4.5.1.2 Renormalisation to the Dirac Fermions S_Ψ

The renormalisation to the Ψ propagator comes from contractions with the remaining external slow $\bar{\Psi}\Psi$ legs

$$\begin{aligned}\hat{S}^<_\Psi &= S^<_\Psi - \frac{1}{2}\langle S^2_{g_\phi}\rangle_>, \\ &= S^<_\Psi + \frac{1}{N}\sum_{n=1}^{N}\int_k^< \bar{\Psi}^<(k)\Sigma(k)\Psi^<(k).\end{aligned} \tag{4.56}$$

The fermion self-energy Σ, shown in Fig. 4.4(c), is

$$\begin{aligned}\Sigma(q) &= 8\pi^2\Lambda^\epsilon g_\phi^2\int_k^> G_\phi(k+q)G_\Psi(k), \\ &= i(\Sigma_0 k_0\gamma_0 + v_F\Sigma_i k_i\gamma_i), \end{aligned}\tag{4.57}$$

$$\begin{aligned}\Sigma_0 &= -16\pi^2\Lambda^\epsilon g_\phi^2\int_k^> \frac{k_0^2}{(k_0^2+c_\phi^2|\boldsymbol{k}|^2)^2(k_0^2+v_F^2|\boldsymbol{k}|^2)}, \\ &= -\frac{2}{c_\phi(c_\phi+v_F)^2}g_\phi^2\delta\ell, \end{aligned}\tag{4.58}$$

$$\begin{aligned}\Sigma_i &= -16\pi^2\Lambda^\epsilon g_\phi^2\int_k^> \frac{c_\phi^2|\boldsymbol{k}|^2/d}{(k_0^2+c_\phi^2|\boldsymbol{k}|^2)^2(k_0^2+v_F^2|\boldsymbol{k}|^2)}, \\ &= -\frac{2(v_F+2c)}{3v_F c_\phi(c_\phi+v_F)^2}g_\phi^2\delta\ell. \end{aligned}\tag{4.59}$$

Note the combinatorial factor of 2. Here and in the proceeding calculations $m_\phi^2 = (m_\phi^2)_* = 0$ such that the theory is tuned to the critical hypersurface. This is justified when analysing the critical fixed points. However, to analyse the RG flow into the broken symmetry state m_ϕ^2 corrections to all parameters would need to be accounted for, but this is not done here.

4.5.1.3 Renormalisation to the Fermion-Boson Yukawa Vertex S_{g_ϕ}

The renormalisation to the Yukawa vertex comes from contractions with the remaining external slow $\bar{\Psi}\Psi\phi$ legs

$$\frac{1}{\sqrt{\tilde{N}}}\hat{S}^<_{g_\phi} = \frac{1}{\sqrt{\tilde{N}}}\left(S^<_{g_\phi} + \frac{1}{6}\langle S^3_{g_\phi}\rangle_>\right),$$

$$= \frac{1}{\sqrt{\tilde{N}}}\left(S^{<}_{g_\phi} + \frac{1}{N}\sum_{n=1}^{N}\int_r^{<} \bar{\Psi}_n \Xi \phi \Psi_n\right), \tag{4.60}$$

where the action has been represented in $r = (\tau, \boldsymbol{r})$ space where it is local. The Yukawa vertex correction Ξ, shown in Fig. 4.4(d), is

$$\begin{aligned}\Xi &= 8\pi^2\Lambda^\epsilon g_\phi^3 \int_k^{>} G\Psi(k)G\Psi(k)G_\phi(k),\\ &= -8\pi^2\Lambda^\epsilon g_\phi^3 \int_k^{>} \frac{1}{(k_0^2 + c_\phi^2\,|\boldsymbol{k}|^2)(k_0^2 + v_F^2\,|\boldsymbol{k}|^2)},\\ &= -\frac{2}{v_F c_\phi (v_F + c_\phi)} g_\phi^3 \delta\ell,\end{aligned} \tag{4.61}$$

where $k_i\gamma_i k_j\gamma_j = \boldsymbol{k}^2$ is used. Note the combinatorial factor of 6.

4.5.1.4 Renormalisation to the Order Parameter Boson Self-Interaction S_{λ_ϕ}

The renormalisation to the bosonic self-interaction vertex comes from contractions with four remaining external slow ϕ legs

$$\begin{aligned}\frac{1}{\tilde{N}}\hat{S}^{<}_{\lambda_\phi} &= \frac{1}{\tilde{N}}\left[S^{<}_{\lambda_\phi} - \frac{1}{2}\langle S^2_{\lambda_\phi}\rangle_{>} - \frac{1}{24}\langle S^4_{g_\phi}\rangle_{>}\right],\\ &= \frac{1}{\tilde{N}}\left[S^{<}_{\lambda_\phi} + \int_r^{<}\left(\frac{1}{N}\Gamma_{\lambda_\phi} + \frac{N}{N}\Gamma_{g_\phi}\right)\phi^4\right].\end{aligned} \tag{4.62}$$

The self-interaction vertex correction Γ_{λ_ϕ} from the self-interaction, shown in Fig. 4.4(e), is

$$\begin{aligned}\Gamma_{\lambda_\phi} &= 288\pi^2\Lambda^\epsilon\lambda_\phi^2\int_k^{>} G_\phi(k)G_\phi(k),\\ &= \frac{36}{c_\phi^3}\lambda_\phi^2\delta\ell.\end{aligned} \tag{4.63}$$

Note the combinatorial factor of $2\binom{4}{2}\binom{4}{2} = 72$. The self-interaction vertex correction Γ_{g_ϕ} from the fermion loop, shown in Fig. 4.4(f), is

$$\Gamma_{g_\phi} = 8\pi^2\Lambda^\epsilon g_\phi^4\int_k^{>} \mathrm{tr}\, G\Psi(k)G\Psi(k)G\Psi(k)G\Psi(k),$$

$$= g_\phi^4 \delta\ell. \tag{4.64}$$

Note the combinatorial factor of 6. The integration was simplified using the radial integration identity discussed above

$$k_a k_b k_c k_d \to \frac{\delta_{ab}\delta_{cd} + \delta_{ac}\delta_{bd} + \delta_{ad}\delta_{bc}}{d(d+2)} |\boldsymbol{k}|^4, \tag{4.65}$$

as well as the trace identity

$$\mathrm{tr}\, \gamma_a \gamma_b \gamma_c \gamma_d = 4(\delta_{ab}\delta_{cd} - \delta_{ac}\delta_{bd} + \delta_{ad}\delta_{bd}), \tag{4.66}$$

which follows from the anticommuting properties of γ. In combination

$$\mathrm{tr}\, (k_0\gamma_0 + v_F k_i \gamma_i)^4 \to 4(k_0^2 + v_F^2 |\boldsymbol{k}|^2)^2. \tag{4.67}$$

4.5.2 Gross-Neveu-Yukawa Renormalisation Group Equations

Enacting the final step in the RG procedure $\hat{S}^<_{\mathrm{GNY}} \to \hat{S}_{\mathrm{GNY}}$, the one-loop renormalised couplings are obtained

$$\hat{S}_\Psi = \int_k i\bar{\Psi} \left\{ \left[1 - \eta_\Psi \delta\ell + \frac{\Sigma_0}{N} \right] k_0\gamma_0 + v_F \left[1 + (z - 1 - \eta_\Psi)\, \delta\ell + \frac{\Sigma_i}{N} \right] k_i\gamma_i \right\} \Psi, \tag{4.68}$$

$$\hat{S}_\phi = \frac{1}{2} \int_k \phi \left\{ \left[1 - \eta_\phi \delta\ell + \Pi_0 \right] k_0^2 + c_\phi^2 \left[1 + \left(2z - 2 - \eta_\phi \right) \delta\ell + \Pi_i \right] k_i^2 \right.$$
$$\left. + \left[1 + \left(2z - \eta_\phi \right) \delta\ell \right] m_\phi^2 + \Pi_{m_\phi^2} + \frac{\Delta}{N} \right\} \phi, \tag{4.69}$$

$$\hat{S}_{g_\phi} = \frac{1}{\sqrt{\tilde{N}}} \left\{ g_\phi \left[1 + \frac{1}{2} \left(3z - 3 + \epsilon - 2\eta_\Psi - \eta_\phi \right) \delta\ell \right] + \frac{\Xi}{N} \right\} \int \bar{\Psi}\phi\Psi, \tag{4.70}$$

$$\hat{S}_{\lambda_\phi} = \frac{1}{\tilde{N}} \left\{ \lambda_\phi \left[1 + \left(3z - 3 + \epsilon - 2\eta_\phi \right) \delta\ell \right] + \frac{\Gamma_{\lambda_\phi}}{N} + \Gamma_{g_\phi} \right\} \int \phi^4. \tag{4.71}$$

Following the tree-level procedure, the field rescalings (including anomalous dimensions $\eta_{\phi,\Psi}$) ensure the frequency terms are scale invariant

$$\eta_\Psi = \frac{1}{N}\frac{\Sigma_0}{\delta\ell},\ \eta_\phi = \frac{\Pi_0}{\delta\ell}. \tag{4.72}$$

The velocity RG equations are

$$\frac{d}{d\ell}v_F = v_F\left(z - 1 - \eta_\Psi + \frac{1}{N}\frac{\Sigma_i}{\delta\ell}\right) = v_F\left(z - 1 + \frac{1}{N}\frac{\Sigma_i - \Sigma_0}{\delta\ell}\right), \tag{4.73}$$

$$\frac{d}{d\ell}c_\phi^2 = c_\phi^2\left(2z - 2 - \eta_\phi + \frac{\Pi_i}{\delta\ell}\right) = c_\phi^2\left(2z - 2 + \frac{\Pi_i - \Pi_0}{\delta\ell}\right). \tag{4.74}$$

These are solved for $z = 1$ and $c_\phi = v_F$, as $\Sigma_i - \Sigma_0 \propto (v_F - c_\phi)$ and $\Pi_i - \Pi_0 \propto (v_F - c_\phi)$. This indicates that the putative critical fixed point is Lorentz invariant, with isotropic space-time scaling indicated by the dynamical exponent $z = 1$, and a single velocity scale set by v_F. Units of the Fermi velocity are now used, $v_F = c_\phi = 1$.

The RG equation for the Yukawa coupling is

$$\begin{aligned}\frac{d}{d\ell}g_\phi^2 &= g_\phi^2(\epsilon - \eta_\phi - 2\eta_\Psi) + \frac{2}{N}\frac{\Xi}{\delta\ell},\\ &= g_\phi^2\left[\epsilon - \left(2 + \frac{3}{N}\right)g_\phi^2\right].\end{aligned} \tag{4.75}$$

This indicates the existence of a non-trivial fixed point at $(g_\phi^2)_* = \epsilon/(2 + \frac{3}{N})$, which is perturbatively controlled in ϵ and N. The RG equation for the self-interaction is

$$\begin{aligned}\frac{d}{d\ell}\lambda_\phi &= \lambda_\phi(\epsilon - 2\eta_\phi) + \frac{1}{N}\frac{\Gamma_{\lambda_\phi}}{\delta\ell} + \frac{\Gamma_{g_\phi}}{\delta\ell},\\ &= \lambda_\phi\left(\epsilon - 4g_\phi^2\right) - \frac{36}{N}\lambda_\phi^2 + g_\phi^4.\end{aligned} \tag{4.76}$$

4.5.3 Wilson-Fisher and Gross-Neveu-Yukawa Fixed points

In the physical regime $\lambda_\phi > 0$ there are two fixed points, which are shown schematically in Fig. 4.5. The Wilson-Fisher (WF) fixed point, where the fermions are decoupled $(g_\phi^2)_* = 0$, is located at $(\lambda_\phi)_* = \epsilon N/36$ (note that this is $(\lambda_\phi)_* = \epsilon/36$ in the original λ_ϕ). Along with this there is the GNY fixed point at

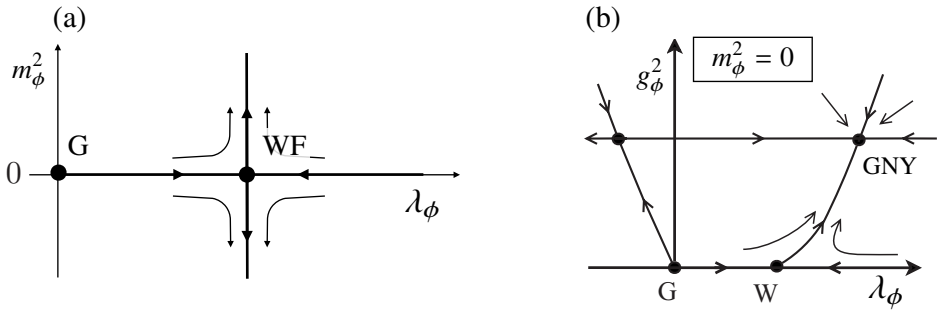

Figure 4.5: Schematic renormalisation group flow diagrams for $d < 3$ spatial dimensions. The (renormalised) bosonic order parameter mass m_ϕ^2 tunes to the critical surface at $(m_\phi^2)_* = 0$, and is the relevant perturbation at the critical fixed points. $m_\phi^2 < 0$ is the broken symmetry region. The boson self-interaction λ_ϕ and fermion-boson Yukawa interaction g_ϕ are relevant perturbations at the non-interacting Gaussian (G) fixed point for $d < 3$. (a) The purely bosonic Wilson-Fisher (WF) diagram where the fermions are (artificially) decoupled $g_\phi = 0$. (b) The fermionic criticality diagram, where the coupling to the fermions is a relevant perturbation at the WF fixed point, and the flow is to the Gross-Neveu-Yukawa (GNY) fixed point. Negative λ_ϕ corresponds to an unbounded action and is unphysical. Figure (b) is adapted from Ref. [20].

$(\lambda_\phi)_* \approx \epsilon(1-\frac{9}{N})/4$. The RG flow in the region of the WF fixed point can be analysed with the stability matrix, which is obtained by linearising around the fixed point, $(g_\phi^2, \lambda_\phi) = ((g_\phi^2)_* + \delta g_\phi^2, (\lambda_\phi)_* + \delta\lambda_\phi)$,

$$\frac{d}{d\ell}\begin{pmatrix}\delta g_\phi^2 \\ \delta\lambda_\phi\end{pmatrix} = \begin{pmatrix}\epsilon & -N\epsilon/9 \\ 0 & -\epsilon\end{pmatrix}\begin{pmatrix}\delta g_\phi^2 \\ \delta\lambda_\phi\end{pmatrix}. \tag{4.77}$$

The positive eigenvalue ϵ of the stability matrix indicates the Yukawa coupling to the Dirac fermions is a *relevant* perturbation at the WF fixed point and cannot be neglected, see Fig. 4.5(b). Hence, this is a simple example where the presence of gapless fermionic excitations change the universal nature of the criticality from the paradigmatic GLW ϕ^4 theory. Instead, the system will flow to the GNY fixed point about which g_ϕ and λ_ϕ are irrelevant perturbations

$$\frac{d}{d\ell}\begin{pmatrix}\delta g_\phi^2 \\ \delta\lambda_\phi\end{pmatrix} = \begin{pmatrix}-\epsilon & 15\epsilon/2N \\ 0 & -\epsilon - 15\epsilon/N\end{pmatrix}\begin{pmatrix}\delta g_\phi^2 \\ \delta\lambda_\phi\end{pmatrix}. \tag{4.78}$$

This identifies the GNY point as a quantum critical fixed point, that is tuned to by the relevant perturbation m_ϕ^2

$$\begin{aligned}\frac{d}{d\ell}m_\phi^2 &= \left(2z-\eta_\phi\right)m_\phi^2+\frac{\Delta}{N\delta\ell},\\ &= 2(1-g_\phi^2+6\lambda_\phi/N)m_\phi^2,\\ &= (2-\epsilon-3\epsilon/2N)m_\phi^2.\end{aligned} \tag{4.79}$$

As discussed earlier, this single positive eigenvalue of the stability matrix defines the correlation length exponent $\nu^{-1}=2-\epsilon-3\epsilon/2N$. In the context of the sublattice CDW it is clear to identify $m_\phi^2\sim(V_1)_c-V_1$, and therefore $\xi\sim\left|m_\phi^2\right|^{-\nu}$. The finite anomalous dimensions are

$$\eta_\Psi=\epsilon/4N,\ \eta_\phi=\epsilon(1-3/2N), \tag{4.80}$$

which indicate the breakdown of the fermion and boson quasiparticle pictures at the fermionic quantum critical point.

In two spatial dimensions $\epsilon=1$ and the large N limit $\nu=1$, $\eta_\phi=1$, and $\eta_\Psi=0$. From these exponents, the order parameter exponent $\beta=1$ is obtained from the standard scaling relations $\alpha+2\beta+\gamma=2$ (Rushbrooke), $\gamma=(2-\eta_\phi)\nu$ (Fisher) by assuming hyperscaling $\alpha=2-\nu(z+d)$, which typically holds below the upper-critical dimension. Therefore, this limit is in good agreement with the Dirac fermion mean-field discussed in Section 2.3.3.

This chiral Ising GNY model has been studied using a number of sophisticated techniques [130, 131] (and references therein) including: four-loop perturbative RG, non-perturbative functional RG, conformal bootstrap and quantum Monte Carlo. State of the art results for the spinful ($N=2$) model using field theoretic methods [131, 142–144] agree rather well: $1/\nu\approx0.88-0.99$, $\eta_\phi\approx0.69-0.77$ and $\eta_\Psi\approx0.02-0.08$. The disparity to Monte Carlo [145] is larger $(1/\nu,\eta_\phi,\eta_\Psi)=(1.2,0.62,0.38)$, which could be due to corrections to scaling when comparing the lattice to field theories [131]. There are similarly extensive studies of the chiral XY (relevant to Kekulé criticality) and chiral Heisenberg (relevant to

antiferromagnetic criticality) GNY models [131].

4.5.3.1 Equivalence to the Gross-Neveu Model

It is noteworthy that there is good agreement at $\epsilon = 1$ between the four-loop $3+1-\epsilon$ expansion [131] of the GNY model and the four-loop $1+1+\epsilon$ expansion [143] of the original Gross-Neveu model ($v_F = 1$)

$$L_{\mathrm{GN}} = \bar{\Psi}\partial_\mu\gamma_\mu\Psi + \frac{V}{N}(\bar{\Psi}\Psi)^2. \tag{4.81}$$

The former is an expansion around the upper critical dimension, while the latter is an expansion around the lower critical dimension. That both models describe the same critical point was first conjectured some time ago by Zinn-Justin [22]. This was based on a comparison of the the one-loop RG equations in large N, which for Eq. (4.81) is

$$\frac{d}{d\ell}V = -\epsilon V + V^2/\pi. \tag{4.82}$$

In the Gross-Neveu model the fermionic interaction is an irrelevant perturbation at weak coupling, and will flow to the Gaussian fixed point of the the Dirac semimetal. The phase transition occurs at the non-trivial critical fixed point $(V)_* = \pi\epsilon$, and for $V > (V)_*$ the system flows to the strong coupling broken symmetry state. Finally, by integrating out ϕ from the GNY model in the region of the GNY fixed point (where λ_ϕ is irrelevant), the equivalence $V \sim g_\phi^2/m_\phi^2$ can be seen [22]. This was already evident from integrating out A in Eq. (4.42).

4.5.4 Correlations Functions and Scaling at Criticality

This discussion loosely follows chapters 4 and 7 of the textbook by Sachdev [1]. The breakdown of the quasiparticle picture can be seen from the correlation functions [20]

$$\langle\bar{\Psi}(\omega,\boldsymbol{k})\Psi(\omega,\boldsymbol{k})\rangle \sim \frac{\omega\gamma_0 + iv_F k_i\gamma_i}{(v_F^2\,|\boldsymbol{k}|^2 - \omega^2)^{\frac{z+1-\eta_\Psi}{2}}}, \tag{4.83}$$

$$\langle\phi^\dagger(\omega,\boldsymbol{k})\phi(\omega,\boldsymbol{k})\rangle \sim \frac{1}{(c_\phi^2\,|\boldsymbol{k}|^2 - \omega^2)^{\frac{2z-\eta_\phi}{2}}}, \tag{4.84}$$

where $\omega = -ik_0$ is the real frequency, following a Wick rotation from imaginary to real time. The key feature is the absence of the well defined quasiparticle excitations, which are otherwise seen from the pole structure away from criticality where $\eta_{\Psi,\phi} = 0$. In contrast, at criticality this is replaced by a dissipative continuum of excitations where $\eta_{\Psi,\phi} > 0$. This is indicated by the branch cuts of $\sim (\boldsymbol{k}^2 - \omega^2)^{-n}$ for non-integer n [1].

The scaling of the correlation functions follows directly from the scaling of the fields, for example

$$\langle \bar{\Psi}'(k')\Psi'(k')\rangle = \langle \bar{\Psi}(k)\Psi(k)\rangle e^{-(z-\eta_\Psi)\ell} \Rightarrow \langle \bar{\Psi}(k)\Psi(k)\rangle \sim k^{\eta_\Psi - z}. \tag{4.85}$$

More generally, the scaling in terms of the correlation length $\xi = e^{(\ell)_*}$ (the characteristic length scale) is

$$\langle \bar{\Psi}(\omega, \boldsymbol{k})\Psi(\omega, \boldsymbol{k})\rangle = \xi^{z-\eta_\Psi} F_{\Psi\pm}(\omega\xi^z, \boldsymbol{k}\xi), \tag{4.86}$$

$$\langle \phi^\dagger(\omega, \boldsymbol{k})\phi(\omega, \boldsymbol{k})\rangle = \xi^{2z-\eta_\phi} F_{\phi\pm}(\omega\xi^z, \boldsymbol{k}\xi), \tag{4.87}$$

where $F_{\Psi,\phi\pm}$ are universal scaling functions above and below the critical point. Note that ξ^{-z} is the scale of the energy gap.

In addition, the quasiparticle residues vanish as power laws in the vicinity of the critical point

$$Z_\Psi \sim (m_\phi^2)^{\nu\eta_\Psi},\ Z_\phi \sim (m_\phi^2)^{\nu\eta_\phi}, \tag{4.88}$$

where the residues are extracted from the scaling of the spectral density (the imaginary part of the correlation function). For example, the non-interacting bosonic spectral density is

$$\begin{aligned} \mathrm{Im}\langle \phi^\dagger\phi\rangle &\sim \lim_{\theta\to 0^+} \mathrm{Im}\frac{1}{c_\phi^2 |\boldsymbol{k}|^2 - (\omega - i\theta)^2}, \\ &\sim \frac{Z_\phi}{2c_\phi |\boldsymbol{k}|}[\delta(c_\phi |\boldsymbol{k}| - \omega) - \delta(c_\phi |\boldsymbol{k}| + \omega)], \end{aligned} \tag{4.89}$$

with the non-interacting bosonic residue $Z_\phi = 1$. The imaginary part is extracted

with the Dirac identity trick $\lim_{\theta\to 0^+} \mathrm{Im}(x - i\theta)^{-1} = \pi\delta(x)$, and partial fractions. The comparison of Eq. (4.89) and Eq. (4.87) implies $Z_\phi \sim \xi^{-\eta_\phi}$. Then, Eq. (4.88) follows from $\xi \sim (m_\phi^2)^{-\nu}$.

4.6 Criticality of Lattice Symmetry Breaking Charge Order

Renormalisation group analysis of the full theory Eq. (4.40) with ϕ and A fields is now presented. The methodology is simply an extension of the Gross-Neveu-Yukawa theory. The renormalisation group equations are obtained to one-loop order using the $\epsilon = 3 - d$ and large N expansions in the Wilson momentum shell scheme.

4.6.1 Lattice Cutoff and Ward-Takahashi Identities

Here it is demonstrated, using the Ward-Takahashi identity, that the emergent gauge invariance implies the A bosonic mass $m_A^2 = 0$ in the low-energy theory. The argument follows Ref. [137]. The conserved Noether currents j_i^a of the infinitesimal global chiral/gauge transformations $\Psi \to e^{i\theta^a T^a}\Psi = \Psi + i\theta^a T^a \Psi$ are [146]

$$\theta^a j_i^a = \frac{\partial L}{\partial(\partial_i \Psi)} i\theta^a T^a \Psi = -i\theta^a \Psi^\dagger \alpha_i T^a \Psi, \tag{4.90}$$

where there is no summation over a. The associated Ward-Takahashi identity asserts that the insertion $\partial_i j_i^a$ into any correlation function vanishes (up to contact terms) $\partial_i \langle j_i^a j_j^b \cdots j_p^f j_q^g \rangle = 0$. The Ward-Takahashi identity for the two current correlator is $\partial_i \langle j_i^a j_j^b \rangle = 0$, where the two current correlators are precisely the $A_i^a A_j^b$ self energies Π_{ij}^{ab}. At one-loop $\Pi_{ij}^{ab} = \delta_{ij}(k_0^2 + \boldsymbol{k}^2 + m_A^2) - k_i k_j$, prior to gauge fixing. The identity $\partial_i \Pi_{ij}^{ab} = 0$ implies, for example, $k_x \Pi_{xx}^{ab} + k_y \Pi_{yx}^{ab} = 0$, or $k_x(k_0^2 + k_y^2 + m_A^2) = k_y(k_x k_y)$, see Eq. (4.13). By dividing both sides by k_x, it can therefore be seen that the mass term is forbidden, $\lim_{q_0\to 0, \boldsymbol{q}\to 0} m_A^2 = 0$. This is expected to hold to infinite order for the low-energy theory. Note that this argument is trivial in the Feynman-'t Hooft gauge where $\Pi_{ij\neq i} = 0$.

The hard-cutoff Λ scheme breaks the emergent gauge invariance of the low-energy theory. The fermion bubble and tadpole diagrams generate constant correc-

tions of $O(\Lambda^{2-\epsilon})$ to the bosonic mass m_A^2, and so $(m_A^2)_*$ is finite at the non-trivial fixed point. In doing so, the Ward-Takahashi identity is violated. This is ultimately related to the fact that the gauge structure is an emergent property of the continuum low-energy field theory and not present on the lattice. In fact the lattice already breaks the gauge invariance by generating a constant correction $\sim (V_1 - 2V_2)\phi^2 + V_2 A^2$ at the level of the lattice Hubbard-Stratonovich transformation, see Eq. (4.10). What this means is that the A fields can have finite expectation values from tuning the lattice interactions past the critical point into the broken symmetry state [135, 136]. It is natural that the cutoff has this effect, as it is related to the inverse lattice constant $\Lambda \sim 1/a$.

Apart from the constant corrections discussed, a consistent set of RG equations are obtained using the gauge invariant minimal subtraction scheme [9]. More so, regardless of these subtleties the coupling $\lambda_{\phi A}\phi^2 A^2$ in Eq. (4.15) implies that the condensation of the mass field ϕ will dynamically generate a finite expectation value for the emergent gauge fields, which is reminiscent of a Higgs mechanism. In any case, in the following the mass terms are shifted such that $(m^2_{\phi,A})_* = 0$, and the constant corrections suppressed in the RG equations, as was enacted in the GNY theory.

4.6.2 Renormalisation Group Equations

The RG equations for the velocities are

$$\frac{d}{d\ell} v_F = (z-1)v_F + \frac{4}{N}\left(\frac{g_\phi^2 \left(c_\phi - v_F\right)}{3c_\phi \left(c_\phi + v_F\right)^2} - \frac{2g_A^2 v_F}{c_A \left(c_A + v_F\right)^2} \right), \tag{4.91}$$

$$\frac{d}{d\ell} c_\phi^2 = 2(z-1)c_\phi^2 + \frac{2g_\phi^2 \left(v_F^2 - c_\phi^2\right)}{v_F^3}, \tag{4.92}$$

$$\frac{d}{d\ell} c_A^2 = 2(z-1)c_A^2 + \frac{4g_A^2 \left(v_F^2 - c_A^2\right)}{3v_F^3}. \tag{4.93}$$

Here the anomalous dimensions $\eta_{\Psi,\phi,A}$ are determined by the scale invariance of the ∂_τ terms. The RG equations for the Yukawa couplings are

$$\frac{d}{d\ell}g_\phi^2 = g_\phi^2\left[\epsilon + 3(z-1) - \frac{2g_\phi^2}{v_F^3} - \frac{4}{N}\left(\frac{g_\phi^2\left(c_\phi + 2v_F\right)}{c_\phi v_F\left(c_\phi + v_F\right)^2} + \frac{4g_A^2\left(c_A + 2v_F\right)}{c_A v_F\left(c_A + v_F\right)^2}\right)\right], \tag{4.94}$$

$$\frac{d}{d\ell}g_A^2 = g_A^2\left[\epsilon + 3(z-1) - \frac{4g_A^2}{3v_F^3} - \frac{4}{N}\left(\frac{2g_\phi^2\left(c_\phi + 2v_F\right)}{3c_\phi v_F\left(c_\phi + v_F\right)^2} + \frac{4g_A^2}{c_A\left(c_A + v_F\right)^2}\right)\right]. \tag{4.95}$$

The RG equations for the boson order parameter field self-interactions are

$$\frac{d}{d\ell}\lambda_\phi = \lambda_\phi\left(\epsilon + 3(z-1) - \frac{4g_\phi^2}{v_F^3}\right) + \frac{g_\phi^4}{v_F^3} - \frac{4}{N}\left(\frac{9\lambda_\phi^2}{c_\phi^3} + \frac{\lambda_{\phi A}^2}{c_A^3}\right), \tag{4.96}$$

$$\frac{d}{d\ell}\lambda_A = \lambda_A\left(\epsilon + 3(z-1) - \frac{8g_A^2}{3v_F^3}\right) - \frac{4}{N}\left(\frac{12\lambda_A^2}{c_A^3} + \frac{\lambda_{\rm YM}^2}{4c_A^3} + \frac{\lambda_{\phi A}^2}{4c_\phi^3} + \frac{\lambda_A\lambda_{\rm YM}}{c_A^3}\right), \tag{4.97}$$

$$\frac{d}{d\ell}\lambda_{\rm YM} = \lambda_{\rm YM}\left(\epsilon + 3(z-1) - \frac{8g_A^2}{3v_F^3}\right) + \frac{8g_A^4}{3v_F^3} - \frac{4}{N}\left(\frac{2\lambda_{\rm YM}^2}{c_A^3} + \frac{12\lambda_A\lambda_{\rm YM}}{c_A^3}\right), \tag{4.98}$$

$$\begin{aligned}\frac{d}{d\ell}\lambda_{\phi A} = {}& \lambda_{\phi A}\left(\epsilon + 3(z-1) - \frac{4g_A^2}{3v_F^3} - \frac{2g_\phi^2}{v_F^3}\right) + \frac{4g_A^2 g_\phi^2}{v_F^3} \\ & - \frac{4}{N}\left(\frac{4\lambda_{\phi A}^2}{c_A c_\phi\left(c_A + c_\phi\right)} + \frac{3\lambda_\phi\lambda_{\phi A}}{c_\phi^3} + \frac{6\lambda_A\lambda_{\phi A}}{c_A^3} + \frac{\lambda_{\rm YM}\lambda_{\phi A}}{2c_A^3}\right).\end{aligned} \tag{4.99}$$

The RG equations for the boson order parameter field masses are

$$\frac{d}{d\ell}m_\phi^2 = m_\phi^2\left(2z - \frac{2g_\phi^2}{v_F^3} - \frac{12\lambda_\phi}{Nc_\phi^3}\right) - m_A^2\frac{8\lambda_{\phi A}}{Nc_A^3}, \tag{4.100}$$

$$\frac{d}{d\ell}m_A^2 = m_A^2\left(2z - \frac{4g_A^2}{3v_F^3} - \frac{2\left(12\lambda_A + \lambda_{\rm YM}\right)}{Nc_A^3}\right) - m_\phi^2\frac{2\lambda_{\phi A}}{Nc_\phi^3}. \tag{4.101}$$

The RG equations are solved to $O(1/N)$ to leading order in ϵ as follows. First, z is chosen to make v_F scale invariant by solving Eq. (4.91). Then, the fixed points of the boson velocities and Yukawa couplings are obtained simultaneously by solving Eqs. (4.92 – 4.95). The boson self-interaction fixed points are then obtained by

solving Eqs. (4.96 – 4.99).

The RG flow in the vicinity of the multicritical fixed point $(m^2_{\phi,A})_* = 0$ is determined by linearisation in the couplings $x_i = (g^2_\phi, g^2_A, \lambda_\phi, \lambda_A, \lambda_{\rm YM}, \lambda_{\phi A}, m^2_\phi, m^2_A)$. At the putative continuous phase transition, the two relevant (positive) eigenvalues of the stability matrix Eq. (4.22) are the inverse correlation length exponents $\nu^{-1}_{1,2} = \nu^{-1}$.

4.6.3 CDW_3 Multicritical Fixed Point

The CDW_3 fixed point is at $m^2_\phi = (m^2_\phi)_*$ and $m^2_A = (m^2_A)_*$. At this multicritical fixed point the Yukawa couplings take the values

$$(g^2_\phi)_* = 2\epsilon\,(1 - 6/N)\,,\ (g_A)^2_* = 3\epsilon\,(1 + 1/2N) \tag{4.102}$$

The resulting critical exponents are collected in Tab. 4.1, and are contrasted with the GNY universality. In addition, there is good agreement from analysis of the CDW_3 fixed point directly in the physical spatial dimension $d = 2$, which is perturbatively controlled by large N (RG equations in Appendix B.2). The spontaneous lattice symmetry breaking (finite g_A) results in the violation of Lorentz invariance with $z = 1 + (g^2_A)_*/2N = 1 + 3\epsilon/2N$ and $c_{\phi,A} = v_F(1 + 3/2N)$. This is in contrast to the emergent Lorentz invariance of GNY fixed points with $z = 1$ and $c_\phi = v_F$ to all orders in N. It is important to highlight that divergent anisotropic velocity renormalisation, preempting a fixed point, is encountered if the independent spatial rotational symmetries of $\boldsymbol{A}^1$ or $\boldsymbol{A}^2$ are artificially broken.

In $N \to \infty$ the correlation length exponents decouple to $\nu_{1,2} = \nu_A = \nu_\phi = 1$. By assuming hyperscaling, the scaling laws can be used to obtain the rest of the critical exponents, as was discussed at the GNY fixed point. The finite anomalous dimensions indicate the breakdown of the quasiparticle picture at the critical point.

4.6.4 Cubic Terms and Fermion-Induced Criticality

The RG analysis indicates the existence of a continuous quantum phase transition. However, relaxing particle-hole symmetry the reduced lattice symmetry group C''_{6v} allows for the cubic term $b\mathrm{Im}[G^3_2 - 3G^2_1 G_2]$, where $G_a = A^a_x + iA^a_y$. If this is finite, the Landau cubic criterion would imply a first order transition of the Landau free

Exponent	GNY ($d = 3 - \epsilon$)	CDW_3 ($d = 3 - \epsilon$)	CDW_3 ($d = 2$)
$z - 1$	0	$\frac{3\epsilon}{2N}$	$\frac{56\sqrt{2}-75}{N}$
η_Ψ	$\frac{\epsilon}{4N}$	$\frac{7\epsilon}{4N}$	$\frac{54\sqrt{2}-72}{N}$
η_ϕ	$\epsilon\left(1 - \frac{3}{2N}\right)$	$\epsilon\left(1 - \frac{6}{N}\right)$	$1 + \frac{24\sqrt{2}-45}{N}$
η_A		$\epsilon\left(1 + \frac{1}{2N}\right)$	$1 + \frac{64\sqrt{2}-87}{N}$
$2 - \nu_1^{-1}$	$\epsilon\,(1 - 3/2N)$	$\epsilon\left(1 + \frac{11+\sqrt{745}}{4N}\right)$	$1 + \frac{84-65\sqrt{2}+\sqrt{1307-714\sqrt{2}}}{N}$
$2 - \nu_2^{-1}$		$\epsilon\left(1 + \frac{11-\sqrt{745}}{4N}\right)$	$1 + \frac{84-65\sqrt{2}-\sqrt{1307-714\sqrt{2}}}{N}$

Table 4.1: One-loop critical exponents at the GNY/Chiral Ising and CDW_3 fixed points to $O(1/N^2)$. The GNY fixed point describes the quantum critical point of the semimetal-insulator transition into the sublattice CDW phase on the honeycomb lattice. The CDW_3 fixed point describes a new fixed point of interacting Dirac fermions where lattice symmetries are spontaneously broken. For the CDW_3 fixed point there is good agreement between the $\epsilon = 3 - d$ expansion and the direct evaluation in the physical dimension $d = 2$ as $N \to \infty$.

energy $f_L \sim m^2 - (b - b_c)m^3 + m^4$. Naive tree-level scaling $[b] = (5z - d)/2$ suggests that this is indeed the case. Yet, the large anomalous dimensions $\eta_A \propto g_A^2$ render the cubic term irrelevant at the $d = 2$ CDW_3 critical point. Therefore the coupling to gapless Dirac fermions induces a continuous transition [23].

To demonstrate this it is sufficient to calculate the leading order RG equation

$$\frac{d}{d\ell}b^2 = b^2\left[\epsilon + 5z - 3 - \frac{4g_A^2}{v_F^3} - \frac{12}{N}\left(\frac{3\lambda_A}{c_A^3} + \frac{\lambda_{YM}}{c_A^3}\right)\right] + O(b^4), \tag{4.103}$$

where the dimensionless coupling is $b^2 \to \frac{8\pi^2\Lambda^\epsilon}{N}b^2$. This required calculating the contractions of $\langle S_b S_\lambda\rangle_>$ with three slow bosonic legs. Crucially, lattice terms are no directly renormalised by the Dirac fermions because of the higher continuous spatial rotational symmetry. At the CDW_3 fixed point Eq. (4.103) reduces to

$$\frac{d}{d\ell}b^2 = 2b^2\left[1 - \epsilon - \frac{24\epsilon}{N}\right] + O(b^4). \tag{4.104}$$

Therefore, to this order b is an irrelevant perturbation for $\epsilon = 1$ ($d = 2$), and the fixed point value is $(b)_* = 0$. In $N \to \infty$, b is marginal to all loop orders [24]. Similar behaviour was found for the Potts clock term $\chi^3 + \chi^{*3} \sim |\chi|^3\cos(3\varphi)$ for of

complex Kekulé XY order parameter χ coupled to Dirac fermions in $d < 3$ spatial dimensions [23]. This highlights that fermion-induced critical points are inherently different from Wilson-Fisher fixed points of conventional order-parameter theories.

Finally, notice that the same discussion applies to the low-energy $\tilde{b}\phi(\boldsymbol{A}^1 \times \boldsymbol{A}^2)$ term with the leading order RG equation

$$\begin{aligned}\frac{d}{d\ell}\tilde{b}^2 &= \tilde{b}^2\left[\epsilon + 5z - 3 - \frac{8g_A^2 + 6g_\phi^2}{3v_F^3} - \frac{4}{N}\left(\frac{4\lambda_A}{c_A^3} + \frac{3\lambda_{\mathrm{YM}}}{c_A^3} + \frac{8\lambda_{\phi A}}{c_\phi c_A(c_\phi + c_A)}\right)\right], \\ &= 2\tilde{b}^2\left[1 - \epsilon - \frac{59\epsilon}{4N}\right]. \end{aligned} \tag{4.105}$$

4.7 CDW_3 Broken Symmetry State

To analyse the nature of the CDW_3 broken symmetry state, the free energy density $f(\phi, \boldsymbol{A}^1, \boldsymbol{A}^2)$ must be minimised. Infinitesimally close to the multi-critical point, f is obtained from integrating over the fermions for static order parameter fields with finite expectation values [141]. Although the criticality is universal, the broken symmetry state is not. Instead it depends on the lattice model and the concomitant path taken through the critical surface $(\delta_\phi, \delta_A) = \delta(\cos\theta, \sin\theta)$ with $\delta_{\phi,A} = (m^2_{\phi,A})_* - m^2_{\phi,A}$.

The analysis proceeds directly in $d = 2$ and is controlled with large N. In the region of the critical surface it is assumed that the couplings are well approximated by their fixed point values $(m^2_{\phi,A})_* = 4\Lambda^2$, $(g^2_\phi)_* = 4\pi\Lambda/N$, $(g^2_A)_* = 2(g^2_\phi)_*$, and $v_F = 1$. Integrating over the fermions obtains the Landau free energy density

$$\begin{aligned} f = -N\int_{-\infty}^{\infty}\frac{dk_0}{2\pi}\int^{\Lambda}\frac{d^2\boldsymbol{k}}{(2\pi)^2}\ln\det\left(-ik_0 + \boldsymbol{\alpha}\cdot\boldsymbol{k} + \frac{(g_\phi)_*}{\sqrt{N}}\phi\alpha_z T^3 + \frac{(g_A)_*}{\sqrt{N}}\boldsymbol{\alpha}\cdot\boldsymbol{A}^a T^a\right) \\ + \frac{m_\phi^2}{2}\phi^2 + \frac{m_A^2}{2}A^2 + \cdots . \end{aligned} \tag{4.106}$$

Here $\cdots$ indicate higher order terms that includes those depending on the lattice model. The free energy is minimised for $\boldsymbol{A}^1 \times \boldsymbol{A}^2 = 0$, as otherwise particle-hole symmetry is broken, which is energetically unfavourable. Evaluating the frequency

and momentum integrals by standard means

$$f(\phi, A) = -\frac{\delta_\phi}{2}\phi^2 - \frac{\delta_A}{2}A^2 + \frac{4-\pi}{4\pi}(g_A)_*(g_\phi^2)_* A\phi^2 + \cdots, \tag{4.107}$$

$$\rightarrow f(\rho, x) = -\frac{\delta}{3}\left((x-1)^2\cos\theta + 2(x+2)^2\sin\theta\right)\rho^2 + \frac{4-\pi}{3\sqrt{3}\pi}(x-1)^2(x+2)(g_A)_*(g_\phi^2)_* A\rho^3 + \cdots. \tag{4.108}$$

To make connection to the lattice model the second line uses the CDW_3 representation

$$\phi = \sqrt{2/3}(\rho - \Delta),\ (\boldsymbol{A}^1, \boldsymbol{A}^2) = \frac{4\rho + 2\Delta}{\sqrt{3}}(C_\alpha C_\beta, C_\alpha S_\beta, S_\alpha C_\gamma, S_\alpha S_\gamma), \tag{4.109}$$

with $C_\alpha = \cos\alpha$, $S_\alpha = \sin\alpha$, and parameterised $\Delta = x\rho$ for $1 \geq x \geq 0$ and $(\delta_\phi, \delta_A) = \delta(\cos\theta, \sin\theta)$. This representation is necessary for $V_2 \gg V_1$ on the honeycomb lattice, where unconstrained charge order has an ill-defined Hubbard-Stratonovich transformation at tree-level. This is evident from the bare Hubbard-Stratonovich bosonic mass Eq. (4.10) $L_{\rm HS} = \sqrt{3/2}(g_\phi)_0\phi^2 + \sqrt{3}(g_A)_0 A^2$, with $(g_\phi)_0 = \sqrt{3/2}(V_1 - 2V_2)$ and $(g_A)_0 = \sqrt{3}/2V_2$. Therefore, it is expedient to constrain the order parameter space to the physically valid CDW_3 region. Numerical simulations and semiclassical analysis [83] have identified the lattice ground state manifold is restricted to $\beta = \gamma$ and $(\alpha, \beta) = \frac{2\pi}{3}(n, m)$ for integers $n, m = 0, 1, 2$. Here α encodes translations and β rotations, which together enumerate the 9 possible charge configurations, displayed in Fig. 3.6. Naturally, the number of patterns is doubled with charge inversion ($\rho, \Delta < 0$).

The continuum free energy is independent of α, β, where $\boldsymbol{A}^1 \times \boldsymbol{A}^2 = 0$ enforces $\beta = \gamma$. Solving for $\frac{\partial f}{\partial \rho} = 0$ obtains the (partially) minimised free energy

$$f_*(x) = -\frac{4\pi^2\left(2(x+2)^2\sin\theta + (x-1)^2\cos\theta\right)^3}{(g_A)_*(g_\phi^2)_* 27(\pi-4)^2(x-1)^4(x+2)^2}\delta^3 + \cdots. \tag{4.110}$$

In general, the higher order, non-universal terms will select the minimizing value of x or Δ (subject to constraints), for a given path θ through the critical surface.

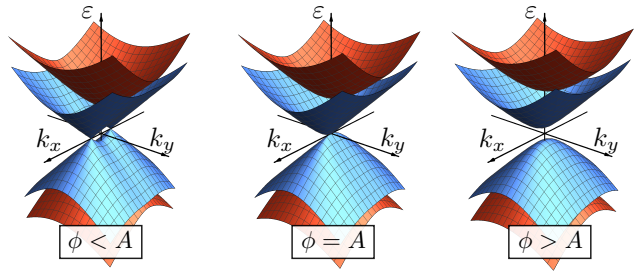

Figure 4.6: Topological phase transition between the Dirac semimetal ($\phi < A$) and band insulator ($\phi > A$), tuned by complementary mass ϕ and non-Abelian gauge A fields. The topological critical point ($\phi = A$) hosts anisotropic excitations with orthogonal relativistic and non-relativistic directions.

It is possible however to obtain the ground state in the limiting cases by assuming generic bounding quartic terms. For $\theta \to \pi/2^-$ it is found that $\Delta/\rho \to 1^-$ and $\phi \to 0^+$. In the other limit, $\theta \to 0^+$, it is found that $\Delta/\rho \to 0^+$, $\phi \to A^+$. In both cases minimisation requires $\beta = \gamma$, which causes $\phi(\boldsymbol{A}^1 \times \boldsymbol{A}^2)$ to vanish independent of particle-hole symmetry. Moreover, the lattice conditions $(\alpha, \beta) = \frac{2\pi}{3}(n, m)$ are determined by the vanishing of the lattice cubic term b, and the maximising of the lattice quartic term $\phi\,\mathrm{Re}[G_1^3 - 3G_1G_2^2]$.

The latter limit, $\theta \to 0^+$, is precisely the condition for the broken symmetry state to host the previously discussed gapless semi-Dirac [47, 48] excitations, which disperse quadratically in the direction defined by the polar angle β and linearly orthogonal to this. From the hybridisation of down-folded Dirac valleys there is a condensation energy gain from the second set of bands that gap with $\pm|\phi + A|$. In the previous chapter, such a metallic CDW_3 state with semi-Dirac quasiparticle excitations was found [68] for the case of the pure V_2 interaction.

4.7.1 Topological Phase Transitions

The broken symmetry state with gapless semi-Dirac excitations ($\phi = A$) can be interpreted as the critical point of the topological Lifshitz phase transition [48] between a semimetal ($\phi < A$) and a topologically trivial band insulator ($\phi > A$) (see Fig. 4.6). This notion for the $d = 2$ topological critical point can be generalised to the case of the three masses $\alpha_z M^a T^a$ for $a = 1, 2, 3$ and additional emergent gauge fields $\boldsymbol{A}^1, \boldsymbol{A}^2, \boldsymbol{A}^3$. This generalisation accounts for Kekulé masses ($M^{1,2}$) and gauge

fields $\boldsymbol{A}^3$, which may be induced by strain on the honeycomb lattice [147]. Implicit summation over repeated indices $a, b, c = 1, 2, 3$ is used, and here $M^2 = M^a M^a$ and $A^2 = \boldsymbol{A}^a \cdot \boldsymbol{A}^a$.

Assuming full global $SU(2)$ gauge rotational symmetry the analytic part of the Landau free energy takes the form (up to quartic order)

$$\begin{aligned} f = {} & C_1 M^2 + C_2 A^2 + C_3 \epsilon^{abc} M^a \boldsymbol{A}^b \times \boldsymbol{A}^c + C_4 M^2 A^2 + C_5 M^a \boldsymbol{A}^a \cdot M^b \boldsymbol{A}^b \\ & + C_6 M^4 + C_7 A^4 + C_8 (\epsilon^{abc} \boldsymbol{A}^b \times \boldsymbol{A}^c)^2 + C_9 \boldsymbol{A}^a \cdot \boldsymbol{A}^b \boldsymbol{A}^a \cdot \boldsymbol{A}^b, \end{aligned} \tag{4.111}$$

with unspecified coupling constants C_i. The $C_3 \epsilon^{abc} M^a \boldsymbol{A}^b \times \boldsymbol{A}^c$ and $C_5 M^a \boldsymbol{A}^a \cdot M^b \boldsymbol{A}^b$ terms must vanish to describe topological transitions. Subject to this, the topological critical point of the Hamiltonian

$$\hat{H} = \boldsymbol{k} \cdot \boldsymbol{\alpha} + \alpha_z M^a T^a + \boldsymbol{\alpha} \cdot \boldsymbol{A}^a T^a, \tag{4.112}$$

exists at $|M| = |A|$. A finite C_3 terms breaks particle-hole symmetry. A finite C_5 term induces a band gap for all finite M and A. These terms can also be identified from the characteristic polynomial $\det(\hat{H} - \varepsilon \hat{1})$. There are a number of obvious extensions including spin, dimensionality and the number of quadratic directions.

4.8 Discussion

Here it was demonstrated that spontaneous lattice symmetry breaking in interacting Dirac systems is described by effective field theories of Dirac fermions coupled to a combination of dynamical mass and emergent gauge order parameter fields. This is a departure from the common wisdom that mass channels solely dominate the energetic landscape [20, 133], which is an expectation motivated by the energetic gain upon condensing into an insulating state (mass fields are defined as those that anticommute with the non-interacting Hamiltonian, thereby acting to open a band gap). As a result, the ensuing criticality considered here is found to be beyond the GNY universality classes. The unconventional dynamical exponent $z > 1$ indicates that the putative emergent Lorentz invariance associated with GNY criticality is

violated.

As a concrete example the lattice symmetry breaking due to CDW_3 order of Dirac fermions on the half-filled honeycomb lattice was analysed. However, the resulting effective field theory with mass and gauge fields has much wider applicability. The important role of emergent gauge fields has been recognised in the context of the Ising nematic transition in d-wave superconductors [18, 135, 136, 148, 149], and there is indeed a close connection with the gauge sector of the field theory presented here.

That $z > 1$ raises the possibility that the long-range Coulomb interactions [19]

$$\hat{n}(\boldsymbol{r})\frac{e^2}{|\boldsymbol{r}-\boldsymbol{r}'|}\hat{n}(\boldsymbol{r}') \rightarrow -i\Psi^\dagger a_0\Psi + \frac{1}{2e^2}a_0\,|\boldsymbol{q}|\,a_0, \tag{4.113}$$

could be relevant and provide further non-trivial scaling at this novel critical point [50]. The one-loop RG equation for the Coulomb coupling [20]

$$\frac{d}{d\ell}e^2 \approx (z-1)e^2 - \delta_{d,3}e^4, \tag{4.114}$$

demonstrates that $z > 1$ defines e as a relevant perturbation. At the new CDW_3 fixed point it is expected that $z \sim 1 + (g_A^2)_* - xe^2$ $(x > 0)$ suggesting such relevance. In contrast, the Coulomb interaction is irrelevant at the $d = 2$ GNY fixed point $z = 1 - xe^2$ $(x > 0)$ [19, 20].

This work shows that complementary combinations of mass and non-Abelian gauge fields provide a natural playground for the study of topological quantum phase transitions. Lifshitz transitions of merging Dirac cones are observed when tuning through the broken-symmetry states close to the multi-critical point. These insights could be relevant for a range of systems, including black phosphorus [150, 151], optical honeycomb lattices [62, 152, 153], artificial graphene [63], $\mathrm{TiO_2/VO_2}$ interfaces [47, 154], and α(BEDT-TTF)$_2$I$_3$ [155]. Additionally, there has been considerable recent interest in the properties of topological quantum critical points [42, 49–56, 156], which in $d = 2$ are commonly described by effective Hamiltonians of the semi-Dirac form $\hat{H} = k_x^2\sigma_x + k_y\sigma_y$. Here anisotropic velocity renormalisation

needs to be regulated with non-perturbative infrared loop resummations [56], which is discussed in more detail in Chapter 5.

A related open question is whether there is a similar description of other exotic Lorentz violating fermions, such as the multifolds in topological chiral crystals [124–126], and what this means for their quantum critical properties [123, 157].

Chapter 5

Quantum Criticality of Semi-Dirac Fermions in 2+1 Dimensions

Semi-Dirac fermions in two spatial dimensions are quasiparticles that disperse linearly in one direction and quadratically in the other. Strong short-range interactions drive instabilities of semi-Dirac fermions. In this Chapter, the instabilities towards staggered charge and spin, as well as superconducting orders are considered. The critical properties of semi-Dirac fermions coupled to dynamical order parameter fields are analysed using the renormalisation group (RG). The RG equations are obtained to one-loop order and analytically controlled by a large number N_f of fermion flavours. The $1/N_f$ corrections are surprisingly small, suggesting that the expansion is well controlled in the physical dimension. The order-parameter correlations inherit the electronic anisotropy of the semi-Dirac fermions, leading to correlation lengths that diverge along the spatial directions with distinct exponents, even at the mean-field level. It is natural to conjecture that the proximity to the critical point may stabilise novel phases with modulated order. The original work in this chapter was made available as a preprint in *Quantum Criticality of Semi-Dirac Fermions in 2+1 Dimensions*, M. Uryszek, E. Christou, A. Jaefari, F. Krüger, B. Uchoa Phys. Rev. B **100**, 155101 (2019) [158].

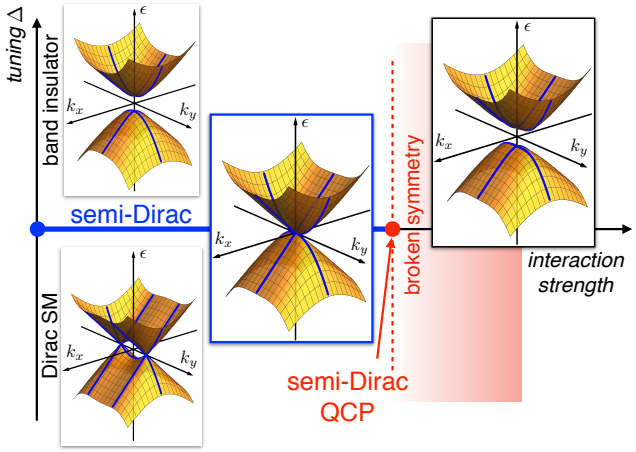

Figure 5.1: Schematic phase diagram. As a function of the band tuning parameter Δ the system undergoes a topological Lifshitz transition between a Dirac semimetal (with a pair of Dirac cones) and a band insulator. At the transition point the system exhibits gapless "semi-Dirac" quasiparticle excitations. Sufficiently strong short-range interactions leads to superconducting, or staggered charge or spin orders, depending on the type of interaction. The symmetry breaking is associated with the opening of a gap in the semi-Dirac spectrum.

5.1 Introduction

Dirac fermions generically describe quasiparticles with relativistic dispersion in the vicinity of special points in the Brillouin zone [15, 36, 43]. In two spatial dimensions (2D), the merging of two Dirac points results in a topological phase transition separating the semi-metallic phase from a gapped insulating one [45, 46]. At the boundary between the two phases, the system exhibits gapless "semi-Dirac" quasiparticle excitations [45, 47] that disperse relativistically (linearly) in one direction and non-relativistically (quadratically) in the other, see Fig. 5.1.

Based on density-functional calculations, semi-Dirac quasiparticles were predicted to occur in single layers of black phosphorus under strain [159]. Following this, the topological transition was observed by surfacing doping such black phosphorus [150, 151]. Semi-Dirac fermions have also been predicted to occur in α-(BEDT-TTF)$_2$I$_3$ salt under pressure [160], VO_2/TO_2 heterostructures [154, 161], and in strained honeycomb lattices [45]. As discussed in this Thesis, it has recently been suggested [68, 120] that strong next-nearest neighbour repulsions between fermions on the honeycomb lattice can lead to a charge ordered state that breaks lattice sym-

metries and exhibits semi-Dirac quasiparticles excitations. In addition, semi-Dirac fermions have strongly anisotropic hydrodynamic transport properties [52], for example the electrical conductivity is metallic in one direction and insulating in the other direction. Even more strikingly, one of the electronic sheer viscosity components vanishes at zero temperature, leading to a generalisation of the previously conjectured lower bound for the viscosity to entropy density ratio [52].

The non-trivial scaling of the quasiparticle kinetic energy gives rise to novel universal behaviour [42, 48–50, 54–56, 162]. Moreover, it is expected that the inherent electronic anisotropy will be reflected in strongly anisotropic order parameter correlations. This can have profound effects on the nature of broken-symmetry states. For instance, in gapped superconducting phases, it has been suggested [51] that an applied magnetic field may lead to the formation of a novel smectic phase with a stripe pattern of flux domains near the quantum critical point. Accessing the universal critical behaviour of 2D semi-Dirac fermions has proven difficult. Because of the different dispersion along the k_x and k_y directions, the generalisation to arbitrary dimension and consecutive ϵ expansion below an upper critical dimension is subtle and not uniquely defined. This is in contrast to the Dirac case discussed in Chapter 4. For a model with d_{L} linear and $d_{\mathrm{Q}} > 0$ quadratic momentum directions, the interactions become marginal at $2d_{\mathrm{L}} + d_{\mathrm{Q}} = 4$, suggesting that the universal critical behaviour of 2D semi-Dirac fermions ($d_{\mathrm{L}} = d_{\mathrm{Q}} = 1$) could be accessible within an ϵ-expansion with $d_{\mathrm{L}} = 1$ and $d_{\mathrm{Q}} = 2 - \epsilon$ [56]. This expansion results in a non-analytic $\sim \epsilon \ln \epsilon$ dependence of the anomalous dimensions of the fermion and order-parameter fields [56]. The non-monotonic behaviour and vanishing of the corrections at $\epsilon = 1$, nevertheless, could indicate that the semi-Dirac case lies outside the validity of the expansion.

In a complementary approach [42] generic short-range four-fermion interactions were analysed in two spatial dimensions with a generalised dispersion k_y^{2n} in the non-relativistic direction. This construction allowed for a controlled ascent from one dimension ($n \to \infty$). At finite n, fermionic interactions are rendered irrelevant at weak coupling, but key aspects of one-dimensional physics such as spin-charge

separation are preserved. Quantum fluctuations beyond 1D, controlled by $\sim 1/n$, enter the RG through loop integrations that involve the dispersion along k_y.

In this Chapter the quantum criticality of semi-Dirac fermions directly in two spatial dimensions is revisited. Universal critical properties are accessed by means of the one-loop momentum-shell RG. Analytic control is achieved by introducing a large number N_f of fermionic flavours. The additional N_f fermion flavours are not involved in the symmetry breaking and remain degenerate across the quantum phase transition. This complementary approach avoids tuning the dimensionality or the form of the dispersion, and as such can act as an independent check to the novel methods discussed above. A similar large N_f procedure was used to analyse the criticality of 2D and 3D semi-Dirac fermions subject to weak, long-range Coulomb interactions [49, 50, 162]. Where as, here the focus is on strong short-range interactions that drive charge, spin and superconducting instabilities. This study is motivated by the leading order RG analysis of Ref. [42], which deemed these to be the dominant instabilities in the context of an extended Hubbard model comprised of on-site (attractive and repulsive) and nearest-neighbour repulsive interactions. These broken symmetry phases possess a fully gapped quasiparticle spectrum and hence maximise the condensation energy gain. The results can be readily compared to the analogous two-loop large N_f analysis of relativistic 2D Dirac fermions [19, 71, 163, 164], unravelling the effects of the peculiar form of the dispersion on the universal behaviour.

It is found that the $1/N_f$ corrections to critical exponents are very small and considerably smaller than for the case of 2D Dirac fermions, suggesting that the expansion is well controlled. The mean-field limit, $N_f \to \infty$, recovers the results obtained from the $d_Q = 2 - \epsilon$ expansion[56], evaluated at $\epsilon = 1$ and $N_f \to \infty$. However the $1/N_f$ corrections differ, as they depend on the specific form of the dimensional-dependent bosonic infrared (IR) propagator, which needs to be included to regularise unphysical divergencies at the critical fixed point. As expected, it is found that the order-parameter correlations inherit the intrinsic anisotropy of the system, e.g. the correlation lengths along different spatial directions diverge with

different powers. It is conjectured that this behaviour could help stabilise exotic modulated ordered phases near the quantum critical point [56]. The $N_f \to \infty$ results are significantly different from the 2D Dirac case. This can be understood by analysing the mean-field Ginzburg-Landau free energy, which is obtained from integrating out the fermions in the broken symmetry state. Spatial anisotropies are encoded in non-analytic gradient terms. It is found that the critical exponents derived from the RG for $N_f \to \infty$ are in agreement with the exponents obtained from the mean-field Ginzburg-Landau functional, suggesting that hyperscaling relations are satisfied.

The rest of this Chapter is organised as follows. Section 5.2 motivates the effective Yukawa actions for spin, charge and superconducting instabilities. Section 5.3 discusses the Wilson RG procedure and the calculation of the RG equations and critical exponents in the large N_f limit. Section 5.4 presents the non-analytic structure of the mean-field theory. Section 5.5 ends the chapter with a discussion of the results.

5.2 Effective Semi-Dirac Field Theory

The effective low-energy field theory of 2D semi-Dirac fermions coupled to dynamical order parameter fields is presented. The non-interacting fermionic action is given by

$$S_\Psi = \sum_{n=1}^{N_f} \int_{\vec{k}} \Psi_n^\dagger(\vec{k}) s_0 \otimes \left[-ik_0\sigma_0 + vk_x\sigma_x + \left(\frac{k_y^2}{2m} + \Delta \right) \sigma_y \right] \Psi_n(\vec{k}), \tag{5.1}$$

where $\vec{k} = (k_0, \boldsymbol{k}) = (k_0, k_x, k_y)$, with k_0 the zero temperature Matsubara frequency, and $\int_{\vec{k}} = \int^\Lambda \frac{d^3\vec{k}}{(2\pi)^3}$, which is subject to an ultraviolet cut-off Λ. Also, v is the velocity in k_x and m is the effective mass in k_y. The Pauli spin s_i and pseudospin σ_i matrices ($i = 0$ for identities) act on the 4-component fermionic spinor fields $\Psi = (\psi_{\uparrow+}, \psi_{\uparrow-}, \psi_{\downarrow+}, \psi_{\downarrow-})$. The pesudospin is some relevant quantum number of the parent lattice model. For example it could be any sublattice, valley, or orbital degree of freedom. The action has been generalised to a large number N_f of fermionic

flavours $\Psi^\dagger\Psi \to \sum_{n=1}^{N_f} \Psi_n^\dagger \Psi_n$.

The poles of the (real frequency) fermionic propagator, or alternatively the eigenvalues of the Hamiltonian $H_0(\boldsymbol{k}) = s_0 \otimes [v k_x \sigma_x + (k_y^2/2m + \Delta)\sigma_y]$, provide the electronic dispersion

$$\varepsilon(\boldsymbol{k}) = \pm\sqrt{(v k_x)^2 + \left(\frac{k_y^2}{2m} + \Delta\right)^2}, \tag{5.2}$$

which is degenerate in spin $s = \uparrow, \downarrow$ and fermion flavour n. The effect of the tuning parameter Δ on the electron dispersion is illustrated in Fig. 5.1. For $\Delta < 0$ the dispersion contains two relativistic Dirac points $\boldsymbol{K}_\pm = \left(0, \pm\sqrt{2m(-\Delta)}\right)$, while for $\Delta > 0$ the dispersion has an energy gap Δ. Hence Δ tunes a transition between a Dirac semimetal and a band insulator. At $\Delta = 0$, the system undergoes a topological Lifshitz transition, corresponding to the merging of two Dirac points. At this point the system exhibits the anisotropic semi-Dirac quasiparticle excitations.

The aim is to describe interaction-driven quantum phase transitions of semi-Dirac fermions. Enforcing $\Delta = 0$ whilst increasing the strength of interactions requires fine tuning. Depending on the experimental system, this may be achieved with strain, pressure, or surface doping [150, 151, 154, 159–161].

5.2.1 Staggered Instabilities

Similar to Chapter 4, the critical theory is constructed from semi-Dirac fermions coupled to a Ginzburg-Landau-Wilson dynamical order parameter theory via a Yukawa coupling. Typically, a theory of this type can be obtained by performing a Hubbard-Stratonovich decoupling of a generic strongly interacting four-fermion interaction in the appropriate order parameter ϕ channel, which is schematically $(\Psi^\dagger\Psi)^2 \to \phi^2 + \Psi^\dagger\phi\Psi$. In contrast to the previous Chapters on the honeycomb lattice, here the microscopic origins of this critical theory are not provided. Instead, it is assumed there is a sufficiently strong fermionic interaction that spontaneously stabilises the order of interest. Similarly, phase competition and multicriticality is left for future investigation.

The local Yukawa action is

$$S_g = g \sum_{n=1}^{N_f} \sum_{i=1}^{N_b} \int_{\vec{r}} \Psi_n^\dagger(\vec{r}) Y_i \phi_i(\vec{r}) \Psi(\vec{r}), \tag{5.3}$$

where $\vec{r} = (\tau, \boldsymbol{r})$ is the imaginary time τ and position $\boldsymbol{r}$ vector. Here N_b is the number of components of the bosonic order parameter field $\boldsymbol{\phi} = (\phi_1, \ldots, \phi_{N_b})$ For the case of staggered charge order $N_b = 1$, and the Yukawa coupling matrix $Y_1 = s_0 \otimes \sigma_z$. In the instance that the pseudospin is a sublattice index, this would correspond to a sublattice charge density wave (CDW). For convenience it will be referred to as CDW order. Likewise, $N_b = 3$ has the natural interpretation as sublattice spin density wave (SDW) order, with $Y_i = s_i \otimes \sigma_z$ for $i = 1, 2, 3 = x, y, z$. Finally, $N_b = 2$ could be interpreted as describing s-wave superconducting (SC) pairing with $Y_i = s_i \otimes \sigma_0$ for $i = 1, 2 = x, y$. Naturally, this requires a redefinition of the spinor basis to the reduced Nambu (particle-hole doubled) space $\tilde{\Psi} = (\psi_{\uparrow+}, \psi_{\downarrow+}, \psi^\dagger_{\downarrow-}, \psi^\dagger_{\uparrow-})$ [165, 166]. In this case $\tilde{H}_0(\boldsymbol{k}) = s_z \otimes [v k_x \sigma_x + (k_y^2/2m + \Delta)\sigma_y]$. These Yukawa terms describe $U(1)$ s-wave pairing with the complex order parameter

$$\Phi = \langle \cos\varphi(\psi_{\uparrow-}\psi_{\downarrow+} + \psi_{\downarrow-}\psi_{\uparrow+} + \text{h.c.}) + i \sin\varphi(\psi_{\uparrow-}\psi_{\downarrow+} + \psi_{\downarrow-}\psi_{\uparrow+} - \text{h.c.}) \rangle, \tag{5.4}$$

where $\boldsymbol{\phi} = (\text{Re}\Phi, \text{Im}\Phi)$. It is natural to associate the flavour symmetry with time reversed points in the Brillouin zone (similar to Dirac valleys), such that the Cooper pair has zero total momentum. A concrete example of a time reversal symmetric tight-binding Hamiltonian with a pair of semi-Dirac points can be found in Ref. [51].

In principle, what has been described is semi-Dirac fermions coupled to Ising Z_2 ($N_b = 1$), XY $O(2)$ ($N_b = 2$) and Heisenberg $O(3)$ ($N_b = 3$) order parameter fields. In each instance, the order parameter fields couple like "masses" to the fermions in the sense that they anticommute with $H_0(\tilde{H}_0)$ and therefore induce an insulating gap upon condensing ($\phi^2 = \boldsymbol{\phi} \cdot \boldsymbol{\phi}$)

$$\varepsilon(\boldsymbol{k}) = \pm \sqrt{(v k_x)^2 + \left(\frac{k_y^2}{2m} + \Delta \right)^2 + (g\phi)^2}, \tag{5.5}$$

which is independent of the basis. These instabilities were found [42] to be dominant from renormalisation group analysis of an extended Hubbard model containing on-site and nearest neighbour interactions. For superconductivity it is required that the on-site interaction is attractive, in which case the textbook microscopic origin would be electron-phonon coupling.

In addition to the $\phi^2 = \boldsymbol{\phi} \cdot \boldsymbol{\phi}$ term that arises from the Hubbard-Stratonovich transformation, the successive elimination of high-energy fermion modes under the renormalisation group will generate gradient terms, as well as a ϕ^4 vertex and higher order terms. However, ϕ^4 and higher order terms turn out to be irrelevant in the RG sense. For now the Ginzburg-Landau-Wilson functional for the order parameter $S_\phi + S_\lambda$ is considered, with

$$S_\phi = \frac{1}{2} \int_{\vec{q}} \boldsymbol{\phi}(\vec{q}) \cdot \left(c_0^2 q_0^2 + c_x^2 q_x^2 + c_y^2 q_y^2 + m_\phi^2 \right) \boldsymbol{\phi}(\vec{q}), \tag{5.6}$$

$$S_\lambda = \lambda \int_{\vec{r}} \phi^4(\vec{r}). \tag{5.7}$$

As was the case for the Gross-Neveu-Yukawa type theories in Chapter 4, here the order parameter mass term tunes through the putative quantum critical point, and the convention $m_\phi^2 \to m_\phi^2 - (m_\phi^2)_*$ is used.

To summarise, the effective field theory describing the criticality of semi-Dirac fermions in 2+1 dimensions, to be considered in the following, is given by

$$S = S_\Psi + S_\phi + S_g + S_\lambda. \tag{5.8}$$

There is a caveat, however. As will be discussed in Section 5.3, the bosonic propagator $G_\phi(\vec{q})$ develops an unphysical singularity under the RG scheme. It is therefore necessary to regularise this divergence by including an infrared contribution in S_ϕ.

5.3 Renormalisation Group Analysis

In this Section, the universal critical behaviour of CDW, SDW and superconducting instabilities in the presence of semi-Dirac fermions is analysed. To do so a similar RG scheme to Chapter 4 is applied.

5.3.1 Shell Procedure

In the following the RG flow is obtained by successively integrating out high-energy modes from the infinitesimal 2+1 dimensional shell (defined for $\Delta = 0$)

$$\Lambda e^{-z\delta\ell} < \sqrt{k_0^2 + \varepsilon^2(\boldsymbol{k})} < \Lambda, \tag{5.9}$$

followed by a rescaling of frequency and momenta at each step,

$$k_0 \to k_0' = k_0 e^{z\,\delta\ell},\ k_x \to k_x' = k_x' e^{z\,\delta\ell},\ k_y \to k_y' = k_y' e^{z_y\,\delta\ell}. \tag{5.10}$$

In the definitions of the 2+1 dimensional shell Eq. (5.9), and the rescaling Eq. (5.10), the frequency k_0 and the momentum along the relativistic direction k_x are treated on an equal footing, and are both rescaled with a dynamical exponent z relative to the k_y direction. This can be viewed as having one space-like (k_y) and two time-like (k_0, k_x) directions. For greater clarity, the scaling dimension z_y of the momentum k_y has been introduced. Later it will be set to $z_y = 1$. Under successive mode decimation and rescaling, the cut-off Λ remains invariant if $z = 2z_y$. The shell integration is performed using the coordinate transformation

$$\begin{aligned} k_0 &= \varepsilon \sin\theta \cos\phi, \\ v k_x &= \varepsilon \sin\theta \sin\phi, \\ \frac{k_y^2}{2m} &= \varepsilon \cos\theta, \end{aligned} \tag{5.11}$$

with $\varepsilon \in [\Lambda e^{-z\delta\ell}, \Lambda]$, $\theta \in [0, \frac{\pi}{2}]$, and $\phi \in [0, 2\pi]$. The Jacobian of the transformation is

$$\rho(\varepsilon, \theta, \phi) = \frac{\sqrt{2m}}{2v} \frac{\sin\theta}{\sqrt{\cos\theta}} \varepsilon^{3/2}. \tag{5.12}$$

5.3.2 Tree-Level Scaling

Under the fermionic field rescaling

$$\Psi'(k') = \Psi(k) e^{-(3z + z_y - \eta_\Psi)\frac{\delta\ell}{2}}, \tag{5.13}$$

S_Ψ is scale invariant. The velocity v is an invariant of the flow, as k_0 and k_x scale in the same way, and so it is justified to work in units where $v = 1$. The anomalous dimension η_Ψ is chosen to ensure that the linear terms are scale invariant beyond tree-level. Similarly, the effective mass m associated with the quadratic k_y dispersion remains invariant at tree-level when $z = 2z_y$. Beyond tree-level z will gain $O(1/N_f)$ corrections, and is chosen to ensure m is scale invariant. Thus, it is also justified to work in units where $2m = 1$.

The distinct scaling of momenta, used to ensure the invariance of the cutoff and the fermionic action, mean that the bosonic velocity c_y^2 in S_ϕ will scale differently to c_0^2 and c_x^2. Under the bosonic field rescaling

$$\phi'(k') = \phi(k)e^{-(2z+3z_y-\eta_\phi)\frac{\delta\ell}{2}}, \tag{5.14}$$

c_y^2 is invariant at tree-level, and η_ϕ can ensure invariance beyond this, such that units where $c_y^2 = 1$ are used. However, under this scaling the other bosonic velocities are rendered strongly irrelevant at tree-level with scaling dimensions $[c_0^2] = [c_x^2] = -z$. Therefore, even with loop corrections, both velocities will flow to zero and are effectively omitted from the bare bosonic propagator. Surprisingly, this shell integration has introduced the unphysical divergence in the IR limit $q_y \to 0$,where there is now a pole in the bosonic propagator for all q_0, q_x. The resolution to this problem involves regularisation from the IR bosonic self-energy, which is discussed in Section 5.3.3.

Finally, the field rescalings indicate that the Yukawa coupling is a relevant perturbation $g \to ge^{z_y\delta\ell/2}$, but the bosonic self-interaction is strongly irrelevant $\lambda \to \lambda e^{-z_y\delta\ell}$, and is therefore neglected in the following. It is natural to redefine the Yukawa coupling , $g^2 \to g^2\sqrt{\Lambda}/2N_f$ such that

$$S_g = g\sqrt{\frac{\sqrt{\Lambda}}{2N_f}}\sum_{n=1}^{N_f}\sum_{i=1}^{N_b}\int_{\vec{r}}\Psi_n^\dagger(\vec{r})Y_i\phi_i(\vec{r})\Psi_n(\vec{r}). \tag{5.15}$$

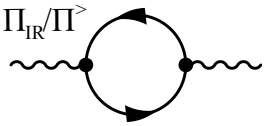

Figure 5.2: The one-loop fermion polarisation bubble diagram that describes the infrared regulator of the bosonic propagator when modes outside of the Wilsonian momentum shell are integrated out. Alternatively it describes the self-energy correction of the bosons when the modes inside the shell are integrated out. The fermion propagator is denoted by the arrowed line.

5.3.3 Infrared Regularisation

In order to regularise the unphysical divergence of the bosonic propagator in the limit $q_y \to 0$, the IR contribution must be included. As pointed out before [50], in 2+1 dimensions the bosonic propagator has different asymptotic forms in the UV and IR limits. Since the RG flow is generated by a successive integration of modes from a shell near the UV cut-off, the IR ($\varepsilon \to 0$) contribution is not generated or renormalised under the RG. Instead the IR boson self-energy needs to be computed separately by integrating the fermion polarisation (see Fig. 5.2) over the frequency and momentum range outside of the infinitesimal shell [50],

$$\Pi_{ij}(\vec{q}) = \frac{g^2}{2}\frac{\sqrt{\Lambda}}{2N_f}\mathrm{tr}\int_{\vec{k}} Y_i G_\Psi(\vec{k}) Y_j G_\Psi(\vec{k}+\vec{q}), \tag{5.16}$$

where the fermionic propagator for the CDW and SDW channels is

$$G_\Psi(\vec{k}) = s_0 \otimes \frac{ik_0\sigma_0 + k_x\sigma_x + k_y^2\sigma_y}{k_0^2 + k_x^2 + k_y^4}. \tag{5.17}$$

The propagator in the SC channel is obtained by replacing $s_0 \to s_z$. For the multicomponent order parameters the polarisation is diagonal, $\Pi_{ij}(\vec{q}) = \Pi(\vec{q})\delta_{ij}$, reflecting the underlying $O(N_b)$ symmetry. It is possible to evaluate the integral in Eq (5.16) analytically for $q_y \to 0$, resulting in

$$\Pi_{\mathrm{IR}}(\vec{q}) = \frac{g^2\sqrt{\Lambda}}{2}\left(q_0^2 + q_x^2\right)^{\frac{1}{4}}. \tag{5.18}$$

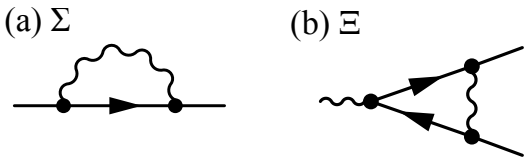

Figure 5.3: The one-loop (a) fermion self-energy and (b) vertex correction to the Yukawa coupling. The bosonic propagator is represented by the wavy line while the fermionic propagator by the straight line. Internal lines are contractions over high-energy shell mode. External lines are modes outside of the shell. The fermion propagator is denoted by the arrowed line. The boson propagators are denoted by the wavy line.

This is achieved using the procedures discussed in Appendix A.1, and an almost identical calculation can be found in Ref. [50]. This IR self-energy contribution to the kernel of $\mathcal{S}_\phi$ regularises the bosonic propagator in the IR at the critical surface ($m_\phi^2 = 0$),

$$G_\phi^{-1}(\vec{q}) = q_y^2 + \frac{g^2\sqrt{\Lambda}}{2}\left(q_0^2 + q_x^2\right)^{\frac{1}{4}}. \tag{5.19}$$

5.3.4 Self-Energy and Vertex Corrections

One-loop UV shell corrections are now calculated. The one-loop bosonic self-energy is

$$\Pi^{>}(\vec{q}) = \frac{g^2}{2}\frac{\sqrt{\Lambda}}{2N_f}\mathrm{tr}\int_{\vec{k}}^{>} Y_i G_\Psi(\vec{k}) Y_j G_\Psi(\vec{k}+\vec{q}), \tag{5.20}$$

where $\int_{\vec{k}}^{>}$ indicates integration over the UV modes within the frequency-momentum shell defined in Eq. (5.9). The IR part is not renormalised under the RG. The important corrections are in the q_y direction and to the bosonic mass m_ϕ^2. To leading order $\Pi^{>}(\vec{q}) \approx \Pi_y q_y^2 + \Pi_{m_\phi^2} m_\phi^2$, and for $\Delta = 0$

$$\Pi_y = \frac{11}{21\pi^2} g^2 z \delta\ell, \quad \Pi_{m_\phi^2} = 0. \tag{5.21}$$

The one-loop fermionic self-energy, shown in Fig. 5.3(a), is

$$\Sigma(\vec{k}) = -g^2\frac{\sqrt{\Lambda}}{2N_f}\sum_{i=1}^{N_b}\int_{\vec{q}}^{>} Y_i G_\Psi(\vec{k}+\vec{q}) Y_i G_\phi(\vec{q}). \tag{5.22}$$

Integrating over the shell,

$$\Sigma(\vec{k}) = s_0 \otimes [\Sigma_0(k_0\sigma_0 + k_x\sigma_x) + (\Sigma_y k_y^2 + \Sigma_\Delta \Delta)\sigma_y] z\delta\ell, \tag{5.23}$$

where for $m_\phi^2 = 0$

$$\Sigma_0 = \Sigma_x = \frac{N_b}{2N_f} F_1(g^2) z\delta\ell,\ \Sigma_y = \frac{N_b}{2N_f} F_2(g^2) z\delta\ell,\ \Sigma_\Delta = 0, \tag{5.24}$$

and the integral functions (see Fig. 5.4) are

$$F_1(x) = \frac{1}{4\pi^2} \int_0^{\frac{\pi}{2}} d\theta\, \frac{(\cos\theta)^{\frac{3}{2}} \sin\theta}{x^{-1}\cos\theta + \sqrt{\sin\theta}}, \tag{5.25}$$

$$F_2(x) = \frac{1}{4\pi^2} \int_0^{\frac{\pi}{2}} d\theta\, \frac{\cos 2\theta + 2\cos 4\theta}{x^{-1}\cos\theta + \sqrt{\sin\theta}} \frac{\sin\theta}{\sqrt{\cos\theta}}. \tag{5.26}$$

Similarly, the one-loop correction to the Yukawa vertex, shown in Fig. 5.3(b), is

$$g\frac{\sqrt{\Lambda}}{2N_f} \Xi Y_i = g^3 \left(\frac{\sqrt{\Lambda}}{2N_f}\right)^{\frac{3}{2}} \sum_{j=1}^{N_b} \int_{\vec{q}}^{>} G_\phi(\vec{q}) Y_j G_\Psi(\vec{q}) Y_i G_\Psi(\vec{q}) Y_j, \tag{5.27}$$

$$\Xi = -\frac{2 - N_b}{2N_f} F_3\left(g^2\right) z\delta\ell, \tag{5.28}$$

$$F_3(x) = \frac{1}{4\pi^2} \int_0^{\frac{\pi}{2}} d\theta\, \frac{1}{x^{-1}\cos\theta + \sqrt{\sin\theta}} \frac{\sin\theta}{\sqrt{\cos\theta}}. \tag{5.29}$$

Note that the vertex correction to the Yukawa coupling g has opposite sign for the CDW ($N_b = 1$) and SDW ($N_b = 3$) instabilities and vanishes in the case of the SC ($N_b = 2$), as reported in previous studies [56].

5.3.5 Renormalisation Group Equations

Following from the definitions set in Section 5.3.2

$$\eta_\Psi = \frac{\Sigma_0}{\delta\ell} = \frac{N_b}{2N_f} F_1(g^2) z, \tag{5.30}$$

$$z = 2z_y + \frac{\Sigma_y}{\delta\ell} - \eta_\Psi \Rightarrow z = \frac{2z_y}{1 + \frac{N_b}{2N_f}[F_2(g^2) - F_1(g^2)]}, \tag{5.31}$$

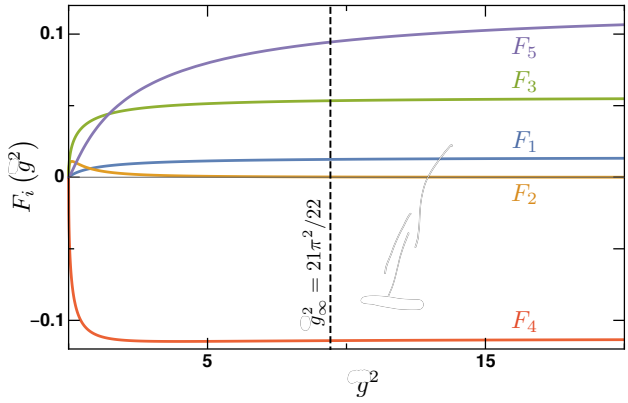

Figure 5.4: The integrals $F_i\left(g^2\right)$ as a function of the dimensionless Yukawa coupling g. To order $1/N_f$, the critical exponents at one-loop order depend on the values of F_i evaluated at the critical point in the $N_f \to \infty$ limit, $g^2_\infty = \lim_{N_f\to\infty} g^2_* = 21\pi^2/22$.

$$\eta_\phi = \frac{\Pi_y}{\delta\ell} = \frac{11}{21\pi^2} g^2 z. \tag{5.32}$$

Therefore, there is the single RG equation for the Yukawa coupling

$$\begin{aligned}\frac{dg^2}{d\ell} &= g^2\left(z_y - 2\eta_\psi - \eta_\phi + 2\frac{\Xi}{\delta\ell}\right),\\ &= g^2\left(z_y - \frac{N_b}{N_f}F_1(g^2)z - \frac{11}{21\pi^2}g^2 z - \frac{2-N_b}{N_f}F_3\left(g^2\right)\right).\end{aligned} \tag{5.33}$$

This depends on the integral functions F_i, which are smooth functions of g^2, as shown in Fig. 5.4.

5.3.6 Fixed Point and $1/N_f$ Expansion

In the following $z_y = 1$. The Yukawa RG equation and z are solved self-consistently order by order in N_f as follows. In $N_f \to \infty$, $z = 2$ and the fixed point is $(g^2_\infty)_* = 21\pi^2/22$. In order to obtain the leading $1/N_f$ correction to the fixed point, the *ansatz* $(g^2)_* = (g^2_\infty)_* + \frac{\delta}{N_f} + O(1/N_f^2)$, is made. To this order the approximation $\alpha_i = F_i\left(g^2_\infty\right)$ is valid. Then to leading order in N_f the following relations are obtained for the non-trivial fixed point values

$$z = 2 + \frac{N_b}{N_f}(\alpha_1 - \alpha_2), \quad \eta_\Psi = \frac{N_b}{N_f}\alpha_1, \quad \eta_\phi = \frac{g^2_*}{g^2_\infty}, \tag{5.34}$$

$$\frac{g_*^2}{g_\infty^2} = 1 - \frac{N_b}{2N_f}(5\alpha_1 - \alpha_2) - 2\frac{2 - N_b}{N_f}\alpha_3. \tag{5.35}$$

The above $1/N_f$ corrections are small, and about an order of magnitude smaller than for the purely relativistic case of Dirac fermions in 2+1 dimensions [71]. In the latter case, the $1/N_f^2$ corrections computed to two-loop order [163, 164] are comparable to, or even larger than, the $1/N_f$ corrections when $N_f = 1$. Where as for semi-Dirac fermions at one-loop order, the $1/N_f^2$ corrections are proportional to derivatives $F_i'\left(g_\infty^2\right) \simeq 10^{-4}$, and hence are approximately an order of magnitude smaller than the $1/N_f$ correction. This suggests that the $1/N_f$ expansion at the physical dimension is better controlled for the case of semi-Dirac fermions. However, the evaluation of two-loop diagrams would be required to investigate this further.

5.3.7 Critical Exponents

It is easily verifiable that the critical fixed point at g_* is stable along the g axis. Near this multicritical point there are two relevant perturbations, Δ and m_ϕ^2, which are the tuning parameters for the topological phase transition and the broken symmetry state respectively.

Semi-Dirac quasiparticle excitations emerge in the semi-metallic phase when Δ is fine tuned to zero. The case that Δ remains equal to zero across the symmetry-breaking phase transition is first considered. In this case the RG equation for m_ϕ^2 is equal to

$$\frac{dm_\phi^2}{d\ell} = \left(2 - \eta_\phi\right) m_\phi^2 = \nu^{-1} m_\phi^2. \tag{5.36}$$

Then to leading order

$$\nu = 1 - \frac{N_b}{2N_f}(5\alpha_1 - \alpha_2) - 2\frac{2 - N_b}{N_f}\alpha_3. \tag{5.37}$$

The electronic dispersion of semi-Dirac fermions with linear and quadratic directions is strongly anisotropic. Therefore it is expected that the order parameter correlations inherit this anisotropy. For spatially isotropic systems, the correlation length along the imaginary time direction diverges as a power of the spatial correla-

tion length, $\xi_\tau = \xi^z$, where z is the dynamical exponent. For the choice $z_y = 1$, the dynamical exponent z sets the scaling dimension of length along the x direction, implying that $\xi_\tau \simeq \xi_x \simeq \xi_y^z$. The spatial anisotropy of the order-parameter correlations is therefore reflected in correlation length exponents $\nu_x = z\nu$ and $\nu_y = \nu$, along the x and y directions, respectively. In the limit $N_f \to \infty$ this gives $\nu_x = 2$ and $\nu_y = 1$.

Assuming that the system satisfies hyperscaling, the standard scaling relations can be applied to obtain the remaining critical exponents. Josephson's hyperscaling relation yields the specific heat exponent,

$$\begin{aligned} \alpha &= 2 - \nu(2z+1), \\ &\approx -3 + \frac{N_b}{2N_f}(21\alpha_1 - \alpha_2) + 10\frac{2-N_b}{N_f}\alpha_3. \end{aligned} \tag{5.38}$$

Note that the effective dimension that enters in the hyperscaling relation is equal to $D = 2z + 1$ corresponding to one space-like and two time-like directions. Fisher's scaling law gives the susceptibility exponent

$$\gamma = \left(2 - \eta_\phi\right)\nu = 1 + O(1/N_f^2). \tag{5.39}$$

Rushbrooke's scaling law $\alpha + 2\beta + \gamma = 2$ is used to obtain the order-parameter critical exponent

$$\begin{aligned} \beta &= 1 - \frac{1}{2}(\alpha + \gamma), \\ &\approx 2 - \frac{N_b}{4N_f}(21\alpha_1 - \alpha_2) - 5\frac{2-N_b}{N_f}\alpha_3. \end{aligned} \tag{5.40}$$

Finally, from the Widom identity $\gamma = \beta(\delta - 1)$ the field exponent is computed

$$\begin{aligned} \delta &= 1 + \frac{\gamma}{\beta}, \\ &\approx \frac{3}{2} + \frac{N_b}{16N_f}(21\alpha_1 - \alpha_2) + \frac{5}{4}\frac{2-N_b}{N_f}\alpha_3. \end{aligned} \tag{5.41}$$

A complete list of critical exponents with numerical values for the coefficients α_i can be found in Tab. 5.1.

z_y	1
z	$2 + 0.0123\ \frac{N_b}{N_f}$
η_ψ	$0.0125\ \frac{N_b}{N_f}$
η_ϕ	$1 - 0.0310\ \frac{N_b}{N_f} - 0.1069 \frac{2-N_b}{N_f}$
ν	$1 - 0.0310\ \frac{N_b}{N_f} - 0.1069 \frac{2-N_b}{N_f}$
α	$-3 + 0.1307\ \frac{N_b}{N_f} + 0.5345\ \frac{2-N_b}{N_f}$
γ	1
β	$2 - 0.0653\ \frac{N_b}{N_f} - 0.2672\ \frac{2-N_b}{N_f}$
δ	$\frac{3}{2} + 0.0163\ \frac{N_b}{N_f} + 0.0668\ \frac{2-N_b}{N_f}$

Table 5.1: Critical exponents for symmetry-breaking phase transitions of semi-Dirac fermions in 2+1 dimensions, calculated at one-loop order and including $1/N_f$ corrections in the number of fermion flavours. N_b is the number of order-parameter components: $N_b = 1$ for the CDW, $N_b = 2$ for the superconducting and $N_b = 3$ for the SDW instabilities.

5.3.8 Multicriticality

Section 5.3.7 summarised the universal critical behaviour of semi-Dirac fermions associated with spontaneous symmetry breaking due to short-range interactions. The semi-Dirac quasiparticle excitations in the disordered, semimetallic phase are obtained by fine tuning the system to the point of a topological phase transition between a Dirac semimetal with two separate relativistic Dirac points and a band insulator. In the free-fermion action (5.1) the semi-Dirac point corresponds to $\Delta = 0$. Spontaneous symmetry breaking leads to the opening of a gap in the fermion spectrum, making it challenging to ensure $\Delta = 0$ across the transition in any real material.

Since the tuning parameters of the symmetry-breaking and topological phase transitions, m_ϕ^2 and Δ, are both relevant perturbations at the fixed point ($g = g_*$, $\Delta = m_\phi^2 = 0$), the fixed point should be viewed as multicritical. The coupled RG equations for m_ϕ^2 and Δ are

$$\frac{dm_\phi^2}{d\ell} = \left(2 - \eta_\phi\right) m_\phi^2 + z\Pi_{m_\phi^2}, \tag{5.42}$$

$$\frac{d\Delta}{d\ell} = \left(2 - \eta_\Psi\right) \Delta + z\Sigma_\Delta, \tag{5.43}$$

where the renormalisations $\Pi_{m_\phi^2}$ and Σ_Δ are coming from the bosonic self-energy (Fig. 5.2) and fermionic self-energy (Fig. 5.3(a)) and are equal to

$$\Pi_{m_\phi^2} = \frac{2}{3\pi^2} g^2 \Delta, \tag{5.44}$$

$$\Sigma_\Delta = \frac{N_b}{2N_f} \left[F_4\left(g^2\right) \Delta + F_5\left(g^2\right) m_\phi^2 \right]. \tag{5.45}$$

The additional integration functions

$$F_4(x) = \frac{1}{\pi^2} \int_0^{\frac{\pi}{2}} d\theta \, \frac{\cos 2\theta}{x^{-1} \cos\theta + \sqrt{\sin\theta}} \frac{\sin\theta}{\sqrt{\cos\theta}}, \tag{5.46}$$

$$F_5(x) = \frac{1}{\pi^2} \int_0^{\frac{\pi}{2}} d\theta \, \frac{\sqrt{\cos\theta}\sin\theta}{\left(x^{-1} \cos\theta + \sqrt{\sin\theta}\right)^2}, \tag{5.47}$$

are shown in Fig. 5.4. Linearising around the multicritical fixed point obtains the stability matrix M, see Section 4.3. The two positive eigenvalues θ_1 and θ_2 of M are inversely proportional to correlation length exponents, $\nu_i = 1/\theta_i$. These are found to be

$$\nu_1 = 1 - \frac{N_b}{2N_f} \left(5\alpha_1 - \alpha_2 - \frac{28}{11}\alpha_5 \right) - 2\frac{2 - N_b}{N_f}\alpha_3, \tag{5.48}$$

$$\nu_2 = \frac{1}{2} + \frac{N_b}{4N_f} \left(\alpha_1 - \alpha_4 - \frac{14}{11}\alpha_5 \right). \tag{5.49}$$

5.4 Mean-Field Analysis

The critical exponents are expected to recover the mean-field values in the limit $N_f \to \infty$. In this limit, the anomalous dimension of the fermion fields vanishes, $\eta_\Psi = 0$, indicating that Fermi-liquid behaviour is recovered. However, the anomalous dimension of the order parameter field (5.34) remains finite, $\eta_\phi = 1$. This results in a correlation length exponent $\nu = 1/(2 - \eta_\phi) = 1$ and an unusually large order-parameter exponent $\beta = 2$, which are found by using the scaling relations. These exponents are very different from the usual mean-field exponents ($\eta_\phi = 0$, $\nu = \beta = \frac{1}{2}$). This unusual behaviour is a result of the appearance of non-analytic terms in the mean-field free energy, which lead to unconventional quantum criticality and

arise due to the unusual scaling of the density of states $\rho(\varepsilon) \sim \sqrt{\varepsilon}$ around the Fermi points.

The mean-field free energy for a gapped phase of semi-Dirac fermions is equal to [51]

$$f_{\mathrm{mf}}(\phi_0) = \frac{1}{g}\phi_0^2 - \int_{k_x^2+k_y^4\leq\Lambda^2} \frac{d^2\boldsymbol{k}}{(2\pi)^2}\sqrt{k_x^2 + k_y^4 + \phi_0^2}, \tag{5.50}$$

$$f_{\mathrm{mf}}(\phi_0) = a(\delta g)\phi_0^2 + b|\phi_0|^{\frac{5}{2}} + O(\phi_0^4), \tag{5.51}$$

where Λ is the UV energy cut-off, $\delta g = (g_c - g)/g_c$ and $a, b > 0$. As in the case of relativistic Dirac fermions, the mean-field free energy contains a non-analytic term $|\phi_0|^{\frac{5}{2}}$, which arises from the evaluation of the integral in the $\boldsymbol{k} \to 0$ limit. Minimising $f_{\mathrm{mf}}(\phi_0)$ with respect to ϕ_0 one obtains $|\phi_0| \sim |\delta g|^{\beta_{\mathrm{mf}}}$ with $\beta_{\mathrm{mf}} = 2$, in agreement with the RG and scaling analysis in the $N_f \to \infty$ limit. In contrast, as was discussed in Chapter 2, the density of states of Dirac fermions vanishes linearly, $\rho(\varepsilon) \sim \varepsilon$, resulting in the non-analytic cubic term $|\phi_0|^3$ and the mean-field exponent $\beta_{\mathrm{mf}} = 1$.

The spatial anisotropy of the system, which appears in the anisotropic dispersion of the quasiparticles, also reflects in the form of the gradient terms in the Ginzburg-Landau functional. These terms can be computed by allowing for small, long-wavelength modulations of the order parameter. For a finite homogeneous component ϕ_0 one can expand in the momentum $\boldsymbol{q}$ of the modulation. This gives rise to terms $q_x^2\sqrt{|\phi_0|}$ and $q_y^2|\phi_0|^{\frac{3}{2}}$ [51], from which the estimations can be made for the correlation lengths ξ_x and ξ_y along the x and y directions respectively. Since

$$\xi_x^{-2}|\phi_0|^{\frac{1}{2}} \simeq \xi_y^{-2}|\phi_0|^{\frac{3}{2}} \simeq |\delta g|\phi_0^2 \tag{5.52}$$

by dimensional analysis, this leads to the quantum critical scaling

$$\xi_x^2 \sim |\phi_0|^{-\frac{3}{2}}|\delta g|^{-1} \sim |\delta g|^{-(1+\frac{3}{2}\beta_{\mathrm{mf}})}, \tag{5.53}$$

$$\xi_y^2 \sim |\phi_0|^{-\frac{1}{2}}|\delta g|^{-1} \sim |\delta g|^{-(1+\frac{1}{2}\beta_{\mathrm{mf}})}. \tag{5.54}$$

Using $\beta_{\rm mf} = 2$, this simple scaling analysis of the mean-field free energy recovers the correlation length exponents $\nu_x = 2$ and $\nu_y = 1$, in agreement with the RG result in the limit $N_f \to \infty$.

The anisotropic scaling of the correlation length along the x and y directions could have very interesting implications for ordered phases in the vicinity of the quantum critical point. In general, the order parameter becomes relatively softer to spatial modulations along the direction where the quasiparticles have parabolic dispersion, and more rigid in the other direction, permitting the emergence of modulated order and stripe phases [51]. In the superconducting case, the system may effectively respond to an external magnetic field as a type II superconductor in one direction and as a type I in the other [51]. This unconventional state could stabilise stripes of magnetic flux rather than conventional vortex lattices.

5.5 Discussion

The critical behaviour of quantum phase transitions in semi-Dirac fermion systems that are driven by strong short-range interactions have been analysed. Here the focus has been on the staggered charge and spin instabilities, as well as s-wave superconductivity. These fully gap the quasiparticle spectrum in the broken symmetry state, making them energetically favourable.

This criticality was previously studied using an ϵ expansion in the number of quadratically dispersing directions within the Yukawa formalism [56], and by generalising the quadratic dispersion to k_y^{2n}, facilitating a $1/n$ expansion in generic four-fermion interactions around the one-dimensional limit [42]. In the complementary approach presented here, a large number N_f of fermion flavours was introduced to gain analytic control in two spatial dimensions. Using a one-loop RG analysis of the effective Yukawa actions, the critical exponents have been computed up to order $1/N_f$.

The $1/N_f$ corrections to critical exponents depend on the peculiar form of the IR order-parameter propagator in 2+1 dimensions, $G_\phi^{-1} \sim \left(q_0^2 + q_x^2\right)^{\frac{1}{4}} + q_y^2$. This IR contribution, which is not renormalised by integrating out electronic UV modes,

needs to be incorporated to regularise unphysical divergencies [50, 56].

The frequency k_0 and the momentum k_x along the relativistic direction were treated on an equal footing, and a single "dynamical" exponent z that describes the scaling of k_0, k_x relative to the quadratically dispersing direction k_y was introduced. This can be viewed as having one space-like and two time-like directions.

It was found that the $1/N_f$ corrections to critical exponents are smaller than for the case of Dirac fermions, and seem to fall off more rapidly when increasing the order of $1/N_f$. This suggests that the $1/N_f$ expansion is well controlled even when the number of flavours $N_f = O(1)$. However, calculations beyond one-loop order are required to confirm this conjecture.

In the mean-field limit $N_f \to \infty$, the anomalous dimension η_ψ of the fermion fields vanishes, signalling a recovery of conventional Fermi-liquid behaviour. On the other hand, the anomalous dimension of the order-parameter fields remains finite, $\eta_\phi = 1$. This has important consequences. It gives rise to a correlation length exponent of $\nu = 1$ instead of the conventional mean-field $\nu = 1/2$. Since the y direction was defined as the reference length ($z_y = 1, z_x = z = 2$), this corresponds to $\nu_y = z_y \nu = 1$ and $\nu_x = z_x \nu = 2$ along the two spatial directions.

The atypical correlation length exponent and the unusually large order parameter exponent $\beta = 2 + O(1/N_f)$ suggest that the mean-field order-parameter theory is highly unusual [51]. As was discussed, the vanishing density of states at the Fermi level gives rise to a non-analytic $|\phi_0|^{5/2}$ term in the Landau free energy. This results in $\beta_{\mathrm{MF}} = 2$, in agreement with the RG result for $N_f \to \infty$. The highly anisotropic order-parameter correlations correspond to different non-analytic gradient terms in the mean-field theory.

It is interesting to compare to previous results in the literature [42, 56]. The freedom in how to define the scaling dimensions in semi-Dirac systems explains the apparent contradiction with Ref. [42] that reports $\nu = 2$ at leading order, compared to $\nu = 1$ here and in Ref. [56]. A close inspection shows that in this work the relativistic direction was used to define the reference length scale. In the notation used here this corresponds to the choice $z = z_x = 1$ and $z_y = 1/2$, leading to the

same correlation length exponents $\nu_x = 2$ and $\nu_y = 1$. Then to leading order there is complete agreement on the correlation length exponent.

However, there is a strong disparity in the order parameter anomalous dimensions found here $\eta_\phi = 1 + O(1/N_f)$, and in Ref. [56], $\eta_\phi \sim \frac{1}{N_f}\epsilon \ln \epsilon$. Not only does the latter vanish for $\epsilon = 1$, but it is also $O(1/N_f)$. As was discussed in Sec. 5.4, our $\eta_\phi \approx 1$ gives rise to the same order parameter exponent $\beta = 2$ in $N_f \to \infty$ as that from the non-analytic mean-field free energy. This acts as a consistency check of our RG analysis. Likewise, the fermion anomalous dimension $\eta_\psi \sim \frac{1}{N_f}\epsilon \ln \epsilon$ calculated in Ref. [56] vanishes at $\epsilon = 1$, where as here it is finite $\eta_\psi = O(1/N_f)$. These discrepancies may arise from the invalidity of the extrapolation of the novel leading order ϵ expansion to $\epsilon = 1$. At the leading one-loop order, it is not possible to extract the anomalous dimensions from the RG analysis of the model containing four-fermion interactions studied in Ref. [42]. In the future it will be interesting to compare beyond leading order results for the critical exponents in this difficult problem.

Semi-Dirac fermions correspond to an intermediate case between Dirac fermions and ordinary metals in two spatial dimensions. The quadratic dispersion along one of the momentum directions leads to an increased density of states at low energies as compared to Dirac fermions, making instabilities comparatively easier due to the enlarged phase space for quantum fluctuations. An interesting question for future studies is whether the enhanced electronic fluctuations near quantum critical points combined with the anisotropy of the correlations could stabilise novel phases such as modulated order.

Chapter 6

Closing Remarks

Here a summary of the results presented in this Thesis are provided. Detailed discussions can be found at the end of each Chapter. Following this, future lines of research are suggested.

6.1 Summary

In this Thesis the role of strong repulsive fermionic interactions to induce novel quantum criticality, and exotic phases of matter, was investigated in two-dimensional Dirac systems using analytical methods. The focus was on the following three topics: (i) The impact of collective quantum fluctuations in determining the fate of the interaction induced topological Mott insulator, which was predicted at the level of mean-field theory. (ii) The novel fermionic quantum criticality that ensues when translational and rotational lattice symmetries are spontaneously broken, corresponding to an effective field theory containing emergent gauge degrees of freedom. (iii) The interplay of topological and symmetry breaking continuous phase transitions, resulting in a quantum multicritical point with anistropic semi-Dirac quasiparticle excitations. A central theme throughout this work was the pivotal role played by the gapless fermionic quasiparticles.

All three topics were motivated by considerations of the extended fermionic Hubbard model on the honeycomb lattice, which is the prototypical Dirac semimetal at half-filling. From these lattice models low-energy effective field theories of Dirac-like fermions coupled to dynamical order parameter bosons could be derived. The

energetics of the competing broken symmetry states considered in topic (i) were calculated using a self-consistent path integral approach. Here the fermionic modes were formally integrated out and the resulting Gaussian order parameter fluctuations were accounted for. Complementary to this, the universal properties investigated in topics (ii) and (iii) employed a renormalisation group scheme that treated the critical fermions and order parameter bosons on an equal footing.

(i) In Chapter 3 the fate of the topological Mott insulator on the honeycomb lattice was investigated. This phase was first found by a mean-field decoupling of strong next-nearest neighbour repulsions in the bond order channel. The interactions dynamically generate complex Haldane or Kane-Mele type hopping. Hence, the condensation of the bond order parameter signifies the opening of a topologically non-trivial bulk insulating gap, and corresponding protected metallic edge states. However, this phase competes with CDW_3 charge order that extends beyond the primitive unit cell, as well as spontaneously breaking the honeycomb rotational symmetry. The self-consistent path integral approach employed here demonstrated that beyond mean-field collective quantum fluctuations played a crucial part in determining the phase diagram. It was found that fluctuations induce the charge order, thereby stifling the possibility of topological Mott insulating phases. These analytical results were in agreement with the general consensus of the various numerical techniques used to simulate interacting fermions on the lattice. Surprisingly it was discovered that the low-energy quasiparticle excitations of the CDW_3 state are described by gapless semi-Dirac fermions that disperse linearly in one direction, and quadratically in the other. This indicated that the transition was not of the putative semimetal-insulator variety, and would display novel quantum critical properties.

(ii) In Chapter 4 the quantum critical properties of Dirac systems subject to spontaneously broken lattice symmetries were investigated. The work in Chapter 3 provided a concrete lattice model of the semimetal-CDW_3 transition. The universal properties of this transition were analysed with the renormalisation group. The derived critical theory was found to comprise of dynamical order parameters fields that couple to Dirac fermions as mass and emergent gauge fields. Owing to the gap-

less nature of the fermionic excitations, these couplings are relevant perturbations to the paradigmatic Ginzburg-Landau-Wilson fluctuating order parameter theory. As a result, the criticality of the mass sector coupled to Dirac fermions describes the aforementioned semimetal-insulator transitions, and is known to belong to the fermionic Gross-Neveu-Yukawa universality class. At the quantum critical point the Landau quasiparticle picture breaks down, with the quasiparticle residue vanishing as a result of finite anomalous dimensions. An additional defining feature is the emergent Lorentz invariance at the critical fixed point, which is categorised by a single terminal velocity, and isotropic scaling of space and time with dynamical exponent $z = 1$. In contrast, the CDW_3 criticality is described by a novel fixed point that violates Lorentz invariance, with $z > 1$, because of the coupling to the emergent gauge fields. These fields are directly related to the spontaneous breaking of translational and rotational lattice symmetries, and are believed to be generic. In addition, this work showed that complementary combinations of mass and non-Abelian gauge fields provide a natural playground for the study of topological quantum phase transitions, and CDW_3 broken symmetry states are germane to host semi-Dirac excitations.

(iii) Following on from Chapters 3 and 4, in Chapter 5 the quantum multicriticality of Dirac fermions at the intersection of topological and symmetry breaking phase transitions was analysed. In two spatial dimensions the Dirac points of opposite chirality can annihilate, undergoing a topological phase transition to a band insulator. The topological critical point hosts gapless semi-Dirac quasiparticle excitations that disperse linearly in one direction and quadratically in the other. The critical behaviour of quantum phase transitions in semi-Dirac fermion systems that are driven by short-range interactions were analysed using the renormalisation group. Instabilities towards staggered charge and spin instabilities, as well as s-wave superconductivity, were considered. The universal behaviour, even at the mean-field level, was found to be strongly distinct from regular Dirac fermions. In addition, it was found that the order parameter correlations inherit the anisotropy of the semi-Dirac fermions.

6.2 Future Research

The path integral approach employed here is a generic framework to self-consistently include collective quantum fluctuations. For example, a similar approach was employed to look at metallic systems [99–102, 167–169]. In the context of Dirac semimetals it has proven rather successful in comparison to the aggregated numerical lattice simulations. It can be seen as a complementary tool that does not suffer from system size effects, and so is able to probe the region of the critical point. This is particularly true when a problem is not accessible to sign-free quantum Monte Carlo. Furthermore, it complements a renormalisation group study of the critical point, as it can suggest what type of order is energetically favourable in the presence of fluctuations.

Therefore, it is worth applying this method to other nodal systems. A first test of the ability to predict fluctuation induced order would be the π-flux square lattice, where the topological Mott phase that is stable at mean-field is outcompeted by stripe charge order [69, 109]. Beyond this, the increased density of states of semi-Dirac fermions implies an enlarged phase space for quantum fluctuations. These enhanced fermionic fluctuations near quantum critical points combined with the anisotropy of the correlations could stabilise novel phases such as modulated orders. Additionally, it could be fruitful to look at systems with quadratic band touching points on the kagome [114, 115] or checkerboard [116, 117] lattices. Also, it is expected that there are interesting phases in the recently discovered topological chiral crystals [124–126], with multiband touching points.

There are a number of follow up questions to the CDW_3 charge order on the honeycomb lattice. The infinite density matrix RG (iDRMG) simulations found that the charge order was accompanied by bond order. It turns out that both orders couple in the low-energy as $\boldsymbol{A}^i$ (in the notation of Chapter 4), and so the universal properties are not changed. However, the lattice ground state may change from the additional bond order, especially in the presence of finite nearest neighbour interactions.

The novel critical properties found in this Thesis relied on the identification that dynamical order parameters can couple as both mass and emergent gauge fields

to Dirac fermions. This is a departure from the common wisdom that mass channels solely dominate the energetic landscape [20, 133]. Such wisdom is based on the fact that the condensation of mass order parameter fields induces insulating band gaps, which is energetically favourable in the simplest cases. This generically maps the problem onto Gross-Neveu-Yukawa models. However, the important role of emergent gauge fields has been previously recognised in the context of the Ising nematic transition in d-wave superconductors [18, 135, 136], which are also Dirac systems. Here the fourfold lattice rotational symmetry is spontaneously reduced to twofold with an Ising order parameter. In the notation of Chapter 3 the effective Yukawa coupling is $A\Psi^\dagger(\alpha_x + \alpha_y)T^3\Psi$. Similarly, on the π-flux lattice [69, 109], sublattice $(A_x^1\Psi^\dagger\alpha_x T^1\Psi)$ and stripe $(A_y^1\Psi^\dagger\alpha_x T^2\Psi)$ charge order parameters both couple as emergent gauge fields, but this has not been identified in the literature. This case is interesting because topological Mott order couples as a mass field, but is destabilised by beyond mean-field fluctuations. In both instances, the existence of emergent gauge fields is tied to the breaking of lattice symmetries.

To test the predictions in this Thesis there are a number of avenues of study. Naturally, higher loop RG and non-perturbative functional RG calculations are required. In addition, with the advent of "designer Hamiltonian" methods [26, 104] in quantum Monte Carlo, it should be possible to engineer unconventional self-energy terms that have complementary mass and gauge fields, such as for the CDW_3 state. Also, iDMRG simulations are now capable of extracting momentum-dependent excitation spectra of Dirac systems [103].

In Chapter 5 it was discussed that critical theories of semi-Dirac fermions need to be regularised in the vicinity of a critical fixed point. Perhaps this would not be the case if the semi-Dirac point was studied by the complementary combinations of mass and non-Abelian gauge fields identified in Chapter 4. It is conceivable that the encountered divergence of semi-Dirac theories is associated with integrating out some of the emergent gauge degrees of freedom in an uncontrolled manner.

Finally, a question that has not been addressed in the literature is the role of a finite chemical potential on the critical properties of Dirac systems. The chemical

potential is expected to be a relevant perturbation in the RG sense, indicating that the system will flow to some metallic non-Fermi liquid scaling regime. It would be interesting to understand the cross over from the Gross-Neveu-Yukawa criticality. It is expected that there is a competition of energy scales between the chemical potential and the condensation energy gain from spontaneous symmetry breaking. The study of doped Dirac systems could shed new light on the problem of metallic quantum criticality and non-Fermi liquid theory [33].

Appendix A

Appendix: The Fate of the Topological Mott Insulator

A.1 Calculation of Massive Dirac Fermion Polarisation Bubbles

The techniques presenter here are general, but are illustrated for the specific case of the free Dirac fermion propagator dressed with topological Mott broken symmetry states

$$G^{\tau s}_{\sigma\sigma'}(\vec{k}) = \frac{i\omega\sigma^0_{\sigma\sigma'} + v_F[\tau k_x(\sigma_x)_{\sigma\sigma'} + k_y(\sigma_y)_{\sigma\sigma'}] + \tau M_s(\sigma_z)_{\sigma\sigma'}}{k^2 + M_s^2},$$
$$= \frac{g^{\tau s}_{\sigma\sigma'}(\vec{k})}{k^2 + M^2}, \tag{A.1}$$

where $M_s = \frac{3\sqrt{3}V_2}{2}\chi^0$ or $M_s = s\frac{3\sqrt{3}V_2}{2}\chi^z$, $M_s^2 = M^2$, $\vec{k} = (\omega, v_F k_x, v_F k_y)$ and $k^2 = \vec{k}\cdot\vec{k}$. The polarisation bubble components

$$\Pi^{ss'}_{\sigma\sigma'}(\vec{q}) = \sum_{\tau=\pm}\int_{\vec{p}} G^{\tau s}_{\sigma\sigma'}(\vec{k}+\vec{q})G^{\tau s'}_{\sigma'\sigma}(\vec{k}), \tag{A.2}$$

can be calculated using standard field theoretic machinery [139] of Feynman parameters

$$\frac{1}{A^a B^b} = \frac{\Gamma(a+b)}{\Gamma(a)\Gamma(b)}\int_0^1 dx \frac{x^{a-1}(1-x)^{b-1}}{[xA + (1-x)B]^{a+b}}, \tag{A.3}$$

and the integrals of dimensional regularisation

$$\int \frac{d^D k}{(2\pi)^D} \frac{k^{2m}}{[k^2 + M^2]^n} = \frac{1}{(4\pi)^{D/2}} \frac{\Gamma(\frac{D}{2} + m)}{\Gamma(\frac{D}{2})} \frac{\Gamma(n - m - D/2)}{\Gamma(n)} M^{D+2(m-n)}, \tag{A.4}$$

with integer $m \geq 0$ and where the Gamma function $\Gamma(z+1) = z\Gamma(z)$, $\Gamma(n) = (n-1)!$ for positive integer n, and $\Gamma(\frac{1}{2}) = \sqrt{\pi}$. Note that odd powers of k in the numerator vanish by symmetry.

The regulation of ultraviolet divergences $\Lambda \to \infty$ is necessary for internal diagram lines such as the polarisation bubble. The mean-field free energy terms are technically ultraviolet divergent, but can be made cutoff independent by rescaling the coupling $V \to V/\Lambda$.

Application of the above machinery yields

$$\Pi^{ss'}_{\sigma\sigma'}(\vec{q}) = \sum_{\tau=\pm} \int_0^1 dx \int_{\vec{k}} \frac{g^{\tau s}_{\sigma\sigma'}(\vec{k} + (1-x)\vec{q}) g^{\tau s'}_{\sigma'\sigma}(\vec{k} - x\vec{q})}{[k^2 + (-x^2 + x)q^2 + M^2]^2}, \tag{A.5}$$

where the linear transformation $\vec{k} \to \vec{k} - x\vec{q}$ has been used to make the denominator rotationally symmetric in $\vec{k}$. Before applying (A.4) to (A.5), the spherical angular averages are evaluated using the identity [170]

$$\frac{\Gamma(x)\Gamma(y)}{\Gamma(x+y)} = 2 \int_0^{\frac{\pi}{2}} d\theta \, \sin^{2(x-1)}(\theta) \cos^{2(y-1)}(\theta), \tag{A.6}$$

or more specifically

$$\int_{\vec{k}} \omega^{n_\omega} k_x^{n_x} k_y^{n_y} f(k) = \frac{\Gamma(\frac{n_\omega+1}{2})\Gamma(\frac{n_x+1}{2})\Gamma(\frac{n_y+1}{2})}{2\pi\Gamma(\frac{n_x+n_y+n_\omega+3}{2})} \int_{\vec{k}} k^{n_\omega+n_x+n_y} f(k), \tag{A.7}$$

where $f(k)$ is isotropic in $\vec{k}$. Having evaluated the momentum integrals, the Feynman parameter integrals of the general form

$$\int_0^1 \frac{x^m dx}{[-x^2 + x + M^2]^{\frac{2n+1}{2}}}, \tag{A.8}$$

are evaluated with the help of the following recursion relations [170]. Note that

the q dependence has been scaled out for brevity. For $n \geq 0$, $m > 0$ (with $R = -x^2 + x + M^2$)

$$\begin{aligned}
I(n,m) &= \int \frac{x^m dx}{\left[-x^2+x+M^2\right]^{\frac{2n+1}{2}}}, \\
&= \begin{cases} \frac{x^{m-1}}{(2n-m)R^{\frac{2n-1}{2}}} - \frac{2m-2n-1}{2(2n-m)} I(n,m-1) - \frac{(m-1)M^2}{2n-m} I(n,m-2), \ \forall\, m \neq 2n, \\ -\frac{x^{2n-1}}{(2n-1)R^{\frac{2n-1}{2}}} + \frac{1}{2} I(n,2n-1) - I(n-1,2n-2), \ \forall\, m = 2n, \end{cases} \\
I(n,0) &= \int \frac{dx}{\left[-x^2+x+M^2\right]^{\frac{2n+1}{2}}}, \\
&= \frac{2(2x-1)}{(2n-1)(4M^2+1)R^{\frac{2n-1}{2}}} \times \\
&\qquad \left[1 + \sum_{k=1}^{n-1} \left(\frac{8R}{4M^2+1}\right)^k \frac{\prod_{i=1}^{k}(n-i)}{\prod_{j=1}^{k} 2(n-j-\frac{1}{2})}\right], \ \forall\, n \geq 1, \\
I(0,0) &= -\arcsin\left(\frac{1-2x}{\sqrt{4M^2+1}}\right).
\end{aligned}$$

Similarly, for $n = -1$, $m > 0$

$$\begin{aligned}
I(-1,m) &= \int dx\, x^m \sqrt{-x^2+x+M^2}, \\
&= \frac{x^{m-1}R^{\frac{3}{2}}}{m+2} + \frac{2m+1}{2(m+2)} I(-1,m-1) + \frac{(m-1)M^2}{m+2} I(-1,m-2), \\
I(-1,0) &= \frac{(2m-1)\sqrt{R}}{4} + \frac{4M^2+1}{8} I(0,0).
\end{aligned}$$

Finally, it is useful to express the polarisation in terms of the sublattice pseudospin Pauli components $\Pi^{ss'}(\vec{q}) = \sum_\mu \Pi_\mu^{ss'}(\vec{q})\sigma_\mu$ where the sum is over $\mu = 0, x, y, z$. The polarisation components are

$$\begin{aligned}
\Pi_0^{ss'}(\vec{q}) &= \frac{1}{4\pi v_F^2}\left\{ \arctan\left(\frac{q}{2\,|M|}\right)\left[\frac{q^2+\tilde{\omega}^2}{4q} + M^2\frac{q^2-\tilde{\omega}^2}{q^3} + \frac{2}{q}M_s M_{s'}\right] \right. \\
&\qquad \left. + |M|\,\frac{q^2+\tilde{\omega}^2}{2q^2}\right\}, \\
&= \frac{1}{32 v_F^2 q}\left\{ q^2 + \tilde{\omega}^2 + 4M^2\frac{q^2-\tilde{\omega}^2}{q^2} + 8M_s M_{s'} + O(M^3)\right\}, \qquad \text{(A.9)}
\end{aligned}$$

$$\begin{aligned}\Pi_x^{ss'}(\vec{q}) &= -\frac{1}{4\pi v_F^2}\left\{\arctan\left(\frac{q}{2|M|}\right)\left[\frac{2q^2+v_F^2|\boldsymbol{q}|^2}{4q}+M^2\frac{v_F^2|\boldsymbol{q}|^2-2q^2}{q^3}\right]\right.\\ &\quad\left.+|M|\,\frac{2q^2+v_F^2|\boldsymbol{q}|^2}{2q^2}\right\},\\ &= -\frac{1}{32v_F^2q}\left\{2q^2+v_F^2|\boldsymbol{q}|^2+4M^2\frac{v_F^2|\boldsymbol{q}|^2-2q^2}{q^2}+O(M^3)\right\}, \qquad \text{(A.10)}\\ \Pi_y^{ss'}(\vec{q}) &= 0,\\ \Pi_z^{ss'}(\vec{q}) &= 0.\end{aligned}$$

Notice that the quantum anomalous and spin Hall bubbles are distinguished by only one term in $\Pi_0^{ss'}$. Also $\sum_{s=\pm} s\Pi_\mu^{ss'}(\vec{q}) = 0$ for $s' = \pm s$.

In addition, it can be demonstrated that γ will account for renormalisation of the Fermi velocity. The general structure of the polarisation is

$$\Pi(q) \sim \frac{1}{v_F^2 q}(q^2 + M^2 + O(M^3)).$$

Applying the rescaling $\vec{Q} = \vec{q}/v_F\Lambda$ to keep track of factors of v_F, and noting that any factor that can be scaled out of the integrand is negligible (as the logarithm is taken), it is seen that

$$\tilde{\mathcal{S}} \sim v_F V_2 \int_{\vec{Q}} \tilde{\chi}^\dagger\left[1+\gamma V_2 \underbrace{\frac{1}{v_F Q}\left(Q^2+\frac{M^2}{v_F^2}\right)}_{\Pi(Q)}\right]\tilde{\chi}.$$

The internal factors of v_F can be absorbed into the order parameter, and then it is clear that $\Pi \propto 1/v_F$ and so $\gamma < 1$ accounts for the increase of v_F under renormalisation.

A.2 Further Details of the CDW$_3$ Polarisation Calculation

Here details are presented of the calculation of the CDW$_3$ polarisation

$$\tilde{\Pi}_{\vec{q}ij} = \sum_{abcd=1}^{4} \int_{\vec{k}} \mathcal{P}^{\dagger}_{ia} G_{\vec{k}+\vec{q}ab} \mathcal{P}_{bj} \mathcal{P}^{\dagger}_{jc} G_{\vec{k}cd} \mathcal{P}_{di}. \tag{A.11}$$

The spin diagonal fermionic propagator dressed with the charge order is

$$G_{\vec{k}ab} = s^0[-i\omega + v_F \boldsymbol{k} \cdot \boldsymbol{\alpha} + \delta_1 \sigma^z \otimes \sigma^0 + \delta_2 \sigma_z \otimes \tau_x]^{-1}_{ab}, \tag{A.12}$$

with $\delta_1 = 2V_2(\rho - \Delta), \delta_2 = 2V_2(\rho + \Delta/2)$. To apply the field theoretic machinery outlined in Section A.1 it is crucial to express the propagator in terms of massive Dirac fermion propagators $\sim [p^2 + M^2]^{-1}$. Inverting $G^{-1}_{\vec{p}}$ and using partial fractions

$$G_{\vec{k}ab} = \frac{g_{\vec{k}ab}}{4\delta_2\sqrt{v_F^2 k_x^2 + \delta_1^2}} \sum_{\nu=\pm} \frac{\nu}{p^2 + \delta_1^2 + \delta_2^2 - \nu[2\delta_2\sqrt{v_F^2 k_x^2 + \delta_1^2}]}, \tag{A.13}$$

where $g_{\vec{k}}$ is some complicated matrix that is polynomial in $\vec{k}$ and δ_i with combined cubic order. Then expanding the denominator in the critical region, $\rho, \delta_i \to 0$, the propagator can be expressed in terms of "higher order" massive Dirac fermion propagators

$$G_{\vec{k}ab} = \frac{g_{\vec{k}ab}}{[k^2 + \delta_1^2 + \delta_2^2]^2} \sum_{n=0}^{\tilde{N}} \left[\frac{2\delta_2\sqrt{v_F^2 k_x^2 + \delta_1^2}}{k^2 + \delta_1^2 + \delta_2^2} \right]^{2n}. \tag{A.14}$$

Following the procedure in Section A.1, $\tilde{\Pi}_{\vec{q}}$ may be evaluated to arbitrary order in $\tilde{N}$. However, to obtain all terms up to quadratic order in ρ, it is only necessary to use $\tilde{N} = 1$. This procedure is achieved using computer algebra, such as Mathematica. The exact form is too lengthy to show.

A.3 Further Details of the CDW$_3$ Fluctuation Correction Calculation

The fluctuation corrections to the quadratic coefficient are

$$\delta\tilde{\alpha} = V_2 \int_{\vec{q}} \mathrm{tr} \frac{2\gamma N_s \tilde{\Pi}^{(2)}_{\vec{q}}}{U^{-1}_{\boldsymbol{q}} + 2\gamma N_s \tilde{\Pi}^{(0)}_{\vec{q}}}. \tag{A.15}$$

The reduces to

$$\delta\tilde{\alpha} = \frac{V_2 v_2 \Omega}{2\pi^2} \int d^2\vec{\phi} \int_0^1 dq\, q\, \mathrm{tr}[(U^{-1}_{\Lambda\boldsymbol{q}} + \Omega q \tilde{\Pi}^{(0)}_{\vec{\phi}})^{-1} \tilde{\Pi}^{(2)}_{\vec{\phi}}], \tag{A.16}$$

where the rescaling $\vec{q} \to v_F \Lambda \vec{q}$ is made, and the radial component of $\tilde{\Pi}$ is extracted $\tilde{\Pi}^{(n)}_{\vec{q}} = \Omega q^{1-n} \tilde{\Pi}^{(n)}_{\vec{\phi}}$. Here $\vec{\phi} = (\phi_1, \phi_2)$ are the azimuthal and polar angles respectively, and $\Omega = 2\pi\gamma N_s v_2$.

The final difficulty involves inverting the 6×6 matrix. This turns out to be possible in an analytically tractable manner if $U^{-1}_{\boldsymbol{q}}$ is approximated by the zeroth order expansion $U^{-1}_{\boldsymbol{0}}$. This is justified via numerical analysis from which it is found that the higher order terms in $\Lambda\boldsymbol{q}$ do not qualitatively change the phase behaviour over a large range of Λ, implying that the terms neglected are a small perturbation. In terms of 3×3 blocks there are the following structures

$$U_0^{-1} = \begin{pmatrix} A_U & 0 \\ 0 & A_U \end{pmatrix}, \; \Omega q \tilde{\Pi}^{(0)} = \begin{pmatrix} \tilde{A}_0 & \tilde{B}_0 \\ \tilde{B}_0^T & \tilde{A}_0 \end{pmatrix}, \; \tilde{\Pi}^{(2)} = \begin{pmatrix} \tilde{A}_2 & \tilde{B}_2 \\ \tilde{B}_2^T & \tilde{D}_2 \end{pmatrix}. \tag{A.17}$$

The aim is to calculate the inverse of $M = U_0^{-1} + \Omega q \tilde{\Pi}^0$, which can be rewritten as $M = M_1 M_2$ with

$$M_1 = \begin{pmatrix} A_U + A_0 & 0 \\ 0 & A_U + A_0 \end{pmatrix}, \; M_2 = \begin{pmatrix} 1 & B_0 \\ B_0^T & 1 \end{pmatrix}, \; B_0 = (A_U + A_0)^{-1} \tilde{B}_0. \tag{A.18}$$

Using $(M_1M_2)^{-1} = M_2^{-1}M_1^{-1}$ and the properties of the inversion of block matrices

$$M_2^{-1} = \begin{pmatrix} 1 & -B_0 \\ -B_0^T & 1 \end{pmatrix} \begin{pmatrix} (1 - B_0B_0^T)^{-1} & 0 \\ 0 & (1 - B_0B_0^T)^{-1} \end{pmatrix}, \tag{A.19}$$

$$\Rightarrow M^{-1} = \begin{pmatrix} 1 & -B_0 \\ -B_0^T & 1 \end{pmatrix} \begin{pmatrix} \tilde{M} & 0 \\ 0 & \tilde{M} \end{pmatrix}, \tag{A.20}$$

where $\tilde{M} = (1 - B_0B_0^T)^{-1}(A_U + A_0)^{-1}$.

Then evaluating the trace over the block structure results in

$$\begin{aligned} \delta\alpha &= \frac{V_2\nu_2\Omega}{2\pi^2} \int d^2\vec{\phi} \int_0^1 dq\, q\, \mathrm{tr}\{\tilde{M}(\tilde{A}_2 + \tilde{D}_2) - (B_0\tilde{M}\tilde{B}_2^T + B_0^T\tilde{M}\tilde{B}_2\}, \\ \delta\alpha &= \frac{V_2\nu_2\Omega}{\pi^2} \int d^2\vec{\phi} \int_0^1 dq\, q\, \mathrm{tr}\{\tilde{M}\tilde{A}_2 - B_0\tilde{M}\tilde{B}_2^T\}, \end{aligned} \tag{A.21}$$

where $\mathrm{tr}\tilde{M}\tilde{A}_2 = \mathrm{tr}\tilde{M}\tilde{D}_2$. The final result is obtained by evaluating the integrals in the order radial, azimuthal, polar, which yields the result quoted in the main text

$$\begin{aligned} \delta\tilde{\alpha} =& \frac{8V_2\nu_2}{\pi\tilde{\Omega}} \Bigg\{ \\ & \left[384(2+x)^2 + 8(28 - 68x + 31x^2)\tilde{\Omega} + (12 - 20x + 11x^2)\tilde{\Omega}^2\right] \frac{\arctan\left(\frac{\sqrt{\tilde{\Omega}}}{4}\right)}{4\sqrt{\tilde{\Omega}}} \\ & + \frac{16}{3}\Bigg[- (1-x)^2\tilde{\Omega} - \frac{9}{2}(2+x)^2 + (62 - \frac{635}{2}x + \frac{883}{8}x^2)\log(2) \\ & - \frac{3}{2}(1+x)^2 \sum_{\sigma=\pm1} \mathrm{Li}_2\left(\frac{\sigma\sqrt{\tilde{\Omega}(4+\tilde{\Omega})} - \tilde{\Omega}}{2}\right) \\ & + (2 - \frac{5}{2}x + \frac{13}{8}x^2)\log(2 - \tilde{\Omega}) - 16(1 - 5x + \frac{7}{4}x^2)\log(16 + \tilde{\Omega})\Bigg]\Bigg\}. \end{aligned} \tag{A.22}$$

Appendix B

Appendix: Novel Criticality of Dirac Fermions from Lattice Symmetry Breaking

B.1 Gauge Fixing the Emergent Gauge Sector

Here properties of the emergent gauge sector are further discussed, and details are provided of the Fadeev-Popov gauge fixing procedure in the R_ξ gauge [146, 171]. The action is invariant under the local spatial gauge transformation

$$U(\boldsymbol{r}) = \exp\{-ig_A[\theta^1(\boldsymbol{r})T^1 + \theta^2(\boldsymbol{r})T^2 + \theta^3 T^3]\}, \tag{B.1}$$

where it is important to note that $\partial_i\theta^3 = 0$ for $i = x, y$, such that $\theta^a(\boldsymbol{r}) = (\theta^1(\boldsymbol{r}), \theta^2(\boldsymbol{r}), \theta^3)$. Therefore the theory does not posses a local $SU(2)$ gauge structure, which is equivalent to the statement $\boldsymbol{A}^3 = 0$. In addition, $\partial_\tau\theta^a = 0$. The gauge transformation can be built from the infinitesimal θ transformations

$$U(\boldsymbol{r}) = \alpha_0 - ig_A\theta^a(\boldsymbol{r})T^a. \tag{B.2}$$

The gauge covariant derivative is

$$(D_0, \boldsymbol{D}) = (\partial_\tau\alpha_0, \boldsymbol{\partial} - i\frac{g_A}{v_F}\boldsymbol{A}^a T^a). \tag{B.3}$$

Gauge invariance of the Lagrangian requires that under the transformation $\Psi \to U\Psi$, $\Psi^\dagger \to \Psi^\dagger U^\dagger$, the derivative transforms as $\boldsymbol{D} \to U\boldsymbol{D}U^\dagger$. Using the infinitesimal transformation it is clear that the gauge field transforms as

$$\boldsymbol{A}^a T^a \to U\boldsymbol{A}^a U^\dagger + \frac{i}{g_A} U\boldsymbol{\partial} U^\dagger, \tag{B.4}$$

$$\therefore \boldsymbol{A}^a \to \boldsymbol{A}^a - \boldsymbol{\partial}\theta^a - g_A \sum_{b,c=1}^{3} \epsilon^{abc} \boldsymbol{A}^b \theta^c. \tag{B.5}$$

This implies that there is an emergent gauge freedom or redundancy in the low-energy theory for each choice of $\boldsymbol{A}^{1,2}$, as claimed. The issue is that for each physical field configuration of $D[\boldsymbol{A}^{1,2}]$ in the functional integration measure, there are an infinite number of equivalent configurations given by the choice of $\theta^a(\boldsymbol{r})$. To avoid integrating over the emergent infinite degeneracy, it is important to fix the gauge. In the following it will be demonstrated that this is crucial to the path integral definition of the low-energy effective theory. For brevity the spatial part of the theory is considered, and the trivial imaginary time part is neglected. The $\boldsymbol{A}^{1,2}$ sector has the Yang-Mills structure

$$S_F = \frac{1}{4} \int \mathrm{tr} F_{ij} F_{ji}, \tag{B.6}$$

where there are sums over repeated indices $i, j = x, y$. The action is defined in terms of the gauge field strength

$$F_{ij} = \frac{i}{g_A}[D_i, D_j] = \partial_i A_j^a T^a - \partial_j A_i^a T^a - i g_A [A_i^a T^a, A_j^b T^b]. \tag{B.7}$$

Expanding this out and integrating the quadratic terms by parts

$$S_F = \frac{1}{2} \int \left[A_i^a (-\delta_{ij}\partial^2 + \partial_i \partial_j) A_j^a + 2 g_A^2 (\boldsymbol{A}^1 \times \boldsymbol{A}^2)^2 \right]. \tag{B.8}$$

Note that both of these terms are also obtained from integrating over fermion modes in Chapter 4. It is crucial to identify that the kinetic term signifies a non-invertible

propagator, with the matrix structure

$$\begin{pmatrix} A_x^a \\ A_y^a \end{pmatrix}^T \begin{pmatrix} \boldsymbol{k}\cdot\boldsymbol{k} - k_x^2 & -k_x k_y \\ -k_x k_y & \boldsymbol{k}\cdot\boldsymbol{k} - k_y^2 \end{pmatrix} \begin{pmatrix} A_x^a \\ A_y^a \end{pmatrix}, \tag{B.9}$$

which is non-invertible with zero determinant of the kernel.

This is a manifestation of the gauge redundancy. The resolution presented here loosely follows the standard treatment found in the textbooks of Srednicki [146] or Peskin and Schroeder [171], where further technical details may be found.

The following simple example motivates the gauge fixing. The path integral is considered

$$Z \propto \int_{-\infty}^{\infty} dxdy e^{-S(x)}, \tag{B.10}$$

where y is a redundant variable that does not enter the action. The restriction of the integration can be implemented with the delta function, which can be shifted by an arbitrary function $f(x)$

$$Z = \int dxdy\delta(y)e^{-S(x)} = \int dxdy\delta(y - f(x))e^{-S(x)}. \tag{B.11}$$

Equivalently the function $G(x, y)$ can be defined with $G(x, y) = 0$ to have a unique solution at $y = f(x)$ for fixed x. From the properties of the delta function

$$\delta(G(x, y)) = \frac{\delta(y - f(x))}{\partial G/\partial y}, \tag{B.12}$$

where it is assumed $\partial G/\partial y > 0$ at $y = f(x)$. Then at $y = f(x)$

$$Z = \int dxdy\delta(G)\frac{\partial G}{\partial y}e^{-S(x)}. \tag{B.13}$$

This motivates the Fadeev-Popov gauge fixing procedure. Here G is the gauge fixing function

$$G^a(\boldsymbol{r}) = \boldsymbol{\partial}\cdot\boldsymbol{A}^a(\boldsymbol{r}) - w^a(\boldsymbol{r}), \tag{B.14}$$

where w^a is a fixed arbitrary function. The functional generalisation of Eq. (B.12)

is

$$1 = \int D[\theta]\det\left(\frac{\delta G}{\delta\theta}\right)\delta(G), \tag{B.15}$$

which is inserted into $Z \propto \int D[A]e^{-S_F}$ to fix the functional integration over the physical configuration. Under the gauge transformation Eq. (B.5)

$$\frac{\delta G^a(\boldsymbol{r})}{\delta\theta^b(\boldsymbol{r}')} = -\delta^{ab}\partial^2\delta(\boldsymbol{r}-\boldsymbol{r}'), \tag{B.16}$$

which is crucially independent of θ, and so is a trivial multiplicative constant to the Z. The functional integral over A is now restricted by δG. The final step in the so-called R_ξ gauge fixing procedure is to introduce the Gaussian action $S_w = \int w^a w^a/2\xi$, and integrate over w

$$\begin{aligned} Z &\propto \int D[A,w]\delta(\boldsymbol{\partial}\cdot\boldsymbol{A}^a - w^a)e^{-S_w-S_F}, \\ &\propto \int D[A]\exp\left[\frac{1}{2}\int A_i^a(\delta_{ij}\partial^2 + \frac{1-\xi}{\xi}\partial_i\partial_j)A_j^a - 2g_A^2(\boldsymbol{A}^1\times\boldsymbol{A}^2)^2\right]. \end{aligned} \tag{B.17}$$

B.2 Renormalisation Group Equations in $d = 2$

The RG equations are calculated directly in the physical dimensions $d = 2$, controlling the expansion with large N

$$\Psi^\dagger\Psi \to \sum_{n=1}^{N}\Psi_n^\dagger\Psi_n,\ (g_{\phi,A}^2,\lambda_i) \to \frac{8\pi\Lambda}{N}(g_{\phi,A}^2,\lambda_i). \tag{B.18}$$

The RG equations for the velocities are

$$\frac{d}{d\ell}v_F = v_F\left[z-1+\frac{1}{N}\left(\frac{g_\phi^2\left(c_\phi-2v_F\right)}{c_\phi v_F\left(c_\phi+v_F\right)^2} - \frac{8g_A^2}{c_A\left(c_A+v_F\right)^2}\right)\right], \tag{B.19}$$

$$\frac{d}{d\ell}c_\phi^2 = 2(z-1)c_\phi^2 + \frac{g_\phi^2\left(v_F^2-2c_\phi^2\right)}{v_F^3}, \tag{B.20}$$

$$\frac{d}{d\ell}c_A^2 = 2(z-1)c_A^2 + \frac{g_A^2\left(v_F^2-2c_A^2\right)}{2v_F^3}. \tag{B.21}$$

The RG equations for the Yukawa couplings are

$$\frac{d}{d\ell}g_\phi^2 = g_\phi^2\left[3z-2-\frac{2g_\phi^2}{v_F^3}+\frac{1}{N}\left(-\frac{16g_A^2\left(c_A+2v_F\right)}{c_Av_F\left(c_A+v_F\right)^2}-\frac{4g_\phi^2\left(c_\phi+2v_F\right)}{c_\phi v_F\left(c_\phi+v_F\right)^2}\right)\right], \tag{B.22}$$

$$\frac{d}{d\ell}g_A^2 = g_A^2\left[3z-2-\frac{g_A^2}{v_F^3}+\frac{1}{N}\left(-\frac{16g_A^2}{c_A\left(c_A+v_F\right)^2}-\frac{2g_\phi^2\left(c_\phi+2v_F\right)}{c_\phi v_F\left(c_\phi+v_F\right)^2}\right)\right]. \tag{B.23}$$

The RG equations for the boson order parameter field self-interactions are

$$\frac{d}{d\ell}\lambda_\phi = \lambda_\phi\left(3z-2-\frac{4g_\phi^2}{v_F^3}\right)+\frac{g_\phi^4}{v_F^3}+\frac{1}{N}\left(-\frac{4\lambda_{\phi A}^2}{c_A^3}-\frac{36\lambda_\phi^2}{c_\phi^3}\right), \tag{B.24}$$

$$\frac{d}{d\ell}\lambda_A = \lambda_A\left(3z-2-\frac{2g_A^2}{v_F^3}\right)-\frac{g_A^4}{8v_F^3}+\frac{1}{N}\left(-\frac{\lambda_{\phi A}^2}{c_\phi^3}-\frac{48\lambda_A^2}{c_A^3}-\frac{4\lambda_A\lambda_{\rm YM}}{c_A^3}-\frac{\lambda_{\rm YM}^2}{c_A^3}\right), \tag{B.25}$$

$$\frac{d}{d\ell}\lambda_{\rm YM} = \lambda_{\rm YM}\left(3z-2-\frac{2g_A^2}{v_F^3}\right)+\frac{3g_A^4}{2v_F^3}+\frac{1}{N}\left(-\frac{8\lambda_{\rm YM}^2}{c_A^3}-\frac{48\lambda_A\lambda_{\rm YM}}{c_A^3}\right), \tag{B.26}$$

$$\begin{aligned}\frac{d}{d\ell}\lambda_{\phi A} = {}& \lambda_{\phi A}\left(3z-2-\frac{g_A^2+2g_\phi^2}{v_F^3}\right)+\frac{3g_A^2g_\phi^2}{v_F^3}\\ &+\frac{1}{N}\left(\frac{32\lambda_{\phi A}^2}{c_Ac_\phi\left(c_A+c_\phi\right)}-\frac{24\lambda_A\lambda_{\phi A}}{c_A^3}-\frac{12\lambda_\phi\lambda_{\phi A}}{c_\phi^3}-\frac{2\lambda_{\rm YM}\lambda_{\phi A}}{c_A^3}\right).\end{aligned} \tag{B.27}$$

The RG equations for the boson order parameter field masses are

$$\frac{d}{d\ell}m_\phi^2 = 2m_\phi^2\left(z-\frac{g_\phi^2}{v_F^3}\right)+\frac{1}{N}\left(-\frac{12\lambda_\phi m_\phi^2}{c_\phi^3}-\frac{8m_A^2\lambda_{\phi A}}{c_A^3}+\frac{8\Lambda^2\left(3c_A\lambda_\phi+2c_\phi\lambda_{\phi A}\right)}{c_Ac_\phi}\right), \tag{B.28}$$

$$\begin{aligned}\frac{d}{d\ell}m_A^2 = {}& m_A^2\left(2z-\frac{g_A^2}{v_F^3}\right)+\frac{1}{N}\left(-\frac{2m_\phi^2\lambda_{\phi A}}{c_\phi^3}-\frac{2m_A^2\left(12\lambda_A+\lambda_{\rm YM}\right)}{c_A^3}\right.\\ &\left.+\frac{4\Lambda^2\left(c_A\lambda_{\phi A}+c_\phi\left(12\lambda_A+\lambda_{\rm YM}\right)\right)}{c_Ac_\phi}\right).\end{aligned} \tag{B.29}$$

The lattice allowed cubic term is also irrelevant in this treatment

$$\frac{d}{d\ell}b^2 = b^2\left[5z-2-\frac{3g_A^2}{v_F^3}-\frac{12\frac{1}{N}\left(4\lambda_A+\lambda_{\rm YM}\right)}{c_A^3}\right]+O(b^4), \tag{B.30}$$

with the dimensionless coupling $b^2 \to \frac{8\pi\Lambda}{N} b^2$. At the CDW_3 fixed point this reduces to

$$\frac{d}{d\ell} b^2 = 2b^2 \frac{-57 + 32\sqrt{2}}{N} + O(b^4). \tag{B.31}$$

Therefore, to this order b is an irrelevant perturbation and the fixed point value is $b_* = 0$. In $N \to \infty$, b is marginal to all loop orders [24].

Bibliography

[1] S. Sachdev, *Quantum Phase Transitions*, 2nd ed. (Cambridge University Press, 2011).

[2] P. W. Anderson, Science **177**, 393 (1972).

[3] D. Galanakis, E. Khatami, K. Mikelsons, A. Macridin, J. Moreno, D. A. Browne, and M. Jarrell, Philosophical Transactions of the Royal Society A: Mathematical, Physical and Engineering Sciences **369**, 1670 (2011).

[4] L. Landau, E. Lifshitz, and L. Pitaevskij, *Statistical Physics: Part 2 : Theory of Condensed State*, Landau and Lifshitz Course of theoretical physics (Oxford, 1980).

[5] I. Herbut, *A Modern Approach to Critical Phenomena* (Cambridge University Press, Cambridge, 2007).

[6] K. G. Wilson and J. Kogut, Physics Reports **12**, 75 (1974).

[7] M. E. Fisher, Rev. Mod. Phys. **70**, 653 (1998).

[8] J. Cardy, *Scaling and Renormalization in Statistical Physics*, Cambridge Lecture Notes in Physics (Cambridge University Press, 1996).

[9] J. Zinn-Justin, *Quantum Field Theory and Critical Phenomena* (Oxford University Press, 2002).

[10] J. A. Hertz, Phys. Rev. B **14**, 1165 (1976).

[11] S. L. Sondhi, S. M. Girvin, J. P. Carini, and D. Shahar, Rev. Mod. Phys. **69**, 315 (1997).

[12] A. Kopp and S. Chakravarty, Nature Physics **1**, 53 (2005).

[13] A. Abanov and A. Chubukov, Phys. Rev. Lett. **93**, 255702 (2004).

[14] T. Senthil, A. Vishwanath, L. Balents, S. Sachdev, and M. P. A. Fisher, Science **303**, 1490 (2004).

[15] A. H. Castro Neto, F. Guinea, N. M. R. Peres, K. S. Novoselov, and A. K. Geim, Rev. Mod. Phys. **81**, 109 (2009).

[16] P. R. Wallace, Phys. Rev. **71**, 622 (1947).

[17] G. W. Semenoff, Phys. Rev. Lett. **53**, 2449 (1984).

[18] M. Vojta, Y. Zhang, and S. Sachdev, Phys. Rev. Lett. **85**, 4940 (2000).

[19] I. F. Herbut, Phys. Rev. Lett. **97**, 146401 (2006).

[20] I. F. Herbut, V. Juričić, and O. Vafek, Phys. Rev. B **80**, 075432 (2009).

[21] D. J. Gross and A. Neveu, Phys. Rev. D **10**, 3235 (1974).

[22] J. Zinn-Justin, Nuclear Physics B **367**, 105 (1991).

[23] Z.-X. Li, Y.-F. Jiang, S.-K. Jian, and H. Yao, Nature Communications **8**, 314 (2017).

[24] M. M. Scherer and I. F. Herbut, Phys. Rev. B **94**, 205136 (2016).

[25] S.-K. Jian and H. Yao, Phys. Rev. B **96**, 195162 (2017).

[26] T. Sato, M. Hohenadler, and F. F. Assaad, Phys. Rev. Lett. **119**, 197203 (2017).

[27] L. Classen, I. F. Herbut, and M. M. Scherer, Phys. Rev. B **96**, 115132 (2017).

[28] E. Torres, L. Classen, I. F. Herbut, and M. M. Scherer, Phys. Rev. B **97**, 125137 (2018).

[29] L. Janssen, I. F. Herbut, and M. M. Scherer, Phys. Rev. B **97**, 041117 (2018).

[30] B. Roy and V. Juričić, Phys. Rev. B **99**, 241103 (2019).

[31] X. Y. Xu, Y. Qi, L. Zhang, F. F. Assaad, C. Xu, and Z. Y. Meng, Phys. Rev. X **9**, 021022 (2019).

[32] Z.-X. Li, S.-K. Jian, and H. Yao, arXiv:1904.10975 (2019).

[33] S.-S. Lee, Annual Review of Condensed Matter Physics **9**, 227 (2018).

[34] K. von Klitzing, Rev. Mod. Phys. **58**, 519 (1986).

[35] D. J. Thouless, M. Kohmoto, M. P. Nightingale, and M. den Nijs, Phys. Rev. Lett. **49**, 405 (1982).

[36] M. Z. Hasan and C. L. Kane, Rev. Mod. Phys. **82**, 3045 (2010).

[37] F. D. M. Haldane, Phys. Rev. Lett. **61**, 2015 (1988).

[38] C. L. Kane and E. J. Mele, Phys. Rev. Lett. **95**, 146802 (2005).

[39] C. L. Kane and E. J. Mele, Phys. Rev. Lett. **95**, 226801 (2005).

[40] B. A. Bernevig, T. L. Hughes, and S.-C. Zhang, Science **314**, 1757 (2006).

[41] M. König, S. Wiedmann, C. Brüne, A. Roth, H. Buhmann, L. W. Molenkamp, X.-L. Qi, and S.-C. Zhang, Science **318**, 766 (2007).

[42] B. Roy and M. S. Foster, Phys. Rev. X **8**, 011049 (2018).

[43] N. P. Armitage, E. J. Mele, and A. Vishwanath, Rev. Mod. Phys. **90**, 015001 (2018).

[44] M. Hohenadler and F. F. Assaad, Journal of Physics: Condensed Matter **25**, 143201 (2013).

[45] P. Dietl, F. Piéchon, and G. Montambaux, Phys. Rev. Lett. **100**, 236405 (2008).

[46] G. Montambaux, F. Piéchon, J.-N. Fuchs, and M. O. Goerbig, Phys. Rev. B **80**, 153412 (2009).

[47] S. Banerjee, R. R. P. Singh, V. Pardo, and W. E. Pickett, Phys. Rev. Lett. **103**, 016402 (2009).

[48] B.-J. Yang, M. S. Bahramy, R. Arita, H. Isobe, E.-G. Moon, and N. Nagaosa, Phys. Rev. Lett. **110**, 086402 (2013).

[49] B.-J. Yang, E.-G. Moon, H. Isobe, and N. Nagaosa, Nature Physics **10**, 774 (2014).

[50] H. Isobe, B.-J. Yang, A. Chubukov, J. Schmalian, and N. Nagaosa, Phys. Rev. Lett. **116**, 076803 (2016).

[51] B. Uchoa and K. Seo, Phys. Rev. B **96**, 220503 (2017).

[52] J. M. Link, B. N. Narozhny, E. I. Kiselev, and J. Schmalian, Phys. Rev. Lett. **120**, 196801 (2018).

[53] X. Li, J.-R. Wang, and G.-Z. Liu, Phys. Rev. B **97**, 184508 (2018).

[54] S. Han, G. Y. Cho, and E.-G. Moon, Phys. Rev. B **98**, 085149 (2018).

[55] S. Han, C. Lee, E.-G. Moon, and H. Min, Phys. Rev. Lett. **122**, 187601 (2019).

[56] S. Sur and B. Roy, arXiv:1812.05615 (2018).

[57] S. Raghu, X.-L. Qi, C. Honerkamp, and S.-C. Zhang, Phys. Rev. Lett. **100**, 156401 (2008).

[58] S. Rachel, Reports on Progress in Physics **81**, 116501 (2018).

[59] K. S. Novoselov, A. K. Geim, S. V. Morozov, D. Jiang, Y. Zhang, S. V. Dubonos, I. V. Grigorieva, and A. A. Firsov, Science **306**, 666 (2004).

[60] S. Das, J. A. Robinson, M. Dubey, H. Terrones, and M. Terrones, Annual Review of Materials Research **45**, 1 (2015).

[61] K. S. Novoselov, A. K. Geim, S. V. Morozov, D. Jiang, M. I. Katsnelson, I. V. Grigorieva, S. V. Dubonos, and A. A. Firsov, Nature **438**, 197 EP (2005).

[62] L. Tarruell, D. Greif, T. Uehlinger, G. Jotzu, and T. Esslinger, Nature **483**, 302 (2012).

[63] K. K. Gomes, W. Mar, W. Ko, F. Guinea, and H. C. Manoharan, Nature **483**, 306 (2012).

[64] S. Sorella and E. Tosatti, Europhysics Letters (EPL) **19**, 699 (1992).

[65] A. Altland and B. D. Simons, *Condensed Matter Field Theory*, 2nd ed. (Cambridge University Press, 2010).

[66] J. Hubbard, Physical Review Letters **3**, 77 (1959).

[67] R. L. Stratonovich, Soviet Physics Doklady **2**, 416 (1957).

[68] E. Christou, B. Uchoa, and F. Krüger, Phys. Rev. B **98**, 161120 (2018).

[69] C. Weeks and M. Franz, Phys. Rev. B **81**, 085105 (2010).

[70] A. G. Grushin, E. V. Castro, A. Cortijo, F. de Juan, M. A. H. Vozmediano, and B. Valenzuela, Phys. Rev. B **87**, 085136 (2013).

[71] L. Janssen and I. F. Herbut, Phys. Rev. B **89**, 205403 (2014).

[72] L. Classen, I. F. Herbut, L. Janssen, and M. M. Scherer, Phys. Rev. B **93**, 125119 (2016).

[73] F. F. Assaad and I. F. Herbut, Phys. Rev. X **3**, 031010 (2013).

[74] L. Wang, P. Corboz, and M. Troyer, New Journal of Physics **16**, 103008 (2014).

[75] Z.-X. Li, Y.-F. Jiang, and H. Yao, New Journal of Physics **17**, 085003 (2015).

[76] Y. Otsuka, S. Yunoki, and S. Sorella, Phys. Rev. X **6**, 011029 (2016).

[77] H.-K. Tang, J. N. Leaw, J. N. B. Rodrigues, I. F. Herbut, P. Sengupta, F. F. Assaad, and S. Adam, Science **361**, 570 (2018).

[78] M. Golor and S. Wessel, Phys. Rev. B **92**, 195154 (2015).

[79] N. A. García-Martínez, A. G. Grushin, T. Neupert, B. Valenzuela, and E. V. Castro, Phys. Rev. B **88**, 245123 (2013).

[80] M. Daghofer and M. Hohenadler, Phys. Rev. B **89**, 035103 (2014).

[81] T. Đurić, N. Chancellor, and I. F. Herbut, Phys. Rev. B **89**, 165123 (2014).

[82] S. Capponi and A. M. Läuchli, Phys. Rev. B **92**, 085146 (2015).

[83] J. Motruk, A. G. Grushin, F. de Juan, and F. Pollmann, Phys. Rev. B **92**, 085147 (2015).

[84] D. D. Scherer, M. M. Scherer, and C. Honerkamp, Phys. Rev. B **92**, 155137 (2015).

[85] Y. Volpez, D. D. Scherer, and M. M. Scherer, Phys. Rev. B **94**, 165107 (2016).

[86] D. S. de la Peña, J. Lichtenstein, and C. Honerkamp, Phys. Rev. B **95**, 085143 (2017).

[87] M. Kurita, Y. Yamaji, and M. Imada, Phys. Rev. B **94**, 125131 (2016).

[88] M. Bijelic, R. Kaneko, C. Gros, and R. Valentí, Phys. Rev. B **97**, 125142 (2018).

[89] S. Capponi, Journal of Physics: Condensed Matter **29**, 043002 (2017).

[90] G. Jotzu, M. Messer, R. Desbuquois, M. Lebrat, T. Uehlinger, D. Greif, and T. Esslinger, Nature **515**, 237 EP (2014).

[91] M. V. Berry, Proc. R. Soc. Lond. A **392**, 45 (1984).

[92] Y. Aharonov and D. Bohm, Phys. Rev. **115**, 485 (1959).

[93] R. Winkler and U. Zülicke, The ANZIAM Journal **57**, 3 (2015).

[94] N. Nagaosa, J. Sinova, S. Onoda, A. H. MacDonald, and N. P. Ong, Rev. Mod. Phys. **82**, 1539 (2010).

[95] H. Kleinert, Electron. J. Theor. Phys. **8**, 57 (2011), arXiv:1104.5161 .

[96] J. González, F. Guinea, and M. Vozmediano, Nuclear Physics B **424**, 595 (1994).

[97] D. C. Elias, R. V. Gorbachev, A. S. Mayorov, S. V. Morozov, A. A. Zhukov, P. Blake, L. A. Ponomarenko, I. V. Grigorieva, K. S. Novoselov, F. Guinea, and A. K. Geim, Nature Physics **7**, 701 EP (2011).

[98] V. N. Kotov, B. Uchoa, V. M. Pereira, F. Guinea, and A. H. Castro Neto, Rev. Mod. Phys. **84**, 1067 (2012).

[99] F. Krüger, U. Karahasanovic, and A. G. Green, Phys. Rev. Lett. **108**, 067003 (2012).

[100] F. Krüger, C. J. Pedder, and A. G. Green, Phys. Rev. Lett. **113**, 147001 (2014).

[101] G. Abdul-Jabbar, D. A. Sokolov, C. D. O'Neill, C. Stock, D. Wermeille, F. Demmel, F. Kruger, A. G. Green, F. Levy-Bertrand, B. Grenier, and A. D. Huxley, Nat Phys **11**, 321 (2015).

[102] A. G. Green, G. Conduit, and F. Krüger, Annual Review of Condensed Matter Physics **9**, 59 (2018).

[103] Y.-C. He, M. P. Zaletel, M. Oshikawa, and F. Pollmann, Phys. Rev. X **7**, 031020 (2017).

[104] Y.-Y. He, X. Y. Xu, K. Sun, F. F. Assaad, Z. Y. Meng, and Z.-Y. Lu, Phys. Rev. B **97**, 081110 (2018).

[105] N. Ikeda, H. Ohsumi, K. Ohwada, K. Ishii, T. Inami, K. Kakurai, Y. Murakami, K. Yoshii, S. Mori, Y. Horibe, and H. Kitô, Nature **436**, 1136 (2005).

[106] A. J. Hearmon, D. Prabhakaran, H. Nowell, F. Fabrizi, M. J. Gutmann, and P. G. Radaelli, Phys. Rev. B **85**, 014115 (2012).

[107] T. Nagata and N. Ikeda, AIP Advances **8**, 075312 (2018).

[108] T. Liu, B. Douçot, and K. Le Hur, Phys. Rev. B **93**, 195153 (2016).

[109] Y. Jia, H. Guo, Z. Chen, S.-Q. Shen, and S. Feng, Phys. Rev. B **88**, 075101 (2013).

[110] K. Sun, H. Yao, E. Fradkin, and S. A. Kivelson, Phys. Rev. Lett. **103**, 046811 (2009).

[111] O. Vafek, Phys. Rev. B **82**, 205106 (2010).

[112] O. Vafek and K. Yang, Phys. Rev. B **81**, 041401 (2010).

[113] E. McCann and V. I. Fal'ko, Phys. Rev. Lett. **96**, 086805 (2006).

[114] W. Zhu, S.-S. Gong, T.-S. Zeng, L. Fu, and D. N. Sheng, Phys. Rev. Lett. **117**, 096402 (2016).

[115] Y. Ren, T.-S. Zeng, W. Zhu, and D. N. Sheng, Phys. Rev. B **98**, 205146 (2018).

[116] H.-Q. Wu, Y.-Y. He, C. Fang, Z. Y. Meng, and Z.-Y. Lu, Phys. Rev. Lett. **117**, 066403 (2016).

[117] T.-S. Zeng, W. Zhu, and D. Sheng, npj Quantum Materials **3**, 49 (2018).

[118] S. Pujari, T. C. Lang, G. Murthy, and R. K. Kaul, Phys. Rev. Lett. **117**, 086404 (2016).

[119] S. Ray, M. Vojta, and L. Janssen, Phys. Rev. B **98**, 245128 (2018).

[120] E. Christou, F. de Juan, and F. Krüger, arXiv:1906.03892 (2019).

[121] M. M. Anber and J. F. Donoghue, Phys. Rev. D **83**, 105027 (2011).

[122] B. Roy, V. Juričić, and I. F. Herbut, Journal of High Energy Physics **2016**, 18 (2016).

[123] B. Roy, M. P. Kennett, K. Yang, and V. Juričić, Phys. Rev. Lett. **121**, 157602 (2018).

[124] B. Bradlyn, J. Cano, Z. Wang, M. G. Vergniory, C. Felser, R. J. Cava, and B. A. Bernevig, Science **353** (2016).

[125] D. S. Sanchez, I. Belopolski, T. A. Cochran, X. Xu, J.-X. Yin, G. Chang, W. Xie, K. Manna, V. Süß, C.-Y. Huang, N. Alidoust, D. Multer, S. S. Zhang, N. Shumiya, X. Wang, G.-Q. Wang, T.-R. Chang, C. Felser, S.-Y. Xu, S. Jia, H. Lin, and M. Z. Hasan, Nature **567**, 500 (2019).

[126] N. B. M. Schröter, D. Pei, M. G. Vergniory, Y. Sun, K. Manna, F. de Juan, J. A. Krieger, V. Süss, M. Schmidt, P. Dudin, B. Bradlyn, T. K. Kim, T. Schmitt, C. Cacho, C. Felser, V. N. Strocov, and Y. Chen, Nature Physics **15**, 759 (2019).

[127] D. M. Basko, Phys. Rev. B **78**, 125418 (2008).

[128] F. de Juan, Phys. Rev. B **87**, 125419 (2013).

[129] F. Gehring, H. Gies, and L. Janssen, Phys. Rev. D **92**, 085046 (2015).

[130] L. N. Mihaila, N. Zerf, B. Ihrig, I. F. Herbut, and M. M. Scherer, Phys. Rev. B **96**, 165133 (2017).

[131] N. Zerf, L. N. Mihaila, P. Marquard, I. F. Herbut, and M. M. Scherer, Phys. Rev. D **96**, 096010 (2017).

[132] I. F. Herbut, V. Juričić, and B. Roy, Phys. Rev. B **79**, 085116 (2009).

[133] S. Ryu, C. Mudry, C.-Y. Hou, and C. Chamon, Phys. Rev. B **80**, 205319 (2009).

[134] C.-Y. Hou, C. Chamon, and C. Mudry, Phys. Rev. Lett. **98**, 186809 (2007).

[135] E.-A. Kim, M. J. Lawler, P. Oreto, S. Sachdev, E. Fradkin, and S. A. Kivelson, Phys. Rev. B **77**, 184514 (2008).

[136] Y. Huh and S. Sachdev, Phys. Rev. B **78**, 064512 (2008).

[137] M. A. Metlitski and S. Sachdev, Phys. Rev. B **82**, 075127 (2010).

[138] R. Shankar, Rev. Mod. Phys. **66**, 129 (1994).

[139] H. Kleinert and V. Schulte-Frohlinde, *Critical Properties of ϕ^4-Theories* (World Scientific, 2001).

[140] T. R. Kirkpatrick and D. Belitz, Phys. Rev. B **91**, 214407 (2015).

[141] M. Moshe and J. Zinn-Justin, Physics Reports **385**, 69 (2003).

[142] B. Knorr, Phys. Rev. B **94**, 245102 (2016).

[143] J. A. Gracey, T. Luthe, and Y. Schröder, Phys. Rev. D **94**, 125028 (2016).

[144] L. Iliesiu, F. Kos, D. Poland, S. S. Pufu, and D. Simmons-Duffin, Journal of High Energy Physics **2018**, 36 (2018).

[145] S. Chandrasekharan and A. Li, Phys. Rev. D **88**, 021701 (2013).

[146] M. Srednicki, *Quantum Field Theory* (Cambridge University Press, 2007).

[147] M. Vozmediano, M. Katsnelson, and F. Guinea, Physics Reports **496**, 109 (2010).

[148] M. Vojta, Y. Zhang, and S. Sachdev, International Journal of Modern Physics B **14**, 3719 (2000).

[149] M. Vojta, Y. Zhang, and S. Sachdev, Phys. Rev. B **62**, 6721 (2000).

[150] J. Kim, S. S. Baik, S. H. Ryu, Y. Sohn, S. Park, B.-G. Park, J. Denlinger, Y. Yi, H. J. Choi, and K. S. Kim, Science **349**, 723 (2015).

[151] J. Kim, S. S. Baik, S. W. Jung, Y. Sohn, S. H. Ryu, H. J. Choi, B.-J. Yang, and K. S. Kim, Phys. Rev. Lett. **119**, 226801 (2017).

[152] T. Uehlinger, G. Jotzu, M. Messer, D. Greif, W. Hofstetter, U. Bissbort, and T. Esslinger, Phys. Rev. Lett. **111**, 185307 (2013).

[153] M. Tarnowski, M. Nuske, N. Fläschner, B. Rem, D. Vogel, L. Freystatzky, K. Sengstock, L. Mathey, and C. Weitenberg, Phys. Rev. Lett. **118**, 240403 (2017).

[154] V. Pardo and W. E. Pickett, Phys. Rev. Lett. **102**, 166803 (2009).

[155] A. Kobayashi, S. Katayama, Y. Suzumura, and H. Fukuyama, Journal of the Physical Society of Japan **76**, 034711 (2007).

[156] L.-K. Lim, J.-N. Fuchs, and G. Montambaux, Phys. Rev. Lett. **108**, 175303 (2012).

[157] I. Boettcher, arXiv:1907.05354 (2019).

[158] M. D. Uryszek, E. Christou, A. Jaefari, F. Krüger, and B. Uchoa, Phys. Rev. B **100**, 155101 (2019).

[159] A. S. Rodin, A. Carvalho, and A. H. Castro Neto, Phys. Rev. Lett. **112**, 176801 (2014).

[160] S. Katayama, A. Kobayashi, and Y. Suzumura, Journal of the Physical Society of Japan **75**, 054705 (2006).

[161] H. Huang, Z. Liu, H. Zhang, W. Duan, and D. Vanderbilt, Phys. Rev. B **92**, 161115 (2015).

[162] G. Y. Cho and E.-G. Moon, Scientific Reports **6**, 19198 EP (2016).

[163] A. N. Vasil'ev, S. É. Derkachev, N. A. Kivel', and A. S. Stepanenko, Theoretical and Mathematical Physics **94**, 127 (1993).

[164] J. A. Gracey, International Journal of Modern Physics A **09**, 567 (1994).

[165] I. F. Herbut, Phys. Rev. Lett. **104**, 066404 (2010).

[166] B. Roy, V. Juričić, and I. F. Herbut, Phys. Rev. B **87**, 041401 (2013).

[167] C. J. Pedder, F. Krüger, and A. G. Green, Phys. Rev. B **88**, 165109 (2013).

[168] U. Karahasanovic, F. Krüger, and A. G. Green, Phys. Rev. B **85**, 165111 (2012).

[169] G. J. Conduit, A. G. Green, and B. D. Simons, Phys. Rev. Lett. **103**, 207201 (2009).

[170] I. S. Gradshteyn and I. M. Ryzhik, *Table of Integrals, Series, and Products*, 7th ed. (Elsevier/Academic Press, 2007).

[171] M. E. Peskin, D. V. Schroeder, and E. Martinec, "An Introduction to Quantum Field Theory," (1995).